Gravitational Waves from Feynman Diagrams

Lucien Huber

9/13/2022

The goal of this thesis is to explain the nascent field of scattering amplitudes in gravitational wave physics. We explore the context in which these tools are revolutionizing the field, and then go into detail of their construction and application.

We begin with a brief overview of the topic and the academic context. The next chapter is devoted to the theoretical foundations of gravitational waves, and their important sources. In the third chapter we discuss the detection of these waves, highlighting the importance of the theoretical templates. The fourth chapter explores the theoretical methods for producing full wave templates, such as Effective One-Body (EOB) and Numerical Relativity (NR) as well as the expansions and approximations used for the inspiral: the Post-Newtonian (PN) and Post-Minkowski (PM) approximations.

The fifth chapter is the main focus of the thesis, and is devoted to the scattering amplitude techniques that can be applied to the general relativistic two-body problem. We begin with the Effective Field Theory (EFT) matching technique to motivate the production of gravitational amplitudes. The Kosower Maybee and O'Connell (KMOC) formalism, defining the classical limit of wave functions, is explained in detail. Finally, amplitudes in a simplified theory, Scalar Quantum Electrodynamics (SQED) are computed, with a focus on automation of calculations. The corresponding graphs, filters, Feynman rules and further simplifications are all implemented in a cocktail of the relevant languages. We also compare the results obtained with those found in the literature.

In the last chapter we provide some concluding remarks and a brief outlook.

Table of contents

Preface

This document represents my, Lucien Huber, master thesis, the last step in my master's degree at ETH Zurich. It can be viewed as either a webpage at https://lcnhb.github.io/GWAmplitudes, or downloaded as a PDF file. All code used for the thesis is provided in the GitHub repository https://github.com/lcnhb/GWAmplitudes.

Acknowledgements

I would like to thank my supervisor, Prof. Babis Anastasiou, for his trust, his support, and kindness throughout the last half year that has led to this thesis. Without his curiosity towards this new subject, I would have never discovered and learned about this wonderful world at the confluence of two great physical theories, General Relativity (GR) and Quantum Field Theory (QFT) . I would also like to extend this thanks to the rest of the theoretical particle physics group a ETH. Dr Achilleas Lazopoulos, Dr. Ben Ruijl, Dr. Valentin Hirschi, Rayan Haindl, Dario Kermanschah, Zeno Capatti, Matilde Vicini, and Julia Karlen, the many shared lunches, coffee breaks, and discussions have been a incredible source of inspiration and motivation for me. In particular, I would like to thank Ben for his help with all things FORM, Zeno for our very insightful discussions and your great suggestions, and Julia for reading through the first draft of this thesis.

I would also like to thank my girlfriend, for her patience, understanding and support. I would also like to thank her for keeping me grounded and reminding me that there is more to life than physics!

Finally, I would like to thank my parents for their unconditional love and support, and without whom I would not be here today.

1 Introduction

The detection of GWs by the LIGO and Virgo collaborations in 2016 [1] has sparked a new era of GW astronomy. The first detections were of Binary Black Hole (BBH) mergers. More recently, Binary Neutron Star (BNS) mergers [2] as well as Neutron Star - Black Hole (NS-BH) mergers have been detected [3]. Future observatories will further increase sensitivity and will be able to detect a wide range of astrophysical sources. Studying these GWs signals gives us a very powerful new window into the universe. It allows us to study the properties of neutron stars and black holes, and the physics of compact object mergers, but also gives us a powerful testing apparatus for general relativity.

To detect these faint signals LIGO and Virgo have been made to be extraordinarily sensitive instruments. This sensitivity had been the main barrier to overcome ever since GW were first predicted by Einstein. Whilst sensitive measurements generally demand, and thus drive equally precise theoretical predictions, for GW astronomy, the case for theoretical models is even stronger. Indeed, theoretical models are necessary components to the detection mechanisms used at current laser interferometers. The faint signals of strain due to the passage of a GW are often buried in the noise of the detector. To counteract this, experimental physicists make use of matched filtering, an approach where a template signal is cross correlated to the detector output. The template is a model of the signal provided by theoretical physicists based on physical models. The upper bound to physical content of the detection is thus in fact set by the physical content of the template and therefore of the theoretical model. Additionally, the more precise the template, the higher the signal-to-noise ratio, the more probable and precise the detection. Theoretical models are thus a crucial component of the detection process, and there is a strong incentive to improve their precision and breadth of applicability.

In recent years, an unlikely ally in this precision race has arisen, based on QFT techniques [4–7]. This is seemingly an impossibility as QFT and GR have historically been the two irreconcilable theories that 'together' span the whole range of scales in the universe. QFT and the standard model, describe physics at the smallest scales, where quantum effects dominate. This is the physics of colliders, and condensed matter. The standard model is our best guess as to the nature of the fundamental constituents of 'matter' and 'light'.

GR on the other hand describes physics at the largest scales, where gravity dominates. It was developed by Einstein as the successor to the

Newtonian theory of gravity, which was not able to account for orbital mechanics such as the precession of the perihelion of mercury. Having passed every experimental test we have thrown at it, GR is by far the best theory of gravity we have yet. It can describe cosmological phenomena, as well as the compact objects known as black holes.

These two physics leviathans do not get along, unfortunately. GR is a theory of geometry, and QFT is a theory of interactions. We can try to write and interpret one in the language of the other, but in either case difficulties arise. Writing GR in terms of perturbative QFT one introduces the graviton, the spin 2 quantum of gravity. Disappointingly, such a theory breaks down at high energies, and is un-renormalisable . In fact the presence of black holes, that dominate the high energy spectrum of GR, is a testament to that fact [8]. On the other hand, whilst one can write QFTs on a curved background, this does not quantize gravity itself, and therefore does not really address the problem. Background independent theories such as loop quantum gravity does not yet have semiclassical limit collapsing to GR. String theory, on the other hand, introduces spurious dimensions that need to be compactified, which leads to uncountably many solutions. In short, there is no satisfactory theory of that combines GR and QFT consistently.

Surprisingly, one can still use the powerful tools of one theory to tackle problems in the other. Specifically, considering the classical limit of QFT, allows the extraction of perturbative gravitational dynamics from an initially quantum description of the setup. This is interesting because the tools developed for high energy physics have become extremely powerful and efficient theoretical machines, often making use of diagrammatic reasoning. Tools such as Feynman diagrams, differential equations [9–11] and more recently generalized unitarity [12–15], all yielding efficient computations for scattering amplitudes, can all be applied to *classical* orbital dynamics in GR. This is exactly the subject of this thesis.

Specifically we are interested in the diagrammatic objects that arise when framing the two body problem similarly to particle collisions. Diagrammatics are interesting as they are an abstraction of the problem that enables efficient reasoning about and automation of the solutions. We will explain where these tools shine in the broader context of waveform approaches such as EOB , Nonrelativistic General Relativity (NRGR) , PM and PN approximations.

This thesis is organized as follows. In Chapter 2 we deal with the theoretical foundations of GWs, exploring how they arise through the linearized Einsteins' field equations. The subsequent Chapter 3 discusses the experimental apparatuses that are used to detect GWs. We describe at the techniques used to extract the signals from the noise, and motivate precise theoretical predictions. In Chapter 4 we look at how to generate partial and full waveforms. We explore the EOB and NR frameworks. Motivated by the need for more precise ingredients to input into EOB, in Chapter 5 we explain the state of the art formalisms that incorporate

amplitude tools into the program. We describe the conservative EFT matching approach, where the system does not lose energy to its environement. Taking into account the loss of energy due to GWs necesitates another method: the KMOC formalism, which makes up the second half of the chapter. In this context, we take a deeper look at amplitude computing tools. We conclude with a discussion of the challenges that lie ahead, and the future of GW astronomy.

2 Gravitational Wave Generation

We start by looking at where and how GWs are generated. We will see that GR predicts the existence of GWs, and we will explore under what conditions they are observable.

2.1 GWs

To this day, the most fundamental theory of gravity is GR , due to Einstein. It formulates spacetime as a Riemannian manifold with curvature, determined by mass distribution. This curvature is encoded in the metric $g_{\mu\nu}$. Objects then move in this deformed spacetime following Equation of Motions (EOMs) written in terms of $g_{\mu\nu}$. Interaction is thus caused by the dependence of $g_{\mu\nu}$ on mass distribution, which itself evolves through $g_{\mu\nu}$. The physical laws that governs the interaction between mass and curvature are manifested in Einstein's field equations,

$$\boxed{R_{\mu\nu} - \frac{g_{\mu\nu}}{2}R + \Lambda g_{\mu\nu} = -8\pi G T_{\mu\nu}}. \tag{2.1}$$

The Left-Hand Side (LHS) of this equation contains several objects that only depend on the metric $g_{\mu\nu}$. $R_{\mu\nu}$ is the Ricci tensor[1], a contraction of the Riemann curvature tensor $R^{\beta}{}_{\mu\nu\rho}$. The Riemann tensor[2] encodes the curvature of spacetime, in terms of the non-commutativity of covariant derivatives. When they do, it means that they have collapsed to regular derivatives, and thus the Levi-civita connection[3] must have vanished. This is only possible if the metric is flat, $g_{\mu\nu} = \eta_{\mu\nu}$. The Riemann curvature tensor is exclusively composed of the metric, its first, second derivatives, and it is linear in the second derivative of the metric. In fact, it is the only possible tensor of this form. The second term on the LHS is the Ricci scalar, a further contraction of the Ricci Tensor: $R = g^{\mu\nu}R_{\mu\nu}$. The final term on the LHS is just a proportional constant factor of the metric, Λ, called the cosmological constant. It can be measured and has a low known upper bound. It is in part responsible for the expansion of the universe.

[1] The Ricci Tensor is given by:
$$R_{\mu\nu} := R^{\alpha}{}_{\mu\alpha\nu} = g^{\alpha\beta}R^{\alpha\mu\beta\nu} \tag{2.2}$$

[2] The Riemann Tensor is given by:
$$R^{\beta}{}_{\mu\nu\rho} = \Gamma^{\beta}{}_{\mu\nu,\rho} - \Gamma^{\beta}{}_{\mu\rho,\nu} - \Gamma^{\alpha}{}_{\mu\rho}\Gamma^{\beta}{}_{\alpha\nu} + \Gamma^{\alpha}{}_{\mu\nu}\Gamma^{\beta}{}_{\alpha\rho}. \tag{2.3}$$

[3] The Levi-Civita Connection is given by:
$$\Gamma^{\alpha}{}_{\mu\nu} = \frac{1}{2}g^{\alpha\rho}\left\{g_{\rho\nu,\mu} + g_{\rho\mu,\nu} - g_{\mu\nu,\rho}\right\} \tag{2.4}$$

11

The Right-Hand Side (RHS) of eq. 2.1 encodes the distribution of mass and energy in the universe, through the stress-energy tensor $T_{\mu\nu}$, which depends on the dynamical properties of the system. It is further multiplied by the Gravitational constant G. In empty space, $T_{\mu\nu}$ is zero.

Equation 2.1 can be recast in a form where the Ricci scalar has been substituted by the trace of the stress-energy tensor,

$$R_{\mu\nu} = -8\pi G\left(T_{\mu\nu} - T^{\alpha}_{\alpha}\frac{g_{\mu\nu}}{2}\right) + \Lambda g_{\mu\nu} \tag{2.5}$$

Both eq. 2.1 & eq. 2.5 with $\Lambda = 0$ admit wave solutions. In order to see this, let us look at these equations in the weak field approximation. We take the metric to be a small perturbation around the Minkowskian background,

$$g_{\mu\nu} = \eta_{\mu\nu} + h_{\mu\nu}, \tag{2.6}$$

where $h_{\mu\nu}$ is the expansion parameter (thus considered small). Note that if we restrict ourselves to first order in $h_{\mu\nu}$ then all raising and lowering of indices is done with $\eta_{\mu\nu}$. Since the LHS of eq. 2.1 is composed of the Ricci tensor and scalar, let us see how these behave in the weak approximation. Both are in fact made up of Levi-Civita connections, which to first order in $h_{\mu\nu}$ is given by:

$$\Gamma^{\alpha}_{\mu\nu} = \frac{1}{2}\eta^{\alpha\rho}\left\{h_{\rho\nu,\mu} + h_{\rho\mu,\nu} - h_{\mu\nu,\rho}\right\} + \mathcal{O}(h^2) \quad . \tag{2.7}$$

Plugging eq. 2.7 into the definition of the Ricci tensor we see that the terms with products of the connection vanish, and we are left with the derivative terms:

$$R_{\mu\nu} = \frac{\eta^{\alpha\rho}}{2}\left[h_{\rho\alpha,\mu\nu} + h_{\mu\nu,\rho\alpha} - h_{\mu\alpha,\rho\nu} - h_{\nu\rho,\mu\alpha}\right] + \mathcal{O}(h^2) = R^{(1)}_{\mu\nu} + \mathcal{O}(h^2) \tag{2.8}$$

The linearized Ricci scalar is then just $R^{(1)} = \eta^{\mu\nu}R^{(1)}_{\mu\nu}$. The symmetry of the Einstein Field Equations (EFE) under general diffeomorphisms implies the existence of gauge freedom. In particular, eq. 2.1, admits an infinite number of solutions, and in fact we can map a solution into another by changing coordinates in such a way that the equation isn't affected. To fix this ambiguity we choose a coordinate system ('gauge choice') by imposing the harmonic coordinate conditions:

$$g^{\alpha\beta}\Gamma^{\mu}_{\alpha\beta} = 0 \tag{2.9}$$

The harmonic coordinate conditions demand the vanishing of the trace of the Levi-Civita connection. They have a simplified form in the weak

approximation, which we can access by plugging eq. 2.7 into eq. 2.9, giving:

$$(\eta^{\alpha\beta} + h^{\alpha\beta})\frac{1}{2}(\eta^{\mu\rho} + h^{\mu\rho})\left[h_{\alpha\rho,\beta} + h_{\beta\rho,\alpha} - h_{\alpha\beta,\rho}\right] = 0$$
$$\eta^{\mu\rho}\eta^{\alpha\beta}\left[2h_{\alpha\rho,\beta} - h_{\alpha\beta,\rho}\right] + \mathcal{O}(h^2) = 0$$
$$\eta^{\alpha\beta}h_{\alpha\rho,\beta} = \frac{1}{2}h_{\alpha\beta,\rho}\eta^{\alpha\beta} + \mathcal{O}(h^2). \tag{2.10}$$

The last equation, truncated to first order, is called the de-Donder gauge condition:

$$h_{\mu\nu}{}^{,\mu} = \frac{1}{2}h^{\alpha}{}_{\alpha,\nu} \tag{2.11}$$

In the de-Donder gauge we can simplify the terms in eq. 2.8 to:

$$\eta^{\alpha\beta}h_{\alpha\mu,\nu\beta} = \frac{1}{2}\eta^{\alpha\beta}h_{\alpha\beta,\mu\nu}, \tag{2.12}$$

and

$$\eta^{\alpha\beta}h_{\beta\nu,\mu\alpha} = \frac{1}{2}h_{\alpha\beta,\mu\nu}. \tag{2.13}$$

With these two relations the expression for the linearized Ricci tensor eq. 2.8 simplifies to

$$R^{(1)}{}_{\mu\nu} = \frac{1}{2}\eta^{\alpha\beta}h_{\mu\nu,\alpha\beta} = \frac{1}{2}\Box_{SR}h_{\mu\nu}. \tag{2.14}$$

Where we have defined the Special Relativity (SR) D'Alembertian differential operator as: $\Box_{SR} = \eta^{\mu\nu}\partial_\mu\partial_\nu$ We can plug eq. 2.14 into eq. 2.5, with $\Lambda = 0$ and up to first order in $h_{\mu\nu}$, we get the linearized Einstein field equations for a system of harmonic coordinates:

$$\Box_{SR}h_{\mu\nu} = -16\pi G(\overbrace{T_{\mu\nu} - \frac{\eta_{\mu\nu}}{2}T^{\alpha}{}_{\alpha}}^{S_{\mu\nu}}), \tag{2.15}$$

$$h^{\alpha}{}_{\mu,\alpha} = \frac{1}{2}h^{\alpha}{}_{\alpha,\mu}. \tag{2.16}$$

Recall raising and lowering indices is done with the Minkowski metric. The tensor $S_{\mu\nu}$ encodes the behavior of the source of GWs. One could also plug eq. 2.14 into eq. 2.1, with $\Lambda = 0$, and express it in terms of the trace reversed perturbation: $\bar{h}_{\mu\nu} = h_{\mu\nu} - \frac{1}{2}h^{\alpha}{}_{\alpha}\eta_{\mu\nu}$. Then, we obtain similar and simpler equations at the cost of a more complex perturbation: [4] [5]

$$\Box_{SR}\bar{h}_{\mu\nu} = -16\pi G T_{\mu\nu} \tag{2.17}$$

[4] Note that the inverse change of variables is just: $h_{\mu\nu} = \bar{h}_{\mu\nu} - \frac{1}{2}\bar{h}^{\alpha}{}_{\alpha}\eta_{\mu\nu}$.

[5] We eliminate the trace of the stress-energy tensor by using: $R = 8\pi G T^{\alpha}{}_{\alpha}$. We can write $R^{(1)} = -\frac{1}{2}\Box_{SR}\bar{h}^{\alpha}{}_{\alpha}$, in de Donder gauge, which is precisely the extra term dropping out of $\Box_{SR}h_{\mu\nu}$ when we express it in terms of $\bar{h}_{\mu\nu}$.

13

$$\bar{h}_{\mu\nu},^\nu = 0. \tag{2.18}$$

We can easily recover the conservation equation for the stress-energy tensor. We take the divergence of eq. 2.17 and use eq. 2.18 to get:

$$T_{\mu\nu},^\nu = 0. \tag{2.19}$$

Let us look at what sorts of solutions come out of these equations.

2.2 Homogenous solutions

The first step is to consider the homogeous solution, as all solutions will involve these terms. Setting $T_{\mu\nu} = 0$ or $S_{\mu\nu} = 0$ yields the wave equation in the absence of sources,

$$\Box_{SR} h_{\mu\nu} = 0. \tag{2.20}$$

[6] Associated to changes in coordinates of the form $x^\mu \to x^\mu + \xi^\mu$ with $\Box_{SR}\xi^\mu = 0$.

The de-Donder gauge (eq. 2.16) and the remaining gauge freedom[6] restricts the possible forms of this solution to having only helicity ± 2 physically significant components (see [16]). Let us look at generic forms of the solution. The metric $h_{\mu\nu}$ ought to be real-valued, thus we seek real solutions of the form

$$h_{\mu\nu} = \varepsilon_{\mu\nu} e^{ik\cdot x} + \varepsilon^*{}_{\mu\nu} e^{-ik\cdot x}, \tag{2.21}$$

where $\varepsilon_{\mu\nu}$ is the polarization tensor, k is the wave vector and we define: $k \cdot x \equiv \eta_{\mu\nu} k^\mu k^\nu = k_\mu x^\mu$. The polarization tensor is a symmetric rank-2 tensor, since $h_{\mu\nu}$ is. Substituting eq. 2.21 into $\Box_{SR} h_{\mu\nu} = 0$ gives $k_\mu k^\mu \equiv k^2 = 0$.[7] [8] From eq. 2.16 we have

[7] Assuming non-zero perturbation $h_{\mu\nu}$ of course.

[8] This is saying that the wavevector for the wave is null, thus that the wave propagates at the speed of light.

$$\varepsilon^\mu{}_\nu k_\mu = \frac{1}{2}\varepsilon^\alpha{}_\alpha k_\nu. \tag{2.22}$$

As said at the beginning of this subsection, we still have some remaining gauge freedom, which we now fix, choosing the following coordinate change $x^\mu \to x^\mu + \zeta^\mu$ where:

$$\zeta^\mu = \mathring{i}A^\mu e^{ik\cdot x} = -\mathring{i}A^{*\mu} e^{-ik\cdot x} \tag{2.23}$$

In the new coordinates, the tensor perturbation takes the form:

$$h'_{\mu\nu} = h_{\mu\nu} - \frac{\partial \zeta_\mu}{\partial x^\nu} - \frac{\partial \zeta_\nu}{\partial x^\mu} = \varepsilon'_{\mu\nu} e^{ik\cdot x} + \varepsilon'^*{}_{\mu\nu} e^{-ik\cdot x}. \tag{2.24}$$

with

$$\varepsilon'_{\mu\nu} = \varepsilon_{\mu\nu} + k_\mu A_\nu + k_\nu A_\mu \tag{2.25}$$

14

Equations -eq. 2.22 and -eq. 2.25 reduce the free components in the polarization tensor to just two. Additionally these equations conspire to yield a traceless polarisation tensor $\varepsilon^\alpha_\alpha = 0$, with $\varepsilon_{0\mu} = 0$ (see [17]). This in turn implies that the metric perturbation itself is traceless, and thus becomes equal to its trace-reversed counterpart. This is the so-called transverse traceless gauge:

$$h_{0\mu} = 0, \quad h^\alpha_\alpha = 0, \quad h_{\mu\nu}{}^{,\nu} = 0. \tag{2.26}$$

The metric perturbation in this gauge is written as: $h^{TT}{}_{ij}$.

2.3 Inhomogenous solutions

With the homogenous part of eq. 2.15 accounted for, we are now ready to derive the inhomogenous part. The solution of eq. 2.15 in the presence of a source term will be heavily inspired by the analogous problem in electromagnetism, where one learns that any linear differential equation:

$$\hat{\mathscr{L}}\phi = J \tag{2.27}$$

is solved using green's functions. If we define the following retarded Green's function

$$\mathscr{G}_{\text{ret}}(x^\mu - x'^\mu) = -2\pi\delta((x - x')^2)\Theta(t > t'), \tag{2.28}$$

which satisfies,

$$\Box_{SR}\mathscr{G}_{\text{ret}}(x^\mu - x'^\mu) = -2\pi\delta^4(x^\mu - x'^\mu). \tag{2.29}$$

Then, the solution to

$$\Box_{SR}h_{\mu\nu} = -16\pi G S_{\mu\nu} \tag{2.30}$$

is given by

$$h_{\mu\nu}(x) = 8G \int d^4x' \ \mathscr{G}_{\text{ret}}(x^\mu - x'^\mu)S_{\mu\nu}(x'). \tag{2.31}$$

Indeed plugging in eq. 2.31 into eq. 2.30,

$$\Box_x h_{\mu\nu} = 8G \int d^4x' \left(\underbrace{(\Box_x\mathscr{G}_{\text{ret}}(x^\mu - x'^\mu)}_{= -2\pi\delta(x^\mu - x'^\mu)})S_{\mu\nu}(x') = -16\pi G S_{\mu\nu}(x). \tag{2.32}$$

One gets the parallel solution to the trace reversed equation eq. 2.17 by swapping S with T and all h with $\bar{h}$.

15

We can perform the $x'^0 = t'$ integration in eq. 2.31, with the Dirac delta function, which sets t' to be the retarded time, $t' = t - |x^\mu - x'^\mu| = t_r$, i.e:

$$h_{\mu\nu}(x) = 8G \int d^3\mathbf{y}\, S_{\mu\nu}(t, \mathbf{y})\, dt'\, \frac{\delta(t' - (t - |\mathbf{x} - \mathbf{y}|))}{2|\mathbf{x} - \mathbf{y}|} \qquad (2.33)$$

$$h_{\mu\nu}(\mathbf{x}, t) = 4G \int d^3\mathbf{y}\, \frac{S_{\mu\nu}(t - |\mathbf{x} - \mathbf{y}|, \mathbf{y})}{|\mathbf{x} - \mathbf{y}|}. \qquad (2.34)$$

We can interpret $h_{\mu\nu}(\mathbf{x}, t)$, as the perturbation obtained by summing up all the radiation from point-sources located at $(\mathbf{x} - \mathbf{y}, t_r)$ on the past light cone. Put differently $h_{\mu\nu}(\mathbf{x}, t)$ is the gravitational radiation produced by the source $S_{\mu\nu}$. Additionally, the form of the time argument of the source tensor, imposed by the definition of the Green's function, shows that the radiation propagates with velocity $= 1 = c$. The solution given by eq. 2.34 satisfies the harmonic coordinate condition of eq. 2.15, since

$$T_{\mu\nu;\mu} = 0 \implies T_{\mu\nu,\mu} + \underbrace{\Gamma\Gamma}_{non-linear} = 0 \implies T_{\mu\nu,\mu} = 0, \qquad (2.35)$$

where we have ingored the non-linear terms encoded in the Levi-Civita connections. Then,

$$S^{\mu\nu}{}_{,\mu} = \partial_\mu \left(T_{\mu\nu} - \frac{\eta^{\mu\nu}}{2} T^\alpha{}_\alpha \right) = -\frac{\eta^{\mu\nu}}{2} T^\alpha{}_{\alpha,\mu}. \qquad (2.36)$$

Also

$$S^\mu{}_\mu = T^\mu{}_\mu - \frac{\delta^\mu_\mu}{2} T^\alpha{}_\alpha = -T^\alpha{}_\alpha. \qquad (2.37)$$

Thus

$$S^{\mu\nu}{}_{,\mu} = \frac{1}{2} S^\alpha{}_{\alpha,\mu} \eta^{\mu\nu}$$
$$S^\mu{}_{\nu,\mu} = \frac{1}{2} S^\alpha{}_{\alpha,\nu}. \qquad (2.38)$$

Then

16

$$
\begin{aligned}
h^{\mu}{}_{\nu,\mu} &= 8G\frac{\partial}{\partial x^{\mu}}\int \mathrm{d}^4 x'\ \mathscr{G}_{\mathrm{ret}}(x^{\mu}-x'^{\mu})S^{\mu}{}_{\nu}(x')\\
&= 8G\int \mathrm{d}^4 x'\ \frac{\partial\mathscr{G}_{\mathrm{ret}}(x^{\mu}-x'^{\mu})}{\partial x^{\mu}}S^{\mu}{}_{\nu}(x')\\
&= -8G\int \mathrm{d}^4 x'\ \frac{\partial\mathscr{G}_{\mathrm{ret}}(x^{\mu}-x'^{\mu})}{\partial x'^{\mu}}S^{\mu}{}_{\nu}(x')\\
&= \underbrace{8G\mathscr{G}_{\mathrm{ret}}(x^{\mu}-x'^{\mu})S^{\mu}{}_{\nu}(x')}_{=0\ \text{at the boundary}} + 8G\int \mathrm{d}^4 x'\ \mathscr{G}_{\mathrm{ret}}(x^{\mu}-x'^{\mu})\frac{\partial S^{\mu}{}_{\nu}(x')}{\partial x'^{\mu}}\\
&= 8G\int \mathrm{d}^4 x'\ \mathscr{G}_{\mathrm{ret}}(x^{\mu}-x'^{\mu})\frac{1}{2}\frac{\partial S^{\alpha}{}_{\alpha}(x')}{\partial x'^{\mu}}\\
&= \quad \dots \quad \text{repeat in reverse}\\
&= \frac{\partial}{\partial x^{\mu}}\left\{8G\int \mathrm{d}^4 x'\ \mathscr{G}_{\mathrm{ret}}(x^{\mu}-x'^{\mu})\frac{1}{2}S^{\alpha}{}_{\alpha}(x')\right\}\\
&= \frac{1}{2}h^{\alpha}{}_{\alpha,\mu}.
\end{aligned}
\tag{2.39}
$$

2.4 Gravitational Wave Sources

Now that we have the general form of the solutions to the linearized Einstein equations, we can proceed to the analysis of sources of GWs. The first step is to analyse the equations in the frequency domain. We will use the following notation:

$$
\mathscr{F}_t\,[\phi]\,(\omega,\mathbf{x}) = \int \mathrm{d}t\,\phi(t,\mathbf{x})\mathrm{e}^{i\omega t}
\tag{2.40}
$$

$$
\mathscr{F}_{\omega}^{-1}\,[\phi]\,(t,\mathbf{x}) = \int \frac{\mathrm{d}\omega}{2\pi}\mathscr{F}_t\,[\phi]\,(\omega,\mathbf{x})\mathrm{e}^{-i\omega t}
\tag{2.41}
$$

Let us look at frequency domain of the soludtion given in eq. 2.34. We have

$$
\begin{aligned}
\mathscr{F}_t\left[h_{\mu\nu}\right](\omega,\mathbf{x}) &= \int \mathrm{d}t\,h_{\mu\nu}(t,\mathbf{x})\mathrm{e}^{i\omega t}\\
&= 4G\int \mathrm{d}^3\mathbf{y}\ \mathrm{d}t\,\frac{S_{\mu\nu}(t-|\mathbf{x}-\mathbf{y}|,\mathbf{y})}{|\mathbf{x}-\mathbf{y}|}\mathrm{e}^{i\omega t}\\
&= 4G\int \mathrm{d}^3\mathbf{y}\ \mathrm{d}t_r\,\frac{S_{\mu\nu}(t_r,\mathbf{y})}{|\mathbf{x}-\mathbf{y}|}\mathrm{e}^{i\omega t_r}\mathrm{e}^{i\omega|\mathbf{x}-\mathbf{y}|}\\
&= 4G\int \mathrm{d}^3\mathbf{y}\,\frac{\mathscr{F}_{t_r}\left[S_{\mu\nu}\right](\omega,\mathbf{y})}{|\mathbf{x}-\mathbf{y}|}\mathrm{e}^{i\omega|\mathbf{x}-\mathbf{y}|}.
\end{aligned}
\tag{2.42}
$$

We can now apply various approximations to this form of the perturbation:

1. Consider a compact source, centered on the origin of our coordinate system. This implies that $S_{\mu\nu}$ is peaked and compactly supported in a region around the origin. We look at the radiation only in the so called *wave zone*, at a distance $r = |\mathbf{x}|$ much larger than the dimensions of the source $R = |\mathbf{y}|_{\mathrm{max}}$.
2. We assume that $r \gg \frac{1}{\omega}$, i.e long wavelengths don't dominate.
3. We assume that $r \gg \omega R^2$, i.e. the ratio of R to the wavelength is not comparable to the ratio of r to R. Using this approximation we can write:

$$
\begin{aligned}
|\mathbf{x} - \mathbf{y}| &= r\left(1 - 2\hat{\mathbf{x}} \cdot \mathbf{y} + \frac{\mathbf{x'}^2}{r^2}\right)^{1/2}, \\
|\mathbf{x} - \mathbf{y}| &\approx r\left(1 - \frac{\hat{\mathbf{x}} \cdot \mathbf{y}}{r}\right) \quad \text{with: } \hat{\mathbf{x}} = \frac{\mathbf{x}}{r}.
\end{aligned}
\tag{2.43}
$$

[9] We just add the condition that $\frac{1}{\omega} \gg R$, that is the source radius is much smaller than the wavelength.

If we additionally further separate the scales in the following way[9]

$$
r \gg [\frac{1}{\omega}, \omega R^2] \gg R,
\tag{2.44}
$$

[10] The approximations all conspire to be able to neglect the $\mathbf{y}$ dependence of $\frac{e^{i\omega|\mathbf{x}-\mathbf{y}|}}{|x-y|}$ in the integral.

Then eq. 2.42 becomes much simpler[10]:

$$
\mathscr{F}_t\left[h_{\mu\nu}\right](\omega, \mathbf{x}) = 4G\frac{e^{i\omega r}}{r} \int \mathrm{d}^3\mathbf{y}\, \mathscr{F}_t\left[S_{\mu\nu}\right](\omega, \mathbf{y}).
\tag{2.45}
$$

Now, let us look at the Fourier transform of the source term. By definition, we have

$$
\mathscr{F}_t\left[S_{\mu\nu}\right](\omega, \mathbf{y}) = \mathscr{F}_t\left[T_{\mu\nu}\right](\omega, \mathbf{y}) + \tfrac{1}{2}\eta_{\mu\nu}\mathscr{F}_t\left[T^\alpha_\alpha\right](\omega, \mathbf{y})
\tag{2.46}
$$

Thus we can study the Fourier transform of $T_{\mu\nu}$, $\mathscr{F}_t\left[T_{\mu\nu}\right]$ instead. Using the conservation equation eq. 2.19 in Fourier t-space, we obtain:

$$
-\mathscr{F}_t\left[T_{i\mu}\right]^{,i} = i\omega\mathscr{F}_t\left[T_{0\mu}\right]
\tag{2.47}
$$

This equation becomes algebraic when we further Fourier transform in $\mathbf{x}$-space:

$$
\hat{T}_{\mu\nu}(k^\alpha) = \hat{T}_{\mu\nu}(\omega, \mathbf{k}) = \int \mathrm{d}^3\mathbf{y}\, \mathscr{F}_t\left[T_{\mu\nu}\right](\omega, \mathbf{y})e^{i\mathbf{k}\cdot\mathbf{y}}
\tag{2.48}
$$

Then the conservation equation becomes:

$$
k^\mu T_{\mu\nu}(\omega, \mathbf{k}) = 0
\tag{2.49}
$$

These four equations relate the time components of $\hat{T}_{\mu\nu}$ to the spatial ones. We now apply eq. 2.47 to itself to obtain:

$$\mathscr{F}_t\left[T_{ij}\right]^{,ij} = -\omega^2 \mathscr{F}_t\left[T_{00}\right] \tag{2.50}$$

which, when multiplied by $x_m x_n$, and integrated over $\mathbf{x}$ gives[11]

$$\int d\mathbf{x}\, \mathscr{F}_t\left[T_{mn}\right](\omega, \mathbf{x}) = -\frac{\omega^2}{2}\int d\mathbf{x}\, x_m x_n \mathscr{F}_t\left[T_{00}\right](\omega, \mathbf{x}). \tag{2.53}$$

Notice that the integral on the RHS is in fact the Fourier transform of the quadrupole moment tensor of the energy denisty:

$$I_{mn} = \int x_m x_n T_{00}(t, \mathbf{x})\, d^3x. \tag{2.54}$$

We call its Fourier transform $\hat{I}_{mn}(\omega)$ and we can finally rewrite eq. 2.45 as:

$$\mathscr{F}_t\left[h_{\mu\nu}\right](\omega, \mathbf{x}) = -2G\omega^2 \frac{e^{i\omega r}}{r}(\hat{I}_{mn}(\omega) + \tfrac{1}{2}\eta_{\mu\nu}\hat{I}^n{}_n(\omega)) \tag{2.55}$$

Going back t-space we have:

$$\begin{aligned}
h_{\mu\nu}(t, \mathbf{x}) &= -\frac{G}{\pi r}\int d\omega\, e^{-i\omega(t-r)}\omega^2(\hat{I}_{mn}(\omega) + \tfrac{1}{2}\eta_{\mu\nu}\hat{I}^n{}_n(\omega)) \\
&= \frac{G}{\pi r}\frac{d^2}{dt^2}\int d\omega\, e^{-i\omega(t_r)}(\hat{I}_{mn}(\omega) + \tfrac{1}{2}\eta_{\mu\nu}\hat{I}^n{}_n(\omega)) \\
&= \frac{2G}{r}\frac{d^2}{dt^2}(I_{mn}(t_r) + \tfrac{1}{2}\eta_{\mu\nu}I^n{}_n(t_r))
\end{aligned} \tag{2.56}$$

This equation has a nice physical interpretation. The gravitational wave produced by a non-relativistic source is proportional to the second derivative of the quadrupole moment of the energy density at the time t_r where the past light cone of the observer intersects the source. The nature of gravitational radiation is in stark contrast to the leading electromagnetic contribution which is due the change in the *dipole* moment of the charge density. The change of the dipole moment can be attributed to the change in center of charge (for Electromagnetism (EM)), or mass (for GR). While a center of charge is free to move around, the center of mass (of an isolated source) is fixed by the conservation of momentum, so the dipole moment is zero.

The quadrupole moment, on the other hand, is sensitive to the shape of the source, which a gravitational system can modify. We observe that the quadrupole radiation is subleading when compared to dipole radiation. Thus on top of the much smaller coupling constant, gravitational radiation is also weakened by this fact, and thus is usually orders of magnitude weaker than electromagnetic radiation.

[11] Two integrations by parts cancel the $x_m x_n$ term in the LHS and since boundary terms are 0 (the source is finite) we have

$$\int dx\, x_m x_n \mathscr{F}_t\left[T_{ij}\right]^{,ij} = \int dx\, x_m x_n{}^{,ij}\mathscr{F}_t\left[T_{ij}\right] \tag{2.51}$$

The hessian of $x_m x_n$ is $(\delta^i_m + \delta^i_n)(\delta^j_n + \delta^j_m)$, but since $T_{\mu\nu}$ is symmetric the integral is

$$\int d\mathbf{y}\, 2\mathscr{F}_t\left[T_{mn}\right](\omega, \mathbf{y}) \tag{2.52}$$

In summary, any object that is modifying its shape is a source of GWs. All orbiting systems therefore are sources of GWs . However as outlined above, only significant 'changes in shape' have a chance to be detectable. We will now explore these phenomena.

2.4.1 Compact binaries

How could one construct a very powerful source of GWs ? An example would be that of two highly-massive bodies (such that T_{00} is large) that orbit each other. Furthermore in order for the GWs emitted by the system to be detectable they must orbit close enough to each other that their quadrupole moment is large. For these very massive objects to be close enough for a small orbit, they have to be very compact. Assuming that is the case, a funny thing happens, as these objects orbit each other, they emit GWs , and in doing so they lose energy[12]. Thus they slow down, and their orbit shrinks. This continues until the orbit is so small that the objects merge into a single object. Of course this is a significant change of shape and thus we have a constructed (if not all on purpose) a very powerful source of GWs . Such objects are called compact binaries.

To Leading Order (LO) in G the motion of the binary is described by a newtonian circular orbit. In baricentric coordinates, such a system is in fact equivalent to effective one body [13] of reduced mass $\mu = \frac{m_1 m_2}{M}$ orbiting in a gravitational potential of mass $M = m_1 + m_2$, at a distance R equal to the distance between the two bodies forming the binary. The orbit is characterized by a balancing act between the gravitational attraction due to the potential and the centripetal force due to the motion of the reduced mass:[14]

$$\frac{GM\mu}{(R)^2} = \frac{\mu u^2}{R},$$

(2.57)

where u is the norm of tangential velocity, and R is the distance between the two objects. eq. 2.57 gives us the the norm of the velocity

$$u = \sqrt{\frac{GM}{R}}.$$

(2.58)

Thus the orbital period is simply, in the case of

$$T = \frac{2\pi R}{u} = 2\pi \sqrt{\frac{R^3}{GM}}.$$

(2.59)

This also gives us angular frequency:

$$\Omega = \frac{2\pi}{T} = \sqrt{\frac{GM}{R^3}}.$$

(2.60)

[12] Of course this happens in every orbiting system just on a time scale that is neglible. Only systems which are massive enough to produce large amounts of radiation actually lose enough energy for it to matter.

[13] This choice of wording is not a coincidence as we shall see

[14] Or equivalently between conserved angular momentum and the derivative of the potential energy.

Thus the EOM $\mathbf{r}(t)$ of the reduced mass is described by a circular orbit in the $x - y$ plane i.e.:

$$\mathbf{r}_{xy}(t) = \begin{pmatrix} R\cos(\Omega t) \\ R\sin(\Omega t) \end{pmatrix}. \tag{2.61}$$

We have not written the third z component of the trajectory as that can be set to zero, for a well chosen set of inertial coordinates. The corresponding trajectory for both masses is simply given by applying the following scaling:

$$\mu\mathbf{r}(t) = m_1\mathbf{r}_1(t) = m_2\mathbf{r}_2(t). \tag{2.62}$$

We can straightforwardly obtain the 00 component of the energy momentum tensor of the system[15] by using the EOM of the reduced mass (eq. 2.61):

$$T_{00}(t, \mathbf{x}) = \mu\delta(x_3)\delta(x_1 - R\cos(\Omega t))\delta(x_2 - R\sin(\Omega t)), \tag{2.63}$$

which when plugged into eq. 2.54, gives us the quadrupole moment of the rotating system:

$$\begin{aligned} I_{11} &= \mu R^2\cos^2(\Omega t) = \mu R^2(1 + \cos(2\Omega t)) \\ I_{22} &= \mu R^2\sin^2(\Omega t) = \mu R^2(1 - \cos(2\Omega t)) \\ I_{12} = I_{21} &= 2\mu R^2(\cos\Omega t)(\sin\Omega t) = \mu R^2\sin(2\Omega t) \\ I_{i3} &= 0. \end{aligned} \tag{2.64}$$

Thus we have roughly:

$$I \sim \mu R^2\cos(2\Omega t) \sim \mu R^2 \sim \mu\left(\frac{GM}{\Omega^2}\right)^{\frac{2}{3}} = \frac{Gm_1m_2}{(m_1 + m_2)^{\frac{1}{3}}}\Omega^{-\frac{4}{3}}, \tag{2.65}$$

where we have expanded in small R in the second relation. The metric perturbation is then given by eq. 2.56 and has norm proportional to:

$$qh \propto \frac{\ddot{I}}{r} \propto \frac{1}{r}\frac{Gm_1m_2}{(m_1 + m_2)^{\frac{1}{3}}}\Omega^{\frac{2}{3}}. \tag{2.66}$$

2.4.2 BH Binaries

Taking the process described above to the limit of more massive and more compact objects one could imagine asking for the most dense objects possible to orbit each other. In GR this object is called a black hole (BH). It is a possible solution to the full fat EFE (eq. 2.1), in a static and isotropic universe, with point like mass at its center. Then the solutions to the equations eq. 2.1 have a unique form [18], called the Schwarzschild solution.

The solution is given by, in spherical coordinates:

$$\mathrm{d}\tau^2 = \left[1 - \frac{R_S}{r}\right] \mathrm{d}t^2 - \frac{\mathrm{d}r^2}{1 - \frac{R_S}{r}} - r^2 \left(\mathrm{d}\theta^2 + \sin^2\theta\,\mathrm{d}\varphi^2\right) \qquad (2.67)$$

where R_S is the Schwarzschild radius, given by:[16]

$$R_S = \frac{2GM}{c^2}. \qquad (2.68)$$

For stellar masses we have $R_S = 2954$ m, quite a lot smaller than the radius of the sun $\sim 7 \cdot 10^8$ m. Note that the metric given in eq. 2.67 exhibits singularities at both $r = R_S$ and $r = 0$. The former is spurious, as it is an artefact of the coordinate choice, while the latter is real, in the sense that coordinate independent scalars formed from the metric (such as the ricci scalar) do in fact blow up as $r \to 0$. This encodes the non-spurious mass singularity that gives rise to the BH phenomena .

If we consider a comparable stellar mass BBH system, we can use the calculations of the previous section to compute the order of magnitude of the perturbation. eq. 2.60 in terms of the Schwarzschild radius gives us the orbital frequency

$$f = \frac{\Omega}{2\pi} = \frac{c}{2\pi}\sqrt{\frac{R_S}{R^3}}, \qquad (2.69)$$

and the metric perturbation is given by eq. 2.66:

$$h = \frac{R_S^2}{rR}. \qquad (2.70)$$

Thus, if we consider BHs separated by ten times their Schwarzschild radius, observed at cosmological distances ~ 100 Mpc, we obtain the values for the scales characterising the binary system:

$$\begin{aligned} R_S &\approx 10^3 \text{ m}, \\ R &\approx 10^4 \text{ m}, \\ r &\approx 10^{23} \text{ m}. \end{aligned} \qquad (2.71)$$

[16] we reinstate the speed of light, as we want to compute orders of magnitudes

Such a system would have an orbital frequency of:

$$f \approx 10^2 \text{ Hz,} \tag{2.72}$$

and would perturb the metric on earth by:

$$h \approx 10^{-21}. \tag{2.73}$$

To have any hope of detecting such systems, one would need to have detectors sensitive to frequency spectra up to hundreds of Hertz, with a strain sensitivity of 10^{-21}. This has been achieved at LIGO and other detectors, and has enabled the detection of such systems.

Non-spinning black holes orbiting around each other are the simplest binary system to model. However, they are extremely unlikely to occur in nature (realistic physical scenarios). The nature of BH formation implies that they necessarily also spin. Spinning black holes, also refered to as Kerr black holes, are characterized by a different metric tensor defining the spacetime surrounding them. The modelling of spinning black holes is still in its infancy and will not be treated it here.

There are many other binary systems that could feasably be detected. Finite-size binaries such as Neutron Stars (NSs) result in tidal phenomena that are not present in the BH case. Also non-binary sytems, such as Cosmic strings, corresponding to early universe topological defects, could produce a detectable stochasitc GW backround.

3 Gravitational Wave Detection

Gravitational waves were first theorized by Einstein, accompanying his theory of general relativity. However, at the time it was not even clear whether they were an artifact of the theory or an observable phenomenon. Of course, as we have seen, GWs are predicted to be extremely weak, and thus there was initially little hope of ever detecting them. As evidence mounted that GR was indeed an incredibly accurate theory of gravity, the interest in GW detection grew. The first detectors, resonant antennas, failed in successfully detecting GWs, as they were simply not sensitive enough. The more modern laser based detectors were the finally able to claim detection, by being extremely sensitive (the modern measurement precision at LIGO is equivalent to measuring the distance to Alpha Centauri 4.367 light-years, to the width of a human hair ~ 40 μm). The first detection was made in 2015 [1], marking the beginning of a new era in astronomy, and maybe even physics itself.

3.1 Laser interferometers

Laser-interferometer-based GW detectors are essentially scaled-up versions of the Michelson interferometer. The device splits a beam of colimated coherent photons (laser) into two, letting them propagate along two axes in an L configuration, before being reflected back to the beam splitter. The two beams, when recombined, interfere with each other, constructively or destructively, depending on the nature of the medium they have traveled through and the length of each arm.

For a gravitational wave to produce a measurable effect on such an apparatus, all the optical equipment should be free to move and be isolated from external vibrations. This is achieved by hanging the mirror on precisely-tuned penduli. When the gravitational wave propagates through the apparatus, it induces a relative movement between the masses, changing the difference $L_x - L_y$ in length of the detectors arms, by an amount ΔL. This effect is exacerbated as the length of the arms $L_x \sim L_y \sim L$ is increased. It follows that the strain is the normalized difference:

$$\frac{\Delta L}{L} = \left[(1/2)\left(1 + \cos^2(\theta)\right)\cos(2\phi)\right]h_+ + [\cos(\theta)\sin(2\phi)]h_\times \equiv h, \quad (3.1)$$

where θ and ϕ are the polar and azimuthal angles of the direction of propagation of the GW . The strain is decomposed into components, h_+ and $h_\times$, which are the plus and cross polarisations of the wave. The strain sensitivity can be further increased by bouncing the light back and forth multiple times along the arms of the interferometer. In current implementations this is achieved using fabry - perot cavities spanning the whole length of the arms.

3.1.1 LIGO and ground based observatories

LIGO implements the measurement apparatus described in the past section. It consists of two detectors, both in the USA, one in Livingston Louisiana and one in Hanford Washington, a separation of 3000 km. Each LIGO detector has two 4 km long arms made up of 1.2 m-wide vacuum tubes, each operating as Fabry-Perot cavities. The light from an effective 750 kW laser bounces back and forth inside these arms around 300 times. Thus, the effective arm length becomes 1200 km, drastically improving sensitivity.

While LIGO was the first to provide detection data, it does not live in a vacuum. In fact for the first published detection, the data analysis teams from LIGO joined forces with those for Virgo, the European gravitational wave detector. The Virgo detector is located in Cascina, Italy, and is similar to LIGO . It has 3 km long arms and a different suspention system. It joined data collection with LIGO in the second observing run in 2017. Finally there are two other detectors that are now part of the collaboration, KAGRA in Japan and GEO600 in Germany. KAGRA is a similar detector to Virgo in scale, but is built underground further isolating it from seismic activity .GEO600 is a smaller detector, with 600 m long arms, built with the objective of being a test bed for future detectors.

Although they exhibit impressive sensitivity, ground based detectors are limited, since they are subject to seismic activity, which can cause vibrations that limits the lower bound of the frequency sensitivity of the detectors. The optics and other higher frequency noise imposes an upper bound to the frequency. In particular ground based detectors are only sensitive to frequencies in the following rough range:

$$[10^0, 10^4] \text{ Hz.} \tag{3.2}$$

In turn this implies that they are sensitive to the comparable, stellar mass [17] compact binaries, which are currently believed to be the most common type of binary systems in the universe. Of course this is not an accident, as these detectors were purpose built for providing evidence of GW in general. In fact, they have been quite successful in this regard, with upwards of 90 detections of GW to date.

[17] and a bit bigger $\sim 1 - 10^3 M_\odot$

Figure 3.1 shows the current library of compact binary systems detected by LIGO -Virg-Kagra, along with those detected through non-GW means.

Fig 3.1: Mass distribution of Detected GW emiting binaries. Credit: Visualization: LIGO-Virgo-KAGRA / Aaron Geller / Northwestern
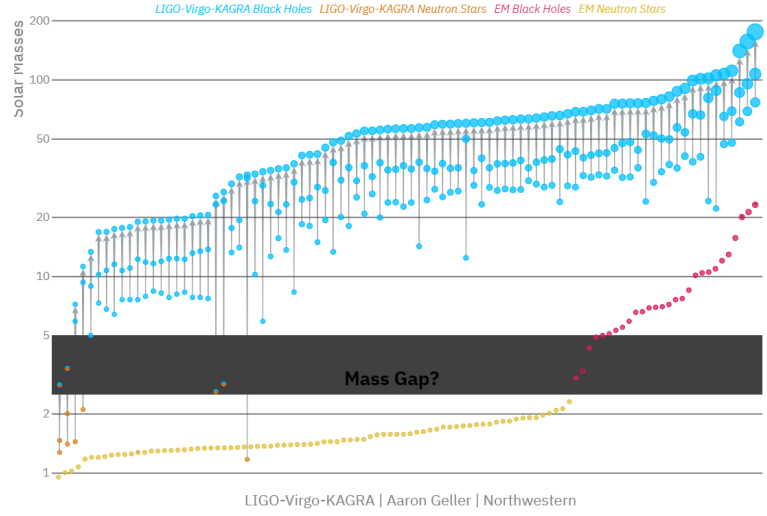
The highlighted band denotes the assumed mass gap that should exist between the neutron star and black hole mass distributions. Note that most of the detections are compatible with the presence of such a gap. However, there are a few detections that are not, and these are particularly interesting. These are binaries with masses too light to be black holes, but too heavy to be neutron stars. A lot of research is ongoing to try and understand what these objects are, and if they are not just measurement artefacts.

3.1.2 LISA

There are many planned next generation GW detectors, from the Einstein telescope to Cosmic explorer. The most interesting one however is LISA, the first genuine space based GW observatory. It is a joint project between ESA and NASA, and is scheduled to launch in 2037. It will consist of three satellites, in triangular formation, at a distance of 2.5 million kilometers of each other. Each of the three LISA spacecraft contains a test mass free-falling within its body. Each spacecraft then measures the distance to its neighboring test mass thus forming a space based laser interferometer.

There are a few key differences with ground based detectors. The first is the size of the arms means it will be sensitive to frequency ranges such as:

$$[10^{-4}, 10^{0}] \text{ Hz.} \tag{3.3}$$

This means that it will be sensitive to the most massive binaries in the universe, supermassive black holes, such as those found at the centers

of galaxies.

The second is that it will be completely isolated from seismic activity, and thus has a much lower noise floor. This combined with the arm length means that LISA is also predicted to be able to observe Extreme Mass Ratio Inspirals (EMRIs), where stellar compact objects ($< 60 M_\odot$) orbit around a massive black hole of around $10^5 M_\odot$ or more. In this configuration the small mass is in a slowly decaying orbit, and thus can spend around 10^5 orbits and between a few months and a few years in the LISA sensitivity band before merging. This will provide us with a very interesting new source of GW , that also allows us to test new approximations, such as those based on mass ratio expansions: Gravitational Self-Force (GSF) .

3.2 Matched filtering

The signals measured by the laser interferometers such as LIGO , provide a measurement of strain over time. This waveform essentially measures the deformation of spacetime when a GW passes through a detector. While some GW signals observed in laser interferometers are clearly identified as such, mainly due to their extraordinary power output, weaker signals are harder to identify. In fact, most of the detections have happened under the noise floor of the detectors. How is this possible? Matched filtering and waveform generation.

Consider some detector output signal s consisting of noise n and a possible true GW signal h_i (or signals, making up a family $\{h_i\}$). The nature of the noise is unpredictable and necessarily probabilistic in nature. We can, however, model the noise as a random variable n that follows a probability distribution P_n dependent on variables that we consider and have measured to be significantly impactful.

In such a probabilistic setup one could try to find the probability that the signal $h_i \in \{h_i\}$ has been detected, conditional on the actual data s. This however is impractical as it requires *a priori* knowledge on the family of possible signals, information that is inaccessible. Instead, we devise a functional $\mathscr{F}[s, h_i]$, (a statistic) dependent on both the data and the supposedly present GW signal. We can then choose a threshold ρ^* above which we claim detection of the signal h_i, i.e. if $\mathscr{F}[s, h_i] > \rho^*$.

The functional that is used is defined in terms of the symmetric inner product $\langle s, h_i \rangle$, that correlates the data s with the template h_i, weighting by detector frequency sensitivity $S_n(f)$:

$$\langle g, h \rangle = 2 \int_{-\infty}^{\infty} \frac{\hat{g}^*(f)\hat{h}(f)}{S_n(|f|)} \, df = 4 \Re \int_0^{\infty} \frac{\hat{g}^*(f)\hat{h}(f)}{S_n(f)} \, df, \qquad (3.4)$$

where $\hat{g}^*$ is the conjugate of the frequency Fourier transform of g. $S_n(f)$ is the *noise power spectral density*, characterising the detector sensitivity defined by:

$$\overline{\hat{n}^*(f_1)\hat{n}(f_2)} = \tfrac{1}{2}\delta(f_1 - f_2)S_n(f_1)\Theta(f_1), \qquad (3.5)$$

where the bar denotes the average over the noise realisation, $\delta(f_1 - f_2)$ is the Dirac delta function, and $\Theta(f_1)$ is the Heaviside step function. We can now define the *signal to noise ratio* for the signal when filtered by h_i as [18]

$$\rho(s, h_i) = \frac{\langle s, h_i \rangle}{\mathrm{rms}\langle n, h_i \rangle} = \frac{\langle s, h_i \rangle}{\sqrt{\langle h_i, h_i \rangle}}. \qquad (3.6)$$

[18] The equality is due to the fact that we average over all realisations of noise, which averrages to uniform: $\overline{\langle h_i, n \rangle \langle n, h_i \rangle} = \langle h_i, h_i \rangle$.

where rms denotes the root mean square. This is the functional $\mathscr{F}[s, h_i]$ we are after and we claim detection if $\rho(h_i) > \rho^*$. The functional $\mathscr{F}[s, h_i] = \rho(s, h_i)$, provided that the noise is normally distributed, is provably the optimal filtering technique, in the sense that it minimises the probability of false positives. For example, if we have a fully gaussian noisy signal $s = n$ then ρ is a normal variable with zero mean and unit variance. If a signal h_i is present, over some again gaussian noise n, then it can be proven that ρ is still normal but centered on $\sqrt{\langle h_i, h_i \rangle}$ with unit variance.

The threshold can be set to correspond to a desired false positive rate $\mathscr{F}$:[19]

[19] The complementary error function is given by $\mathrm{erfc}(z) = \frac{2}{\sqrt{\pi}} \int_z^\infty \mathrm{e}^{-t^2}\, \mathrm{d}t = 1 - \mathrm{erf}(z)$.

$$\mathscr{F} = \sqrt{\frac{1}{2\pi}} \int_{\rho^*}^\infty \mathrm{e}^{-\frac{1}{2}\rho^2}\, \mathrm{d}\rho = \tfrac{1}{2}\,\mathrm{erfc}(\frac{\rho^*}{\sqrt{2}}), \qquad (3.7)$$

or correct detection rate $\mathscr{D}$:

$$\mathscr{D} = \frac{1}{2}\,\mathrm{erfc}\left[\frac{\rho^* - \sqrt{\langle h_i, h_i \rangle}}{\sqrt{2}}\right]. \qquad (3.8)$$

Given a signal and a template, we have described a procedure to determine if the signal is present or not. The physical output of a detection is therefore bounded from above by the physics content of the template. The matched filtering approach is contingent on having a waveform that corresponds to the physical process that is emitting the signal. Usually, these processes can be parametrized by a set of parameter. In the case of a compact binary these parameters are for example, the mass ratio of the binary, the orbit eccentricity, the possible spin etc. The filter waveform must then naturally depend on these parameters, be it heuristically or physically (i.e., from first principles).

3.3 PTA

A PTA consists of an array of several pulsars whose pulse periods (or Time of Arrival (ToA)) are monitored with very high precision by one or more radio telescopes. Pulsars, from **pulsa**ting **r**adio source, are though to be highly magnetized rotating neutron stars. These neutron stars emit strong electromagnetic radiation from their magnetic poles, which when not aligned with rotational poles, emit in the manner of a lighthouse. The measured pulses are extremely regular in nature, with periods ranging from a few milliseconds to a few seconds. Over a year, the variation in the pulse period is on the order of a few microseconds [19]. We can therefor use pulsars as clocks, and infer their variation from their normal cycle time.

GWs propagating between the pulsar and the observer act as anisotropic media. This will cause the pulse to be delayed or sped up, depending on the relative direction of the wave, its polarisation axes and the direction of the pulsar. Given a collection of such pulsars with precisely known periods, evenly distributed in the celestial sphere, then one can use the relative delay of the pulses to measure the direction and nature of the wave. This setup is essentially a blown up version of LIGO with light-year scale arms instead of kilometer scale arms.

Currently, the set of pulsars suitable for this type of measurement is around 40 [20]. Many more pulsars have been measured but not all are suitably regular to be used in PTAs . The frequency range of sensitivity of PTAs has a lower bound set by observation duration and higher bound set by cadence of measurement. Currently, the IPTA [21] has been measuring for 13 years, with measurements being taken every week yielding a sensitivity in a drastically different band than that of LIGO and LISA :

$$[10^{-9}, 10^{-7}]\text{Hz}. \tag{3.9}$$

The nature of sources that can be detected by PTAs is therefore different from that of LIGO and LISA . The PTA sensitivity is more suited to detect stochastic gravitational waves, such as those emitted by early-universe phenomena, or by supermassive black holes ($10^6 - 10^9 M_\odot$) in the centers of galaxies[20].

[20] more massive objects have longer orbital periods

4 Waveform Generation

The matched filtering approach introduced in the previous section motivates the developement of tools for generating waveforms. Specifically, the matched filtering technique is especially sensitive to the phase of the GW , necessitating precise determination of the waveform template's phase. These templates can be varied in physical content, but also in practicality. In all cases they need to be able to cover the set of parameters (the parameter space) that one is interested in exploring. Clearly, if the waveform has been generated purely heuristically, then the physical content of the detection is close to zero. One can only say one has detected a phenomenon that produces this waveform, but not much more. However, if the input parameters are physically meaningful, e.g. the mass ratio of a binary compact inspiraling system, then the waveform constructed purely from this input, if matched to the signal, tells us that a compact binary inspiraling system with this mass ratio has been detected. This is called parameter estimation, and is key to maximizing the physics output of a detection.

Crucially the waveform generation must be able to cover the whole parameter space (for example all feasible mass ratios) to be useful, as one does *not* know in advance the parameters describing the system being observed. Ideally waveform generation should be done in a way that is computationally efficient, as the number of parameters as well as their range to explore is large. Currently, waveform generation is performed in a hybrid way: some waveforms for specific parameter space points, are generated from first principles, while the rest of the parameter space waveforms are interpolated.

In this chapter we will look at the first-principles waveform generation tools currently being developed. More specifically we are going to explore techniques for compact binary waveforms. In this context waveforms may describe inspiralling or scattering binaries. Currently, only the inspiralling binaries have been detected, as these are the systems whose signal LIGO and other detectors are most sensitive to (see Section 3.1.1), other than being by far the most common emitters of high-intensity GWs. As discussed in Section 2.4.1, orbiting and GW emitting compact objects will necessarily inspiral and merge at some point.

For such inspiraling binaries, the waveform features 3 distinct phases: a first *inspiral phase*, a *merger phase* where a remnant compact body is produced as a result of the coalescence of the two objects, and a postmerger, or *ringdown phase*, where the remnant still emits gravitational radiation

while settling to its new stable configuration. Each phase is characterized by different dynamical properties of the orbiting bodies and thus different frameworks are aimed at describing the corresponding features of the waveforms. Even the description of one phase involves different regimes, and thus more specific framework, additionally dependent on the type/initial state of the two orbiting bodies.

For scattering binaries there is hope of detecting them as argued in [22], but they are mainly used as a test-bed for new theories making use of particle physics knowledge. Additionally, one might be able to extend their validity to inspiraling binaries [see 23].

Most of these techniques have two important parts. The first consists in the precise modelling of the evolution of the emitting system. In most cases, this boils down to obtaining the EOMs for the interacting bodies. For scattering, this can just be the amplitude of the event. The second part is extracting the variation of the metric due to the source movement at the measurement point, far away from the source, i.e., the waveform. Of course, the metric at the source is tightly coupled to the dynamics of the system, and thus the approximations conducted at the source also effects the way one extracts the waveform.

The only full, first-principles waveform techniques are NR and EOB [21]. NR is quite unique when compared to other methods. Let us look at it before proceeding to EOB and all the inspiral waveform techniques.

[21] There are a whole family of phenomenological frameworks that we will not discuss
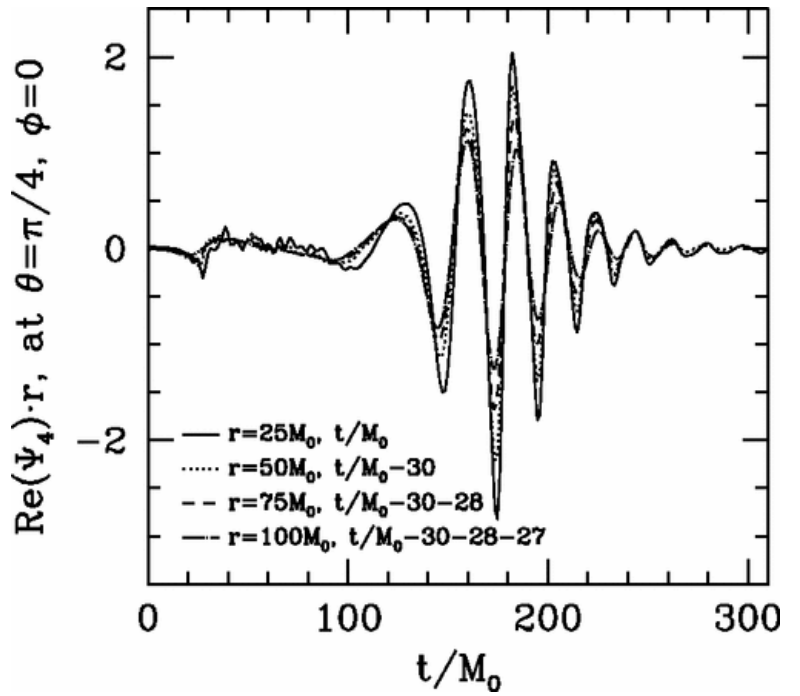
4.1 NR

The most precise, first-principles waveform-generation technique to date is numerical relativity (NR). It was developed as early as the 1960s [24]. Initially and until relatively recently, these numerical methods were unusable because of numerical instabilities. The idea, however, is simple: the EFE are a system of coupled partial differential equations (PDEs) (albeit nonlinear) that can be solved numerically by discretizing the metric. The causes of instability is three-fold. First, the aforementioned non-linearities make the discretization particularly sensitive to extreme variations, such as those close to a BH, which means that one needs a fine mesh to control error buildup. Second, the gauge freedom establishes limits on the type of discretization procedures, so that spurious modes are not introduced. Third, for BHs one needs to consider what to do about the physical metric singularity, as infinity is not a number one can plug into a computer! On top of stability problems, when compact binary objects are considered, the scales involved further complicate things, as one needs enough resolution to resolve the objects, and the deformations on the metric, as well as a large enough volume to have reasonable orbits. This requires a huge amount of lattice nodes, meaning such simulations (even if stable) are extremely computationally expensive.

In 2005 [Pretorious 25] and a little later [Campanelli et al. 26] made a breakthrough advance and were able to fully compute an inspiral-merger-ringdown sequence for a BBH . Pretorius made use of two techniques: Adaptive Mesh Refinement (AMR) and the Generalized Harmonic (GH) formalism. AMR , like its name suggests, is a technique based on a dynamical discretization procedure . The GH formalism, tackles the singularity problem validating the excision of the black hole, and crucially letting that region move. The combination of the procedures, were able to finally slay the proverbial numerical dragon.

These waveforms, such as the one in Figure 4.1, confirmed the predictions made in [Buonanno and Damour 27] that the merger phase of a BBH would not be as complicated as previously thought. As numerical techniques evolved further, they were able to elucidate more and more complex behaviors.

Fig 4.1: The first NR waveform, as presented in [25]

Nowadays, it is the gold standard of waveform generation. Of course it remains increadibly computationally expensive [22] and making any sizable bank of purely NR waveforms is seen as a fools endeavor. To date, only a couple hundred parameter space points have been simulated. NR is used to complement, calibrate and extend the other waveform generation techniques. For example to detect the first signals LIGO and other detectors interpolated between NR-generated parameter space points to reach the ones needed for detection. However, with the advent of LISA on the horizon, a further problem will arise. NR results by nature only take into account the last few orbit cycles before merger. Any more than that and computational time becomes prohibitive. LISA, with its low noise floor, should be able to detect inspiraling but not yet merging

[22] A single waveform with 10 orbits can take a week and tens of thousands of CPU hours

binaries. Doing so will require waveform templates with hundreds of orbits, well out of reach of any modern NR package. Nonetheless, this technique has shown and will continue to show its worth, as no approximations other than discretization are made. The physical content of such waveforms is thus high.

4.2 Inspiral methods

Before continuing to the EOB method, let us look at the techniques that focus on the inspiral part of the waveform. There are broadly speaking three methods that fall in this category. The first we have already encountered at 1st order: PN . It is a perturbative expansion in both relative velocity (slow moving limit) and the coupling constant G (weak field limit) of the EFE . The second is the PM method, which is a perturbative expansion in *only* the coupling constant G. At face value the PM method contains the PN one as a special case, however as at zeroth order, the PM approximation captures straight line motion, and is generally more expressive of scattering. The final approximation can be applied when the mass ratio of the object in question is large. Here one can expand around a fixed but *non-flat* metric, essentially considering one of the objects as a test-particle evolving on a background caused by the heavier object. This is called the GSF formalism.

4.2.1 PN

The PN expansion, is a perturbative expansion of EFE in the orbital regime, which at LO reproduces Newtonian gravity. Consider a system of orbiting bodies with typical values $\bar{M}, \bar{R}, \bar{v}$ for masses, separations, and velocities. Then, the viral theorem states:

$$\langle T \rangle_\tau = -\frac{1}{2}\langle U \rangle \implies \bar{M}\bar{v}^2 \sim \frac{G\bar{M}^2}{\bar{R}} \tag{4.1}$$

thus we can consider the following equivalent small parameters:

$$\bar{v}^2 \sim \frac{G\bar{M}}{\bar{R}} \tag{4.2}$$

We therefore expand in both velocities and coupling constant. This can be achieved either by a classical (albeit quite complicated) perturbative treatment [see 28,29], or a more contemporary EFT-based approach coyly called NRGR [4,30], itself inspired by Non-Relativistic Quantum Chromodynamics (NRQCD) . We call nPM the expansion carried out to $\mathcal{O}(v^{2n})$.

Regardless of method, there are a few shortcomings with this expansion. While it is well suited to describe the *motion* of objects in an orbital

regime, it is not equally effective at describing gravitational radiation far from the source, as it exhibits divergences for $r \to \infty$[23]. This means that in the GW context, the PN expansion is in fact usually coupled to a weak-field approximation (see below), outside of the near zone. This is the region surrounding the source, that is of small extent compared to the wavelength of the emitted radiation:

$$r \ll \lambda \tag{4.3}$$

The PN expansion can also be viewed as an expansion in small 'retardations'. To see this, consider a slowly moving source, such that the time derivatives of the metric generated by this source will be smaller than the spatial derivatives by a factor $\mathcal{O}(v)$,

$$\frac{\partial}{\partial t} = \mathcal{O}(v) \frac{\partial}{\partial x^i}, \tag{4.4}$$

or $\partial_0 = \mathcal{O}(\epsilon)) \partial_i$. Thus the d'Alembertian operator, applied to the metric is, to lowest order, a Laplacian operator

$$-\frac{1}{c^2} \frac{\partial^2}{\partial t^2} + \nabla^2 = \left[1 + O\left(\epsilon^2\right)\right] \nabla^2. \tag{4.5}$$

This means that retardation effects, due to the time derivative, are small corrections. In the PN expansion we are consequently trying to compute some quantity $F(t - r)$, such as a component of the metric, which is intrinsically a function of the retarded time $t_r = t - r$, from its expansion for small retardation r,

$$F(t_r) = F(t) - r\dot{F}(t) + \frac{r^2}{2}\ddot{F}(t) + \dots \tag{4.6}$$

Importantly, the derivatives should bring down factors proportional to frequency Ω of the emitted radiation. Thus this is in fact an expansion in $r\Omega \sim r/\lambda$, which is only valid in the near zone as defined by eq. 4.3, and breaks down outside of this zone, in the so called *radiation zone*. A serious consequence of this fact is that the pure, naive PN expansion is unable to account for outgoing or incoming radiation, and thus unable to describe isolated systems. This is where the PM expansion comes in.

4.2.2 PM

The PM expansion is a weak field expansion of EFE, in the coupling constant G. It thus covers all orders in velocity of the PN expansion, at any fixed G order. We usually call nPM the corresponding $\mathcal{O}(G^n)$-truncated expansion. Historically, it was derived with the objective of being the radiation zone partner to the PN expansion, as it provides a description of the propagation of the waves up to the observer. When used with the PN expansion in such a way, the PM expansion is used to

solve the vacuum EFE . It is usually set up to compute a version of the metric perturbation that is exact:[24]

$$\mathsf{h}_{\mu\nu} = \sqrt{-g}g^{\mu\nu} - \eta^{\mu\nu}. \qquad (4.7)$$

The PM expansion is then given as

$$\sqrt{-g}g^{\mu\nu} = \eta^{\mu\nu} + G\mathsf{h}_1{}^{\mu\nu} + G^2\mathsf{h}_2{}^{\mu\nu} + ..., \qquad (4.8)$$

meaning that:

$$\mathsf{h}^{\mu\nu} = \sum_{n=1}^{\infty} G^n \mathsf{h}_n{}^{\mu\nu}. \qquad (4.9)$$

The EFE for this metric perturbation, when imposing De-Donder gauge conditions (eq. 2.16), is given by

$$\Box_{SR}\mathsf{h}^{\mu\nu} = -16\pi G\mathsf{h}^{\mu\nu}\tau^{\mu\nu}. \qquad (4.10)$$

where $\tau^{\mu\nu}$ is the effective energy momentum tensor given by:

$$\tau^{\mu\nu} = (-g)T^{\mu\nu} - \frac{1}{16\pi G}\Lambda^{\mu\nu}. \qquad (4.11)$$

$\Lambda^{\mu\nu}$ contains all non-linear terms of the Einstein tensor, and its definition can be obtained by comparing with eq. 2.1. Thus, it depends on the metric and thus on $\mathsf{h}_{\mu\nu}$ in a highly non-linearly fashion . We can write it as:

$$\Lambda^{\mu\nu} = L^{\mu\nu}[\mathsf{h}, \mathsf{h}] + M^{\mu\nu}[\mathsf{h}, \mathsf{h}, \mathsf{h}] + N^{\mu\nu}[\mathsf{h}, \mathsf{h}, \mathsf{h}, \mathsf{h}] + \mathcal{O}(\mathsf{h}^5). \qquad (4.12)$$

Here the number of h's in the argument of L, M and N indicates the order of the non-linear term. In a vaccuum eq. 4.10 reduces to

$$\Box_{SR}\mathsf{h}^{\mu\nu} = \Lambda^{\mu\nu}, \qquad (4.13)$$

which we can solve iteratively order by order:

$$\begin{aligned}
\Box_{SR}\mathsf{h}_1{}^{\mu\nu} &= 0, \\
\Box_{SR}\mathsf{h}_2{}^{\mu\nu} &= L^{\mu\nu}[\mathsf{h}_1, \mathsf{h}_1], \\
\Box_{SR}\mathsf{h}_3{}^{\mu\nu} &= M^{\mu\nu}[\mathsf{h}_1, \mathsf{h}_1, \mathsf{h}_1] + L^{\mu\nu}[\mathsf{h}_1, \mathsf{h}_2] + +L^{\mu\nu}[\mathsf{h}_2, \mathsf{h}_1]
\end{aligned} \qquad (4.14)$$

This method can be supplemented by a multipolar expansion of the $\mathsf{h}_n{}^{\mu\nu}$, truncated to the specific PM order we are interested in. This combined expansion was pioneered by [Bonnor and Rosenhead 31], then formalised by [Thorne 32], and finally applied in this present context by [Blanchet 33].

In terms of source dynamics, it is more appropriate (and uniquely able) to describe inherently relativistic phenomena, such as gravitational scattering. Its wider scope of applicability comes at the cost of a higher computational complexity, as at higher orders one encounters intricate families of relativistic integrals. Note that we have in fact computed the 1 PM approximation already in the Chapter 3 when we linearized the EFE. Higher orders are far more difficult to obtain, especially for sources such as BBH .

With the rise of amplitude techniques from high energy physics, both EFT and full theory results have been successful in extracting previously unreachable orders. Such techniques are perfectly suited to compute relativistic scattering as they were developed for this specific task. We will see this in the next chapter.

4.3 EOB

The second full-waveform generation technique is the Effective One-Body (EOB) formalism. It was initially developed by [Buonanno and Damour 34], as a non-perturbative re-summing of the PN expansion. It was later extended to include the merger and ringdown effects in [27]. Thus, it became the first full waveform generating technique to actually produce a waveform. It has gotten progressively more powerful, as the PN expansions have gotten better. More recently PM results have also been included [35]. Additionally EOB can be combined with NR to produce a very accurate waveform, with less computational overhead than NR alone.

As its name suggests, the EOB framework combines all the PN, PM and NR data into a Hamiltonian describing the motion of a single body. It is inspired by solutions of two-body problems in Newtonian gravity which make use of barycentric coordinates to turn it into a one body problem. Further inspiration came from the two body problem in Quantum Electrodynamics (QED) [see 36] .

Consider two bodies, with masses m_1 and m_2, positions $\mathbf{q}_1$, $\mathbf{q}_1$ and momenta $\mathbf{p_1}$ and $\mathbf{p_2}$ respectively. The system can be described by the following Hamiltonian:

$$\mathcal{H}_{\text{newton}}(\mathbf{q}_1, \mathbf{q}_1, \mathbf{p_1}, \mathbf{p_2}) = \frac{\mathbf{p_1}^2}{2m_1} + \frac{\mathbf{p_2}^2}{2m_2} - \frac{Gm_1m_2}{|\mathbf{q}_1 - \mathbf{q}_1|} \qquad (4.15)$$

One then transforms this Hamiltonian into one describing the relative motion $\mathbf{q} = \mathbf{q}_1 - \mathbf{q}_1$. One can formalize this by defining a new set of generalized coordinates, through a canonical transformation. We can go even further and employ a generating function for the transformation,

ensuring that Hamilton's equations remain unchanged in form (see [37]).
To describe relative motion, we use Jacobi coordinates $(\mathbf{Q}, \mathbf{q})$:

$$\begin{pmatrix} \mathbf{q}_1 \\ \mathbf{q}_2 \end{pmatrix} \rightarrow \underbrace{\begin{pmatrix} \frac{m_1}{M} & \frac{m_2}{M} \\ 1 & -1 \end{pmatrix}}_{=A} \begin{pmatrix} \mathbf{q}_1 \\ \mathbf{q}_2 \end{pmatrix} = \begin{pmatrix} \mathbf{Q} \\ \mathbf{q} \end{pmatrix} \qquad (4.16)$$

If we now define the following generating function for the transformation, depending on the old positions coordinates $\mathbf{q}_i$ and the new momenta $\mathbf{P}_i$:

$$f_{II}(\mathbf{q}_i, \mathbf{P}_i) = \mathbf{P}_i A^{ij} \mathbf{q}_j, \qquad (4.17)$$

then the old momenta are given by

$$\mathbf{p_i} = \frac{\partial f_{II}}{\partial \mathbf{q}_i} = \mathbf{P}_i A^{ij} \iff \mathbf{P}_i = [A^{-1}]^{ij} \mathbf{p_j}. \qquad (4.18)$$

Where we can directly invert this equation and obtain the new momenta as:

$$\begin{pmatrix} \mathbf{P} \\ \mathbf{p} \end{pmatrix} = \begin{pmatrix} \mathbf{P}_1 \\ \mathbf{P}_2 \end{pmatrix} = \begin{pmatrix} 1 & 1 \\ \frac{m_2}{M} & -\frac{m_1}{M} \end{pmatrix} \begin{pmatrix} \mathbf{p_1} \\ \mathbf{p_2} \end{pmatrix} \qquad (4.19)$$

As expected, we obtain that one of the momenta describes the center of mass momentum $\mathbf{P} = \mathbf{p_1} + \mathbf{p_2}$. The other positions are by construction given by $\frac{\partial f_{II}}{\partial \mathbf{q}_1} = \mathbf{Q}$ and $\frac{\partial f_{II}}{\partial \mathbf{q}_2} = \mathbf{q}$ i.e the same as equation eq. 4.16. Finally the new Hamiltonian $\mathscr{H}_{\mathrm{rel}}(\mathbf{Q}, \mathbf{q}, \mathbf{P}, \mathbf{p})$ can be directly obtained from the generating function:[25]

$$\mathscr{H}_{\mathrm{rel}}(\mathbf{Q}, \mathbf{q}, \mathbf{P}, \mathbf{p}) = \mathscr{H}_{\mathrm{newton}}(\mathbf{Q}, \mathbf{q}, \mathbf{P}, \mathbf{p}) + \cancelto{0}{\frac{\partial f_{II}}{\partial t}} = \frac{\mathbf{P}^2}{2M} + \frac{\mathbf{p}^2}{2\mu} - \frac{Gm_1 m_2}{|\mathbf{q}|}, \qquad (4.22)$$

where $M = m_1 + m_2$ is the total mass, and $\mu = \frac{m_1 m_2}{M}$ is the reduced mass. If we change coordinates to a frame where the $\mathbf{Q}$ is at rest, i.e. $\mathbf{P} = 0$, the Hamiltonian collapses to a one body Hamiltonian. The two-body problem we started with can now be though of as the one body problem of a test-particle of mass μ orbiting an external mass M.

In Newtonian gravity, a small change of coordinates makes the two body problem exactly solvable. In much the same way, EOB generalizes this framework to general relativity. The defining trick used above is to transform to 'better' coordinates. A first step is to demand that for straight line motion the Center of Momentum (COM) energy $E_{\mathrm{COM}} = P^0$, where P it the 4-momentum of the entire-system, is equal to the Hamiltonian. We then have:[26]

[25] We just plug in the definition of the old momenta in terms of the new (eq. 4.18):

$$\mathbf{p_1} = \frac{m_1}{M} \mathbf{P} + \mathbf{p}, \qquad (4.20)$$

$$\mathbf{p_2} = \frac{m_2}{M} \mathbf{P} - \mathbf{p}. \qquad (4.21)$$

[26] In the COM frame, the spatial part of the total momentum is zero (by definition), and thus we have:

$$P_0^2 = P^2 = (p_1 + p_2)^2 = p_1^2 + p_2^2 + 2 p_1 \cdot p_2. \qquad (4.23)$$

$$\mathcal{H} = \sqrt{M^2(1 + 2\nu(\gamma - 1))}, \qquad (4.24)$$

where $\nu = \frac{\mu}{M}$ is the symmetric mass ratio, and $\gamma = \frac{1}{\sqrt{1-v^2}} = \frac{p_1{}^\mu p_{2\mu}}{m_1 m_2}$ is the relative Lorentz-factor. Note that for non-interacting systems we have $p_\mu p^\mu = \mu^2$ and we can define the effective Hamiltonian:

$$\mathcal{H}_{\text{eff}} = p^0 = \sqrt{\mu^2 + \mathbf{p}^2} = \mu\gamma. \qquad (4.25)$$

We can substitute this into the Hamiltonian above, and add back a generic system momentum $\mathbf{P}$ and obtain

$$\mathcal{H}_{\text{eob}} = \sqrt{M^2(1 + 2\nu(\frac{\mathcal{H}_{\text{eff}}}{\mu} - 1)) + \mathbf{P}^2} \qquad (4.26)$$

This Hamiltonian (with $\mathcal{H}_{\text{eff}}$ given by eq. 4.25) now describes straight line motion in a relativistic framework. The key point is that we can take $\mathcal{H}_{\text{eff}}$ to be a gravitational test mass Hamiltonian, with some specific deformations and this will match the PN result. Consider a test mass in a Schwarzschild background eq. 2.67, i.e. we consider the case of non-spinnning black holes. We can start from the reduced-mass shell expression:

$$g^{\mu\nu}p^\mu p^\nu = -\mu^2 \qquad (4.27)$$

where $g^{\mu\nu}$ is given by eq. 2.67, where we can set $\theta = \frac{1}{2}\pi$ to fix the orientation[27]. Just as before, the effective Hamiltonian is the 0th component of the momentum, which is implicitly given by eq. 4.27:

$$\mathcal{H}_S = \sqrt{A_S(\mu^2 + A_S p_r^2 + \frac{L^2}{r^2})}, \qquad (4.28)$$

where $A_S = \frac{1}{1-R_S/r}$, p_r and $L = p_\phi$ are the radial and angular momentum respectively. We then allow deformations from this Hamiltonian defining

$$\mathcal{H}_{\text{eff}}(r, p_r, \phi, L) = \sqrt{A(\mu^2 + A\bar{D}p_r^2 + \frac{L^2}{r^2}) + Q}, \qquad (4.29)$$

where $A, \bar{D}, Q$ are the so-called EOB potentials. $A, \bar{D}$ correspond to the radial potentials of the effective metric, while Q contains terms quadratic in the momentum. We can then match these to PN results, by matching observables.

This is more than a neat trick as this Hamiltonian, when well-matched, fits the gold standard NR result up to the merger, well out of the PN

regime. Crucially, this Hamiltonian framework does not take into account radiation reaction by construction since it is based on conserved energy. These dissipative effects are included after the fact, as friction terms in the EOM. The usual conservative EOM is straightforwardly obtained through Hamiltonians equations:

$$\dot{r} = \frac{\partial \mathcal{H}_{\text{eff}}}{\partial p_r}, \quad \dot{p}_r = -\frac{\partial \mathcal{H}_{\text{eff}}}{\partial r}$$

$$\omega = \dot{\phi} = \frac{\partial \mathcal{H}_{\text{eff}}}{\partial L}, \quad \dot{L} = -\frac{\partial \mathcal{H}_{\text{eff}}}{\partial \phi}^{\;0}. \tag{4.30}$$

Note that, as expected, the angular momentum is conserved. We will now spoil this conservation, by adding friction forces, also called radiation reaction forces to the EOMs governing radial and angular momentum dynamics:

$$\dot{p}_r = -\frac{\partial \mathcal{H}_{\text{eff}}}{\partial r} + f_r,$$

$$\dot{L} = f_\phi. \tag{4.31}$$

We can now express the energy loss:

$$\dot{E} = \frac{\mathrm{d}\mathcal{H}_{\text{eff}}}{\mathrm{d}t} = \frac{\partial \mathcal{H}_{\text{eff}}}{\partial r}\dot{r} + \frac{\partial \mathcal{H}_{\text{eff}}}{\partial p_r}\dot{p}_r + \frac{\partial \mathcal{H}_{\text{eff}}}{\partial L}\dot{L} = f_r\dot{r} + f_\phi\omega. \tag{4.32}$$

Such dissipative effects are accounted for by matching to PN results for the angular momentum and energy fluxes, which are given by the so called balance laws:

$$\langle \mathcal{F}_L \rangle = -\langle \dot{L} \rangle = -\langle f_\phi \rangle,$$

$$\langle \mathcal{F}_E \rangle = -\langle \dot{E} \rangle = -\langle f_r\dot{r} + f_\phi\omega \rangle. \tag{4.33}$$

We have denoted averaging with angle brackets. With this we obtain as full of a picture of the inspiral as possible given the inputs, namely PN . The matching can also be done with PM and NR results, further increasing the validity and precision of EOB . Of course we are still missing the merger and ringdown phases. The merger, or plunge was predicted in [27] to be simply the peak in the waveform. This waveform is connected smoothly to a ringdown waveform, defined by a sum of quasi-normal modes of the remnant after merger. Thus one obtains a sort of frankenstein waveform, pooling resources from PN , PM , NR and BH perturbation theory. Importantly, when well matched, this waveform is almost as accurate as NR results, but with the added benefit of being able to be computed in a reasonable amount of time. Of course it is still only as powerful as the inputs to which we match, namely the PN or PM results. We will explore how to compute PM results using amplitudes in the next section.

5 Scattering amplitudes and GWs

Whilst we have almost no hope to detect any GW scattering events with current experiments, scattering calculations can still be very useful in the quest for orbital waveforms. Most importantly, while experimental data is not driving gravitational scattering theory, particle scattering experiment and theory have been an enormously fruitful endeavor for High energy physics. The back and forth between precise measurements (such as those conducted at the ??) and precise predictions for particle scattering, has pushed the boundaries of the calculations possible. It would be therefore very beneficial if one could apply the large knowledge acquired for small non-gravitationally interacting particles, to large compact orbiting bodies.

Such techniques as EFT, double copy, generalized unitarity, Integration by Parts (IBP) reduction, differential equations methods, all standing on the shoulders of Feynman perturbative techniques have been applied to the scattering problem in gravity. A key part of applying tools originally developed for mostly quantum systems is controlling the classical limit, and is part of the solution to implementing gravity in a QFT framework, a historically difficult endeavor. Once scattering data is obtained one needs to extract the relevant observables. This may be in an effort to compare results from the different methods, in which case gauge and diffeomorphism invariance are key. It can also be to extract the relevant information for detection and data extraction, in which case the GW waveform is the relevant observable. In the latter case one is mostly interested in the orbital waveform, and thus a map from unbound to bound orbits is necessary.

Multiple formalisms have arisen to map the scattering problem to an orbital one, and the quantum formalism to a classical one. One key way is to map scattering data to the potential (as present in a Hamiltonian for example). In fact this has been developped as early as the 1970s in [38,39]. Further developments happened in [7,35,40−43]. Here we will follow the treatment in [44], where one uses the conservative part of such scattering amplitudes to match to an EFT and subsequently to map to the potential. Recently efforts to add disipative effects have been succesful aswell [see 45]. This potential can then be used as input to the EOB formalism. Furthermore, [23]; [46], have shown a path forward in directly extending unbound data to bound orbits, obviating the need to use a potential and EOB at all.

Finally as mentioned in the last chapter, scattering can stand on its own and is still usefull, unextended to the orbital case. The PM approximation can be computed from scattering amplitudes in an EFT framework [47]. We can also explore the classical observables possible in scattering scenarios. This has been developped in [5] and was extended to local observables[28] such as waveforms in [48].

In this chapter we will first look at how one uses amplitude data to extract orbital and scattering waveforms. We will then look at the KMOC formalism to directly extract observables. Finally we will look at obtaining these amplitudes, combining all the methods and comparing to results such as those in [5,49].

5.1 Scattering amplitudes

In QFT one way to encode scattering data is through a scattering amplitude. Consider a process where one starts out with a set of particles described by a state $|i\rangle$, we let them interact, and end up with a final state $|f\rangle$. The scattering amplitude is then defined as the probability amplitude for this process to occur. It is simply given by

$$\langle i|S - 1|f\rangle = (2\pi)^4 \delta^{(4)}(p_f - p_i) i\mathscr{A}_{fi}, \tag{5.1}$$

where S is essentially the operator that 'does the scattering'. We subtract the identity from it, forming what some call the transfer matrix T as we only are interested in processes where something happens (i.e. not everything stays the same). In the above equation we also define the *scattering matrix element $\mathscr{A}_{fi}$* [see 50] or *invariant Feynman amplitude* [see 51], by factoring out a normalised spacetime delta-function imposing conservation of momentum on the external fields, and a complex unit. The key point is that this amplitude can be computed using graphical techniques. This makes use of the Lehmann Symanzik and Zimmermann (LSZ) [52,53] formalism where such an amplitude $\mathscr{A}_{fi}$, can be computed from products of time ordered correlation functions of the given QFT. These are also called Green's functions, which can then be encoded by sums of Feynman diagrams. The diagrams are generated by applying Feynman rules which can be readily obtained from an action describing the theory. This technique will be exemplified in the following sections.

5.2 From amplitude to potential

Let us now look at how to map the amplitude to the gravitational potential, for use in the EOB formalism. We will follow the treatment in [44]. We first start with defining the effective theory that describes

[28] local as in not time integrated and thus presenting time dependent dynamics

our problem as two scalar fields f_1 and f_2 with masses m_1 and m_2 interacting through a long range potential $V(r)$. It is simply the EFT for non-relativistic fields. This EFT is described by the following action:

$$S = \int \mathrm{d}t\, \mathscr{L}_{\text{kin}} + \mathscr{L}_{\text{int}}, \tag{5.2}$$

where the kinetic term is given by:

$$
\begin{aligned}
\mathscr{L}_{\text{kin}} = &\int \tilde{\mathrm{d}}^{D-1}\mathbf{k}\, f^*{}_1(-\mathbf{k})\Big(\mathring{i}\partial_t - \sqrt{\mathbf{k}^2 + m_1}\Big) f_1(\mathbf{k}) \\
&+ \int \tilde{\mathrm{d}}^{D-1}\mathbf{k}\, f^*{}_2(-\mathbf{k})\Big(\mathring{i}\partial_t - \sqrt{\mathbf{k}^2 + m_2}\Big) f_2(\mathbf{k})
\end{aligned}
\tag{5.3}
$$

and the interaction term is given by:

$$\mathscr{L}_{\text{int}} = -\int \tilde{\mathrm{d}}^{D-1}\mathbf{k}\, \tilde{\mathrm{d}}^{D-1}\mathbf{k}'\, V(\mathbf{k}, \mathbf{k}')\, f^*{}_1(\mathbf{k}') f^*{}_2(-\mathbf{k}') f_1(\mathbf{k}) f_2(-\mathbf{k}). \tag{5.4}$$

This theory is obtained from the full one by integrating out all the massless force carriers , which are consequently encoded in the potential $V(\mathbf{k}, \mathbf{k}')$ and taking the non-relativistic limit $|\mathbf{k}|, |\mathbf{k}'| \ll m_{1,2}$. In a classical system we consider the particles to be separated by a minimum distance, called impact parameter $|\mathbf{b}|$, and consider that their compton wavelength $\ell_c \sim \frac{1}{|\mathbf{k}|}, \frac{1}{|\mathbf{k}'|}$ [29] is much smaller than this separation:

^{29} note the use of natural units

$$|\mathbf{b}| \ll \ell_c \simeq \frac{1}{|\mathbf{k}|}, \frac{1}{|\mathbf{k}'|} \tag{5.5}$$

This ensures that the particles are not interacting quantum mechanically in any significant way. Interestingly this heirachy of scales can be rewritten as:

$$\mathbf{J} \sim |\mathbf{k} \times \mathbf{b}| \gg 1 \tag{5.6}$$

Thus any two body classical system has large angular momentum. We can thus extract the classical part of any quantity by taking the LO contribution in the inverse of angular momentum, or equivalently:

$$\frac{1}{J} \propto \frac{1}{|b|} \sim |\mathbf{k} - \mathbf{k}'| \propto \frac{1}{\kappa} \tag{5.7}$$

Where we used in the first step that angular momentum is proportional to separation. We then applied the fact that in scattering scenarios the impact parameter is proportional to the inverse of the momentum transfer $\sim \frac{1}{|\mathbf{q}|}$ where :

$$q = (0, \mathbf{q}) = (0, \mathbf{k} - \mathbf{k}'). \tag{5.8}$$

The last relation in eq. 5.7 holds due to the virial theorem. Where κ is the coupling constant, which in the case of gravity is $\kappa = 4\pi G$. Since the potential must encode the coulomb potential $\kappa/|\mathbf{k} - \mathbf{k}'|^2 \propto J^3$, it must scale similarly. We thus formulate the following ansatz for the potential:

$$V(\mathbf{k}, \mathbf{k}') = \sum_{n=0}^{\infty} \frac{\kappa^n}{|\mathbf{k} - \mathbf{k}'|^{D-1-n}} c_n \left(\frac{\mathbf{k}^2 + \mathbf{k}'^2}{2} \right) \tag{5.9}$$

Note that higher order terms in the potential could be formed by any combination of momentum invariants $\mathbf{k}^2$, $\mathbf{k}'^2$, and $\mathbf{k} \cdot \mathbf{k}'$, however not all combinations of these are independent. The ansatz is chosen such that only the combination $|\mathbf{k} - \mathbf{k}'|$ and $\mathbf{k}^2 + \mathbf{k}'^2$ is present, the others being combinations reachable by field redefinition, or vanishing on-shell, such as $\mathbf{k}^2 - \mathbf{k}'^2$. Note as-well that we work in $D = 4 - 2\epsilon$ dimensions such that the integrals are dimensionally regulated [see 54]. This means that an ϵ-power corresponds to a logarithm[30].Finally note that in gravity this is precisely a PM expansion!

[30] the third term in the sum is given by $\kappa^3 \ln(\mathbf{k} - \mathbf{k}')^2 c_3 \left(\frac{1}{2}\mathbf{k}^2 + \mathbf{k}'^2 \right)$

5.2.1 EFT amplitude

The first step in establishing a link to the potential from a generic scattering amplitude computed in the full theory is to compute the amplitude in the EFT. We first identitify the Feynman rules from the action. The kinetic term encodes the propagator:

$$= \frac{\mathring{\imath}}{k_0 - \sqrt{\mathbf{k}^2 + m_{1,2}^2} + \mathring{\imath}0}$$

Propagator rule

where the $\mathring{\imath}0$ is the Feynman prescription for avoiding the poles. The interaction term encodes the vertex:

$$= \mathring{\imath}V(\mathbf{k}, \mathbf{k}')$$

Vertex rule

The key point is that the EFT amplitude for two-to-two scattering must be equal to the full amplitude at every order in the coupling constant κ. The expression for the EFT amplitude will contain the coefficient functions from eq. 5.9 since they will be present as vertex terms. Particle number

[31] as pair production is kinematically forbidden

must be conserved in the non-relativistic limit [31], so the amplitude is a sum of bubble diagrams:

EFT amplitude

We can consequently neatly organise the amplitude into a sum of terms with specific loop counts. We can also equivalently organise it into a sum of terms with specific κ powers. We write,

$$\mathscr{A}_{\text{EFT}} = \sum_{L=0}^{\infty} \mathscr{A}_{\text{EFT}}^{L\text{loop}} = \sum_{i=1}^{\infty} \mathscr{A}_{\text{EFT}}^{(i)}. \tag{5.10}$$

Notably, these partitions do not line up for the EFT since the vertex contains all powers of the coupling. This is in contrast to the full theory where usually they yield the same partition. We will eventually want to partition over the coupling power to compare the full theory.

Since every vertex has degree 4, and we have two scalars in and two scalars out, it is convient to define a 2-body propagator. We can already integrate over the energy component of the loop momentum, since the vertex does not have an energy dependence:[32]

[32] the 4-momentum conservation at each vertex means that the energy components of the two propagating momenta must carry along the energy component of the initial state $E = E_1 + E_2$. This can be encoded by demanding that $\omega_1 + \omega_2 = E$. Taking the COM frame for the intial momenta means that the 3 momenta of each propagator must cancel i.e. $\mathbf{k}_1 + \mathbf{k}_2$

$$i\Delta_2(\mathbf{k}) = \int \tilde{\text{d}}\omega \, \frac{i}{\omega - \sqrt{\mathbf{k}^2 + m_1^2}} \frac{i}{E - \omega - \sqrt{\mathbf{k}^2 + m_2^2}} = \frac{i}{E - \sqrt{\mathbf{k}^2 + m_1^2} - \sqrt{\mathbf{k}^2 + m_2^2}}, \tag{5.11}$$

where the integral is performed using the residue theorem, closing the contour in either half plane, where in either case a pole is present. Note that we define $E = E_1 + E_2$ to be the COM energy of the two inital states:[33]

[33] which is equal to the outgoing energy

$$E_{1,2} = \sqrt{\mathbf{p}^2 + m_{1,2}^2} = \sqrt{\mathbf{p}'^2 + m_{1,2}^2}, \tag{5.12}$$

where $\mathbf{p}$ and $\mathbf{p}'$ are the initial and final three-momenta of the two states [34] in the COM frame. Finally we can write what the diagram at loop level $L > 0$ encodes:

[34] for example in the initial state one scalar field will have 3-momentum $\mathbf{p}$, and the other $-\mathbf{p}$

$$\mathscr{A}_{\text{EFT}}^{L\text{loop}} = \int \prod_{i=1}^{L} \tilde{\text{d}}^{D-1}\mathbf{k}_i \, V(\mathbf{p}, \mathbf{k}_1)\Delta_2(\mathbf{k}_1) \cdots \Delta_2(\mathbf{k}_L)V(\mathbf{k}_L, \mathbf{p}'). \tag{5.13}$$

This integral can be perfomed in the non-relativistic limit, as done by [55] up to 3PM, using IBP reduction yielding, up to 2PM, the amplitudes of the EFT:[35]

$$\mathscr{A}_{\text{EFT}}^{(1)} = -\frac{4\pi G c_1}{\mathbf{q}^2}$$

$$\mathscr{A}_{\text{EFT}}^{(2)} = \pi^2 G^2 \Big(-\frac{2c_2}{|\mathbf{q}|} + \frac{1}{E\xi|\mathbf{q}|}\Big[(1-3\xi)c_1^2 + 4\xi^2 E^2 c_1 c_1'\Big]$$

$$\int \tilde{\mathrm{d}}^{D-1}\boldsymbol{\ell} \, \frac{32E\xi c_1^2}{\boldsymbol{\ell}^2(\mathbf{q}+\boldsymbol{\ell})^2(\boldsymbol{\ell}^2 + 2\mathbf{p}\boldsymbol{\ell})}\Big), \tag{5.14}$$

where $\xi = \frac{E_1 E_2}{(E_1 + E_2)^2}$ is the reduced energy ratio. The arguments of the coeffient functions c_1 are kept iplicit and a prime denotes a derivative with respect to $\mathbf{p}$. Additionally we define $\mathbf{q} = \mathbf{p}' - \mathbf{p}$ to be the 3-momentum transfer. Now provided we obtain the amplitude of the full theory, and carefully apply the same limiting procedures, we have that

$$\mathscr{A}_{\text{EFT}}^{(i)} = \mathscr{A}_{\text{full}}^{(i)} \quad \forall i. \tag{5.15}$$

This enables us to fix the coefficients in the potential ansatz eq. 5.9, and fullfils the promised map from amplitude to potential. Importantly we must apply the limiting procedure applied above, i.e. the classical and non relativitic limit. We can summarise this by setting the following heirarchy:

$$m_1, m_2 \ll J|\mathbf{q}| \ll |\mathbf{q}|. \tag{5.16}$$

For the full theory this can be encoded as restricting to a specific kinematic regime, following the method of regions. We consider all the possible loop-momentum scalings, first due to the classical limit:

Region	Momentum $\ell = (\omega, \boldsymbol{\ell})$
hard	(m, m)
soft	$(|\mathbf{q}|, |\mathbf{q}|)$

The soft region is responsible for the classical limit in this language, as we consider a small $|\mathbf{q}|$ expansion. We will infact explore this fact in a different light in Section 5.3. Taking the NR limit corresponds to a subregion of the soft region, the so-called potential region:

$$(\omega, \boldsymbol{\ell}) \sim (|\mathbf{q}|, |\mathbf{q}|), \tag{5.17}$$

where we use that the NR expansion is a given by

$$|\mathbf{p}| \ll m \tag{5.18}$$

and thus equivalently[36] by a small relative velocity:

$$|\mathbf{u}| \ll 1. \tag{5.19}$$

To summarise, to obtain the form of the potential, we first compute the amplitude in an EFT, absorbing all force carrying particles into an effective vertex. Making an ansatz for the potential we can go ahead and compute this amplitude in the non-relativistic limit. This same amplitude can be computed in the full theory, but by still taking the limiting procedure we drastically reduce the kinematic region, simplifying calculations (in fact eliminating diagrams) and allowing us to match order by order the EFT amplitude. This fixes the coefficents postulated for the potential.

Unfortunately the procedure desribed above, and in fact *any* procedure trying to make contact with EOB through expanding the gravitiational potential, automatically does not capture the full physics. The crucial point that makes compact binaries interesting is that they are not isolated, energy conserving systems. The energy of the system is lost to the gravitational waves that enable us to detect them. Any conservative dynamics, by construction, cannot capture this loss of energy. In the context of EOB this radiation reaction was added after the fact, through direct modifications of the EOMs obtained from Hamilton's equations. It is not clear how to incorporate dissipative data from the amplitude in the EOB framework.

One way to not encounter this difficulty is to fully bypass the EOB framework and try to obtain observables directly from the amplitude. This is the subject of the following sections.

5.3 KMOC

The setup of the KMOC framework ([5]) is very general, and is aimed at taking the classical limit of a scattering event in an unspecified theory. We will later on apply it to SQED and gravity.

5.3.1 Conventions

First let us define our conventions. Throughout this section we use relativistically natural units, i.e. we do *not* set $\hbar = 1$. This will essentially be the small parameter that multiplies the soft momenta, that defined the region in Section 5.2. In this section we will further motivate this classical limit, in more detail, by taking the generally accepted limit that makes quantum physics collapse to classical physics:

$$\hbar \to 0. \tag{5.20}$$

We still retain $c = 1$, meaning that, using dimensional analysis we have that $[L][T]^{-1} = 1 \implies [L] = [T]$, length and time are measured in the same units. Correspondingly, energy is measured in units of mass:

$$E = mc^2 \implies [E] = [m] = [M] \tag{5.21}$$

and $\hbar$ has the following units:

$$E = \hbar\omega \implies [M] = [\hbar][T]^{-1} \implies [\hbar] = [T][M]. \tag{5.22}$$

Thus momentum p has units of $[p] = [M]$ mass and Wavenumber $[\breve{p}] = [\frac{p}{\hbar}] = [T]^{-1}$ has units of inverse time. We will denote the on-mass-m-shell measure by $\mathrm{d}\Phi(p)$ [37]:

[37] Repeated integration will be denoted $\mathrm{d}\Phi_n(p_1, \ldots, p_n)$

$$\int \mathrm{d}\Phi(p) \cdots = \int \frac{\mathrm{d}^3\mathbf{p}}{2\hbar\omega_{\mathbf{p}}(2\pi)^3} \cdots = \int \tilde{\mathrm{d}}^4 p \, \tilde{\delta}^{(+)}(p^2 - m^2) \ldots, \tag{5.23}$$

where quantities denoted by bars absorb the relevant factors of 2π, such that $\tilde{\mathrm{d}}^n p = \frac{\mathrm{d}^n p}{(2\pi)^n}$. Additionally we have defined $\hbar\omega_{\mathbf{p}} = \sqrt{\mathbf{p}^2 + m^2}$ to be the on-shell energy and $\delta^{(+)}$ is the normalised positive energy on-shell delta function:

$$\tilde{\delta}^{(+)}(p^2 - m^2) = (2\pi)\delta(p^2 - m^2)\Theta(p^0) = \tilde{\delta}(p^2 - m^2)\Theta(p^0) \tag{5.24}$$

5.3.2 Intital State

With our conventions at hand, let us set the stage for the problem. Imagine we want to scatter two particles, be they massive black holes, or tiny electrons into each other, with a constant particle number (i.e. a classical two in two out scattering). As mentioned in Section 5.1, in QFT the framework that formalizes scattering of definite particle number states is called the LSZ reduction.

Let us look at it in more detail. The first component is to define the states we want to scatter. Suppose our theory has single particle states $|p\rangle$, with mass m, eigenstates of the momentum:

we work in the Heisenberg picture here

$$\mathbb{P}^\mu|p\rangle = p^\mu|p\rangle \quad \text{where} \quad p^0 = \hbar\omega_{\mathbf{p}} = \sqrt{\mathbf{p}^2 + m^2}. \tag{5.25}$$

These states can be seen as special cases (the plane wave states) of wavepacket states:[38]

[38] A plane wave state $|f\rangle = |p\rangle$ would be given by $\breve{f}(k) = 2\hbar\omega_{\mathbf{k}}\tilde{\delta}^{(3)}(\mathbf{k} - \mathbf{p})$

$$|f\rangle = \int \mathrm{d}\Phi(k)\, \breve{f}(k)|k\rangle, \tag{5.26}$$

[39] Note that the concept of coordinate space wavefunction is ill defined in interacting theories. However for such asymptotic states, the wavefunction outside the bulk (on the infinte time boundary) is that of a free wavefunction

where $\check{f}(k)$ is the momentum space wavefunction or more mathematically the momentum distribution function. Note that it is almost a fourier transform, but not quite, as it is performed on mass shell. If the spacetime 'wavefunction' [39] is given by:

$$f(x) = \int \mathrm{d}\Phi(k)\,\check{f}(k)\mathrm{e}^{-\mathring{\imath}k\cdot x}, \tag{5.27}$$

the $\check{f}(k)$ is consequently given by:

$$\langle k|f\rangle = \check{f}(k) = 2\hbar\omega_{\mathbf{p}}\int \mathrm{d}^3\mathbf{x}\,f(x)\mathrm{e}^{\mathring{\imath}k\cdot x}. \tag{5.28}$$

[40] $f\overleftrightarrow{\partial_\mu}g = f(\partial_\mu g) - (\partial_\mu f)g$

If we now define the following operators:[40]

$$a_f^\dagger(t) = -\mathring{\imath}\int \mathrm{d}^3\mathbf{x}\,f(x)\overleftrightarrow{\partial_0}\phi(x) \tag{5.31}$$

Note that if we replace $f(x)$ by a plane wave state $\mathrm{e}^{-\mathring{\imath}k\cdot x}$ we obtain and define the following:

$$a_{\mathbf{k}}^\dagger(t) = \int \mathrm{d}^3\mathbf{x}\,\mathrm{e}^{-\mathring{\imath}k\cdot x}\Big[\hbar\omega_{\mathbf{k}}f(x) - \mathring{\imath}\partial_0 f(x)\Big] \tag{5.29}$$

$$a_f(t) = \mathring{\imath}\int \mathrm{d}^3\mathbf{x}\,f^*(x)\overleftrightarrow{\partial_0}\phi(x) \tag{5.32}$$

$$\frac{\mathrm{d}a_{\mathbf{k}}(t)}{\mathrm{d}t} = \mathring{\imath}[H_H, A_H(t)] \int \mathrm{d}^3\mathbf{x}\,\mathrm{e}^{\mathring{\imath}k\cdot x}\Big[\hbar\omega_{\mathbf{k}}f(x) + \mathring{\imath}\partial_0 f(x)\Big] \tag{5.30}$$

where $\phi(x)$ is the Heisenberg field operator of our theory. Note that while these operators are time dependent, this dependence is not given by applying the Heisenberg EOMs [41], instead it is present through the time dependence of the wavefunction $f(x)$. It turns out that these operators, suggestively written are the true creation and annilihation operators in the interacting theory.

Now we can actually define a general one particle state $|f\rangle$ as the result of a creation operator acting on the physical vacuum. Crucially however this only makes sense in the boundary of the bulk, i.e. at asymptotic times $t \to \pm\infty$[42]. Inside the bulk, any thusly created state would infact not have definite particle number. This definitely makes sense in the scattering problem because if you consider the whole system as a state, it only has definite particle number at asymptotic times, and inside the bulk the scattering happens, and the particle number is not conserved (at least quantum mechanically).

[42] see [51] or [53] for a more in depth discussion of this point

Consequently we only define asymptotic states, denoting them by an in subscript if they were created at $t \to -\infty$ and out if they were created at $t \to +\infty$. Thus we define a generic single particle in state as:

$$|f\rangle_{\mathrm{in}} \overset{\mathrm{def}}{=} \lim_{t\to-\infty} a_f^\dagger(t)|\Omega\rangle = a_{f;\mathrm{in}}^\dagger|\Omega\rangle = \int \mathrm{d}\Phi(k)\,\check{f}(k)\underbrace{a_{\mathbf{k}}^\dagger|\Omega\rangle}_{|k\rangle} \tag{5.33}$$

and the corresponding $t \to +\infty$ state where in is replaced with out. It turns out that the extension to multiparticle states is not much more

complicated. The one thing to demand is that the momentum distributions say $\check{f}_1, \check{f}_2, \ldots$ have no common support, i.e. they are not overlapping. In this case a n-particle in state is defined as:

$$|f_1, \ldots, f_n\rangle_{\text{in}} \stackrel{\text{def}}{=} a^\dagger_{f_1;\text{in}} a^\dagger_{f_2;\text{in}} \ldots a^\dagger_{f_n;\text{in}} |\Omega\rangle = \int d\Phi_n(k_1, \ldots, k_n) \, \check{f}_1(k_1) \ldots \check{f}_n(k_n) |k_1, \ldots, k_n\rangle. \tag{5.34}$$

We now have the definitions for asymptotic in and out states for any number of particles. Before continuing to define the setup to scatter our two particles, let us look at the meaning of the position space wavefunction $f(x)$ as defined in eq. 5.27. Consider a sharply peaked, compactly supported momentum distribution $\check{f}(k)$ around a value $\mathbf{p}_0$ and a characteristic width Δp. One such function could be:

$$f(\mathbf{p}; \mathbf{p}_0, \Delta p) = \begin{cases} N e^{-1/(1-|\mathbf{p}-\mathbf{p}_0|^2/\Delta p^2)} & \text{if } |\mathbf{p}_0 - \mathbf{p}| < \Delta p \\ 0 & \text{if } |\mathbf{p}_0 - \mathbf{p}| \geq \Delta p \end{cases}, \tag{5.35}$$

where N is a normalization constant. Now the integrand in eq. 5.27, at large t or $\mathbf{x}$, will be dominated by the stationary phase point $\mathbf{p}_s$ which is given by:[43]

$$0 = -\frac{\partial}{\partial \mathbf{p}_s}(\hbar\omega_{\mathbf{p}_s} t + \mathbf{p}_s \cdot \mathbf{x}) = -\frac{\mathbf{p}_s t}{\hbar\omega_{\mathbf{p}_s}} + \mathbf{x}. \tag{5.38}$$

In the case of a sharply peaked momentum distribution, the coordinate space wavefunction will be largest when the stationary phase point is be the same as the peak of the momentum distribution, i.e. $\mathbf{p}_s = \mathbf{p}_0$ i.e. substituting $\mathbf{p}_s$ into eq. 5.38 gives:

$$\mathbf{x} \simeq \frac{\mathbf{p}_0 t}{\hbar\omega_{\mathbf{p}_0}} = \mathbf{v}_0 t. \tag{5.39}$$

This is precisely the trajectory of the classical relativistic particle. If we have two particles with different peaked momentum distributions their trajectories will have different velocities, but the same positions at time 0. Thus we will shift one of these trajectories by a so called impact parameter b^μ[44], parametrising the relative separtation of the two particles/wavepackets. This can be simply done by multiplying the momentum distribution $\check{f}_1(p)$ by a factor of $e^{\frac{i}{\hbar}b \cdot p}$. We take it to be perpendicular to the initial momenta p_1, p_2. We now can write down the initial state that we are going to study:

$$|\text{in}\rangle = \int d\Phi_2(p_1, p_2) \, \check{f}_1(p_1)\check{f}_2(p_2) e^{\frac{i}{\hbar}b_\mu p_1{}^\mu} |p_1, p_2\rangle_{\text{in}}. \tag{5.42}$$

From now on we will drop the breve and infer from the arguments the type of f we are dealing with. Note that by extracting the impact parameter in this way, the wavefunctions can be identitcal in form, and will still be separate as required.

49

5.3.3 Change in observable

The KMOC framework concerns itself with the change of an observable during a scattering event. For such an observable O, its change can be simply obtained by evaluating the difference of the expectation value of the corresponding Hermitian operator, $\mathbb{O}$, between in and out states

$$\Delta O = \langle \text{out} | \mathbb{O} | \text{out} \rangle - \langle \text{in} | \mathbb{O} | \text{in} \rangle. \tag{5.43}$$

In quantum mechanics, the out states are related to the in states by the time evolution operator, i.e. the S-matrix: $|\text{out}\rangle = S|\text{in}\rangle$ and we can write

In order, we use the unitarity of the S-matrix, then express the S-matrex as the identity (no actual interaction) and the transfer matrix T. The commutators are then expanded and the part with the identity vanish (as $\mathbb{1}$ commutes with everything).

$$
\begin{aligned}
\Delta O &= \langle \text{in} | S^\dagger \mathbb{O} S | \text{in} \rangle - \langle \text{in} | \mathbb{O} | \text{in} \rangle \\
&\overset{S^\dagger S = \mathbb{1}}{=} \langle \text{in} | S^\dagger [\mathbb{O}, S] | \text{in} \rangle \\
&\overset{S = \mathbb{1} + iT}{=} \langle \text{in} | [\mathbb{O}, \mathbb{1} + iT] | \text{in} \rangle - \langle \text{in} | iT^\dagger [\mathbb{O}, \mathbb{1} + iT] | \text{in} \rangle \\
&= \langle \text{in} | i[\mathbb{O}, T] | \text{in} \rangle + \langle \text{in} | T^\dagger [\mathbb{O}, T] | \text{in} \rangle \\
&= \Delta O_\text{v} + \Delta O_\text{r}.
\end{aligned}
\tag{5.44}
$$

If we put in the definition of our in state (eq. 5.42) we have:

$$\Delta O = \int d\Phi_4(p_1, p_2, p_1', p_2') \, f_1(p_1) f_2(p_2) f^*_1(p_1') f^*_2(p_2') \, e^{ib_\mu \frac{p_1^\mu - p_1'^\mu}{\hbar}} \left[\mathscr{I}_\text{v}(O) - \mathscr{I}_\text{r}(O) \right]. \tag{5.45}$$

Where we define the real integrand $\mathscr{I}_\text{r}(O)$ and the virtual integrand $\mathscr{I}_\text{v}(O)$ as the following matrix elements:

$$
\begin{aligned}
\mathscr{I}_\text{v}(O) &= {}_\text{in}\langle p_1' p_2' | i[\mathbb{O}, T] | p_1 p_2 \rangle_\text{in} \\
\mathscr{I}_\text{r}(O) &= {}_\text{in}\langle p_1' p_2' | T^\dagger [\mathbb{O}, T] | p_1 p_2 \rangle_\text{in}.
\end{aligned}
\tag{5.46}
$$

[45] NB: the notation is slightly different in the [49] paper. Here we define

$$O_\text{in} | p_1 p_2 \rangle = \mathbb{O} | p_1 p_2 \rangle \tag{5.47}$$

aswell as,

$$O'_\text{in} \langle p_1' p_2' | = \langle p_1' p_2' | \mathbb{O} \tag{5.48}$$

and finally

$$\underset{p'-p}{\Delta O} = O'_\text{in} - O_\text{in} \tag{5.49}$$

Let us first look at the virtual integrand $\mathscr{I}_\text{v}(O)$:[45]

$$
\begin{aligned}
\mathscr{I}_\text{v}(O) &= {}_\text{in}\langle p_1' p_2' | i[\mathbb{O}, T] | p_1 p_2 \rangle_\text{in} \\
&= {}_\text{in}\langle p_1' p_2' | i\mathbb{O}T | p_1 p_2 \rangle_\text{in} - {}_\text{in}\langle p_1' p_2' | iT\mathbb{O} | p_1 p_2 \rangle_\text{in} \\
&= iO_\text{in}' \, {}_\text{in}\langle p_1' p_2' | T | p_1 p_2 \rangle_\text{in} - iO_\text{in} \, {}_\text{in}\langle p_1' p_2' | T | p_1 p_2 \rangle_\text{in} \\
&= i \underset{p'-p}{\Delta O} \, {}_\text{in}\langle p_1' p_2' | T | p_1 p_2 \rangle_\text{in} \\
&= i \underset{p'-p}{\Delta O} \, \tilde{\delta}^4(p_1 + p_2 - p_1' - p_2') \mathscr{A}(p_1, p_2 \to p_1', p_2').
\end{aligned}
\tag{5.50}
$$

[46] $1 = \sum_X \int d\Phi_{2+|X|}(r_1, r_2, X) | r_1 r_2 X \rangle \langle r_1 r_2 X |$

Where we could consider the states r_1, r_2, X to be the final states after the scattering

Note that the amplitude is from in states to in states! Now for the real integrand $\mathscr{I}_\text{r}(O)$ we insert a complete set of states :[46]

$$\mathscr{I}_r(O) = {}_{\text{in}}\langle p_1' p_2'|T^\dagger[O,T]|p_1 p_2\rangle_{\text{in}}$$

$$= \sum_X \int d\Phi_{2+|X|}(r_1, r_2, X) \, {}_{\text{in}}\langle p_1' p_2'|T^\dagger|r_1 r_2 X\rangle\langle r_1 r_2 X|[O,T]|p_1 p_2\rangle_{\text{in}}$$

$$= \sum_X \int d\Phi_{2+|X|}(r_1, r_2, X) \, \tilde{\delta}^4(p_1 + p_2 - r_1 - r_2 - r_X) \mathscr{A}(p_1, p_2 \to r_1, r_2, r_X)$$

$$\underset{rX-p}{\Delta O} \, \tilde{\delta}^4(p_1' + p_2' - r_1 - r_2 - r_X) \mathscr{A}^*(p_1', p_2' \to r_1, r_2, r_X).$$
$$(5.51)$$

For both integrands we can preform some variable changes and eliminate certain delta functions. We introduce momentum shifts $q_i = p_i' - p_i$ and then integrate over q_2 finally relabelling $q_1 \to q$ [47]. Thus we have

[47] Introducing the momentum shifts modifies the measure in the following way:

$$d\Phi(p_i') = d\Phi(p_i + q_i)$$
$$= \tilde{d}^4 q_i \, \tilde{\delta}((p_i + q_i)^2 - m_i^2)\Theta(p_i^0 + q_i^0)$$
$$(5.52)$$

Now since we also have the on-shell enforcing delta function from $d\Phi(p_i)$ we can rewrite the delta functions:

$$d\Phi(p_i) \, \tilde{\delta}((p_i + q_i)^2 - m_i^2)$$
$$= d\Phi(p_i)\tilde{\delta}(\underbrace{(p_i^2 - m_i^2)}_{\text{redundant}} + 2p_i \cdot q_i + q_i^2)$$
$$= d\Phi(p_i)\tilde{\delta}(2p_i \cdot q_i + q_i^2)$$
$$(5.53)$$

Finally when integrating over q_2 we choose to hit $\tilde{\delta}^{(4)}(p_1 + p_2 - p_1' - p_2') = \tilde{\delta}^{(4)}(q_1 + q_2)$ and thus we just set $q_2 = -q_1$

$$\Delta O_v = \int d\Phi_2(p_1, p_2) \, \tilde{d}^4 q \, \tilde{\delta}(2p_1 \cdot q + q^2)\Theta(p_1^0 + q^0) \, \tilde{\delta}(2p_2 \cdot q - q^2)\Theta(p_2^0 - q^0)$$

$$\times f_1(p_1)f_2(p_2)f_1^*(p_1 + q)f_2^*(p_2 - q) \, e^{-\frac{i}{\hbar}b_\mu q^\mu}$$

$$\times \underset{q}{i\Delta O} \, \mathscr{A}(p_1, p_2 \to p_1 + q, p_2 - q),$$
$$(5.54)$$

$$\Delta O_r = \sum_X \int d\Phi_{2+|X|}(r_1, r_2, X) \, d\Phi_2(p_1, p_2) \, \tilde{d}^4 q \, \tilde{\delta}(2p_1 \cdot q + q^2)\Theta(p_1^0 + q^0)$$

$$\times \tilde{\delta}(2p_2 \cdot q - q^2)\Theta(p_2^0 - q^0)$$

$$\times f_1(p_1)f_2(p_2)f_1^*(p_1 + q)f_2^*(p_2 - q) \, e^{-\frac{i}{\hbar}b_\mu q^\mu}$$

$$\times \underset{rX-p}{\Delta O}\tilde{\delta}^{(4)}(p_1 + p_2 - r_1 - r_2 - r_X)$$

$$\times \mathscr{A}(p_1, p_2 \to r_1, r_2, r_X)\mathscr{A}^*(p_1 + q, p_2 - q \to r_1, r_2, r_X).$$
$$(5.55)$$

We have arrived at an integral expression for the change in observable O. Luckily for us, we will not need to perform these integrals in the classical limit. We will just have carefully chosen replacement rules for the integrated variables! Let us look at this in more detail now.

5.3.4 Classical limit

Since we are concerned with classial observables we need to explore the classical limit of eq. 5.44, i.e. the limit of $\hbar \to 0$. The first target is the wavefunctions. We have multiple conditions on the wavefunctions. The first are those imposed by LSZ reduction. That is,

- Compact support momentum space wavefunction
- Peaked around one value of momenta

Classical limit of the wavefunctions should make sense, thus

1. as $\hbar \to 0$ the position and momentum wavefunction should approach delta functions, centered around their classical values.
2. The overlap between the wavefunction and its conjugate should be nearly full, since they represent the same particle classically.

Consider for example a nonrelativistic wavefunction for a particle of mass m:

$$f(\mathbf{p}) = \exp\left(-\frac{\mathbf{p}}{2\hbar m \ell_c / \ell_\omega^2}\right) \overset{\hbar = \ell_c m}{=} \exp\left(-\frac{\mathbf{p}}{2m^2 \ell_c^2 / \ell_\omega^2}\right), \qquad (5.56)$$

where ℓ_c is the compton wavelength of the particle $\frac{\hbar}{m}$ and ℓ_ω is a characteristic width. This wavefunction grows sharper in the $\hbar \to 0$ limit. If we now take the Fourier transform of $f(\mathbf{p})$ to gives us the position "probability density", we have:[48]

[48] A absorbs the various constants, with $A = \sqrt{2}m\frac{\ell_c}{\ell_\omega}$ and $\mathbf{x}_0$

$$
\begin{aligned}
\mathscr{F}_{\mathbf{p}}^{-1}[f](\mathbf{x}) &= \int \frac{d\mathbf{p}}{2\pi} \exp\left(-\left(\frac{\mathbf{p}}{A}\right)^2\right) \exp\left(-\frac{i}{\hbar}\mathbf{p}\cdot\mathbf{x}\right) \\
&= \frac{1}{2\pi} \underbrace{\int d\mathbf{p} \, \exp\left(-\left(\frac{\mathbf{p}}{A} - \frac{i\mathbf{x}A}{2\hbar}\right)^2\right)}_{\sqrt{\pi}A} \exp\left(-\frac{\mathbf{x}^2 A}{4\hbar^2}\right) \\
&= \frac{\sqrt{2}A}{2\pi} \exp\left(-\frac{\mathbf{x}^2}{2\ell_\omega^2}\right).
\end{aligned}
\qquad (5.57)
$$

This elucidates more clearly the meaning of characterisic width, as ℓ_ω is the width of the wavefunction in position space. Thus, the position space-wavefunction grows sharper in the $\ell_\omega^2 \to 0$ limit. For both wavefunctions to simultaneously grow sharper in the classical limit, we must then have that $\xi = \left(\frac{\ell_c}{\ell_\omega}\right)^2 \to 0$ remembering that the $\hbar \to 0$ limit is just given by the $\ell_c \to 0$ one. Finally the meaning of classical limit in this context is the $\xi \to 0$ limit.

Going back to the general conditions we want a wavefunction $f_i(p_i)$ s.t in the classical limit the momentum reaches it's classical value: $\check{p}_i = m_i \check{u}_i$, with $\check{u}_i$ the classical four-velocity of particle i, normalized to $\check{u}_i^2 = 1$.

$$\langle p_i{}^\mu \rangle = \int d\Phi(p_i)\, p_i{}^\mu |f_i(p_i)|^2 \overset{!}{=} m_i \check{u}_i^\mu (1 + \mathcal{O}(\xi^{\beta'})) \qquad (5.58)$$

where β' encodes the speed at which the classical value is reached in the $\xi \to 0$ limit. The velocity normalization convergence is controlled by β'':

$$\check{u}_i \cdot u_i = 1 + \mathcal{O}(\xi^{\beta''}) \qquad (5.59)$$

And finally wavefunction spread is controlled by β, and must converge to 0:

$$\begin{aligned}
\sigma^2(p_i)/m_i^2 &= \frac{1}{m_i^2}\langle (p_i - \langle p_i \rangle)^2 \rangle \\
&= \frac{1}{m_i^2}(\langle p_i^2 \rangle - \langle p_i \rangle^2) \\
&= \frac{1}{m_i^2}(m_i^2 - (m_i \breve{u}_i(1 + \mathcal{O}(\xi^{\beta'})))^2) \\
&\propto \xi^\beta,
\end{aligned}$$

(5.60)

where $\langle p_i^2 \rangle = m_i^2$ is enforced by the measure $\mathrm{d}\Phi(p)$.

Additionally the wavefunction should be Lorentz invariant, thus naively we would have that $f(p_i^\mu) = f'(p_i^2)$. However the integration measure enforces an on-shell condition: $m_i^2 = p_i^2$. Thus the wavefunction cannot usefully depend on p_i^2, and we need to introduce at least one additional four vector parameter u. The simplest dimensionless combination of parameters it then $\frac{p \cdot u}{m}$. Of course the wavefunction must also depend on ξ and the simplest form of argument will thus be $\frac{p \cdot u}{m\xi}$ so that any p not aligned with u will be strongly suppressed in the $\xi \to 0$ limit.

We now have control over most of the conditions:

- The classical limit is well defined
- The wavefunction spread is controlled
- The arguments of the wavefunction are clear

We can write a general wavefunction that satisfies the above as:

$$f(\frac{p \cdot u}{m}|\breve{u}_i; m_i; \beta^{(i)}).$$

(5.61)

This function can take the form of a gaussian, or something similar to eq. 5.35. Now there is one final requirement, that concerns the overlap of f and f^* must be $\mathcal{O}(1)$, equivalently and more precisely:

$$f^*(p + q) \sim f^*(p) \implies f^*(p + q) - f^*(p) \ll 1 \implies q^\mu \frac{\partial}{\partial p^\mu} f^*(p) \ll 1.$$

(5.62)

Making explicit the $\frac{p \cdot u}{m\xi}$ dependence: $f(p) = \varphi(\frac{p \cdot u}{m\xi})$ for $\varphi(x)$ a scalar function.

$$\implies \frac{q^\mu u_\mu}{m\xi} \frac{\mathrm{d}\varphi^*(x)}{\mathrm{d}x}\bigg|_{\frac{p \cdot u}{m\xi}} \ll 1.$$

(5.63)

Thus we require that for a characteristic value of $q = q_0$ we have:

$$\frac{q_0 \cdot u}{m\xi} = \bar{q}_0 \cdot u \frac{\ell_\omega^2}{\ell_c} \ll 1 \iff \bar{q}_0 \cdot u \ell_\omega \ll \sqrt{\xi},$$

(5.64)

where we denote by a bar, any quantity that has been rescaled by $\hbar$. Thus a momentum p when divided by $\hbar$ will be written $\bar{p}$ and called wavenumber. We will combine this inequality with ones we obtain from the specific cases of integrations required above.

We now want to examine the classical limit of something like eq. 5.54. If we consider just the integration over the initial momenta p_i and the initial wavefunctions with $\tilde{\delta}(2p_i \cdot q + q^2)$, the delta function will smear out to a sharply peaked function whose scale is the same order as the original wavefunctions. As ξ gets smaller, this function will turn back into a delta function imposed on the q integration. Let us examine this statement more closely. We are interested in the classical limit of the integrals such as:

$$d(m, \xi, u, q) = \int d\Phi(p)\, \tilde{\delta}(2p \cdot q + q^2)\Theta(p^0 + q^0)\varphi(\frac{p \cdot u}{m\xi})\varphi^*(\frac{(p+q) \cdot u}{m\xi}).$$
$$(5.65)$$

This integral must be Lorentz invariant and depends on m, ξ, u, q thus it must manifestly only depend on the following Lorentz invariants: $u^2, q^2, u \cdot q, \xi$. One of these is not actually a variable as we will normalise $u^2 = 1$. The rest aren't fully dimensionless, and we can render them dimensionless:

$$[q^2] = [\hbar \bar{q}]^2 = [M]^2 \implies [\ell_c\sqrt{-\bar{q}^2}] = [\frac{\hbar}{m}\sqrt{-\bar{q}^2}] = \frac{[M]}{[M]} = 1,$$

$$[u \cdot q] = [M] \implies [\frac{u \cdot \bar{q}}{\sqrt{-\bar{q}^2}}] = [\frac{u \cdot q}{\sqrt{-q^2}}] = \frac{[M]}{[M]} = 1, \qquad (5.66)$$

$$[\xi] = 1.$$

[49] t $[\frac{1}{\sqrt{-\bar{q}^2}}] = [T] = [L] = [\ell_s]$

If we call $\frac{1}{\sqrt{-\bar{q}^2}} = \ell_s$ a scattering length[49] then our dimensionless ratios become :
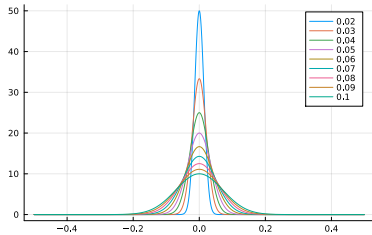
$$\frac{\ell_c}{\ell_s} \quad \text{and} \quad \ell_s \bar{q} \cdot u. \qquad (5.67)$$

The delta function can then be rewritten as:

$$\tilde{\delta}(2p \cdot q + q^2) = \tilde{\delta}(2\hbar m\, u \cdot \bar{q} + \hbar^2 \bar{q}^2) = \frac{1}{\hbar m}\tilde{\delta}(2\bar{q} \cdot u - \frac{\ell_c}{\ell_s^2}) = \frac{\ell_s}{\hbar m}\tilde{\delta}(2\ell_s \bar{q} \cdot u - \frac{\ell_c}{\ell_s}).$$
$$(5.68)$$

Performing the integration over p in eq. 5.65 we obtain symbolically:

$$d(m, \xi, u, q) = \text{peaked function imposing that } 2\ell_s \bar{q} \cdot u = \frac{\ell_c}{\ell_s} \text{ with width } \xi^\beta.$$
$$(5.69)$$

54

Let us disucss the wavefunction and the scales a bit more physically. The characteristic width ℓ_ω is the particle's position uncertainty, $\frac{\hbar}{\ell_\omega}$ is the associated momentum uncertainty. In the classical limit it makes sense that the position uncertainty is neglible with respect to minimum distance between the particles ℓ_s:

$$\ell_\omega \ll \ell_s, \tag{5.70}$$

and the momentum uncertainty is neglible with respect to the masses of the particles:

$$\frac{\hbar}{\ell_\omega} \ll m \implies \ell_c \ll \ell_\omega. \tag{5.71}$$

Putting these together we obtain the goldilocks inequality:

$$\ell_c \ll \ell_\omega \ll \ell_s. \tag{5.72}$$

Now we can go back and look at the arguments of d and we see that

$$\ell_s \bar{q} \cdot u \gg \ell_\omega \bar{q} \cdot u \sim \sqrt{\xi} = \frac{\ell_c}{\ell_\omega} \gg \frac{\ell_c}{\ell_s}. \tag{5.73}$$

Thus in the classical limit we have that d collapses to:

$$d(m, \xi, u, q) \propto \tilde{\delta}(\bar{q} \cdot u). \tag{5.74}$$

Thus the wavefunction-weighted on-shell phase-space integration disappears in the classical limit! The only condition is that the integration momenta take on their physical values. The sequence that we have gone through should be done for all the integrands of type d. We will not do this explicitly every time but instead apply the following rules:

1. Just as for the massless transfer momentum any messenger momentum, be it transfer, virtual-loop or real emmission, shall become a wavenumber: $k \to \hbar\bar{k}$.
2. Replace all couplings with their dimensionless counterparts: $\kappa \to \frac{\kappa}{\sqrt{\hbar}}$ (this is only precisely true for SQED and gravity, which are the applications we are interested in).
3. Eliminate all on-shell integrations by approximating $f(p + \hbar\bar{q})$ by $f(p)$.
4. Laurent expand all the integrands in $\hbar$.
5. Make the integration momenta take on their physical values: $p_i \to m_i \breve{u}_i$.

To make this idea explicit we introduce the following notation, meaning that the steps above have been applied:

$$\left\langle g(p_1, p_2, \dots) \right\rangle \overset{\text{def}}{=} \int \, d\Phi(p_1) \, d\Phi(p_2) \, |f_1(p_1)|^2 |f_2(p_2)|^2 \, g(p_1, p_2, \dots)$$
(5.75)

We can now rewrite eq. 5.44:

$$\Delta O = \Bigg\langle \int \overbrace{\tilde{d}^4 q \, \tilde{\delta}(2p_1 \cdot q + q^2)\Theta(p_1{}^0 + q^0)\tilde{\delta}(2p_2 \cdot q - q^2)\Theta(p_2{}^0 + q^0)}^{d\Psi(q)} \, e^{-\frac{i}{\hbar}q^\mu b_\mu} \Big(\mathscr{I}_{\mathrm{v}}'(O) + \mathscr{I}_{\mathrm{r}}'(O)$$
(5.76)

where

$$\mathscr{I}_{\mathrm{v}}'(O) = i \underset{q}{\Delta O} \mathscr{A}(p_1, p_2 \to p_1 + q, p_2 - q)$$

$$\mathscr{I}_{\mathrm{r}}'(O) = \sum_X \int \, d\Phi_{2+|X|}(r_1, r_2, X) \underset{rX-p}{\Delta O} \tilde{\delta}^{(4)}(p_1 + p_2 - r_1 - r_2 - r_X)$$
(5.77)

$$\times \mathscr{A}(p_1, p_2 \to r_1, r_2, r_X)\mathscr{A}^*(p_1 + q, p_2 - q \to r_1, r_2, r_X).$$

Additionally we want to make clear the dependence on $\hbar$ since we want to eventually take the $\hbar \to 0$ limit. We apply step 1. above, and change integration variables to $\bar{q} = \frac{q}{\hbar}$ and absorb that $\hbar$ dependence into the redefinition of the integrands and the measure:

$$d\Psi(q) = \hbar^2 \, d\overline{\Psi}(\bar{q}) = \hbar^4 \, \tilde{d}^4 \bar{q} \, \frac{1}{\hbar}\tilde{\delta}(2p_1 \cdot \bar{q} + \hbar\bar{q}^2)\Theta(p_1{}^0 + q^0) \frac{1}{\hbar}\tilde{\delta}(2p_1 \cdot \bar{q} + \hbar\bar{q}^2)\Theta(p_2{}^0 + q^0),$$
(5.78)

$$\overline{\mathscr{I}_{\mathrm{v}}'}(O) = \hbar^2 \mathscr{I}_{\mathrm{v}}'(O),$$
$$\overline{\mathscr{I}_{\mathrm{r}}'}(O) = \hbar^2 \mathscr{I}_{\mathrm{r}}'(O).$$
(5.79)

We can finally neatly write:

$$\Delta O = \left\langle \int \, d\overline{\Psi}(\bar{q}) \, e^{-i\bar{q}^\mu b_\mu} \Big(\overline{\mathscr{I}_{\mathrm{v}}'}(O) + \overline{\mathscr{I}_{\mathrm{r}}'}(O) \Big) \right\rangle.$$
(5.80)

Now the $\hbar$ dependence is all in the integrands (ignoring the $\hbar\bar{q}^2$ factors in the delta function). The classical limit of this observable is then simply, dropping the angle brackets, since these dissappear in the classical limit:

$$\Delta O_{\mathrm{classical}} = \lim_{\hbar \to 0} \hbar^{\beta_{LO}} \Big[\int \, d\overline{\Psi}(\bar{q}) \Big(\overline{\mathscr{I}_{\mathrm{v}}'}(O) + \overline{\mathscr{I}_{\mathrm{r}}'}(O) \Big) \Big],$$
(5.81)

56

where β_{LO} is the LO $\hbar$-dependence of the observable. This is so that $\Delta O_{\text{classical}} \sim \hbar^0$ i.e. classical scaling.

5.4 Impulse in KMOC

We can now explore the integrands for a specific observable. Consider the momentum of particle 1, $p_1{}^\mu$, then the change in momentum is essentially the impulse of particle 1. The KMOC formalisms gives us a way to write this as:

$$\Delta p_1{}^\mu = \left\langle \int \mathrm{d}\overline{\Psi}(\bar{q}) \, \exp\left(-i\bar{q}^\mu b_\mu\right)\left(\overline{\mathcal{I}_v'}(p_1{}^\mu) + \overline{\mathcal{I}_r'}(p_1{}^\mu)\right)\right\rangle. \qquad (5.82)$$

We then have:

$$\overline{\mathcal{I}_v'}(p_1{}^\mu) = \hbar^2 i\,\overset{\circ}{q}\, \mathcal{A}(p_1, p_2 \to p_1 + \hbar\bar{q}, p_2 - \hbar\bar{q})$$
$$\overline{\mathcal{I}_r'}(p_1{}^\mu) = \hbar^2 \quad \mathrm{d}\Phi_{2+|X|}(r_1, r_2, r_X)\,(r_1^\mu - p_1^\mu)\,\tilde{\delta}^{(4)}(p_1 + p_2 - r_1 - r_2 - r_X)$$
$$\times\, \mathcal{A}(p_1, p_2 \to r_1, r_2, r_X)\mathcal{A}^*(p_1 + \hbar\bar{q}, p_2 - \hbar\bar{q} \to r_1, r_2, r_X). \qquad (5.83)$$

We can extract $\hbar$ from q and from the amplitude, by extracting each coupling constant κ along with an $\frac{1}{\sqrt{\hbar}}$, thus quartic vertices yield a factor of $\frac{\kappa^2}{\hbar}$ whereas cubic ones yield $\frac{\kappa}{\sqrt{\hbar}}$ [50]. If we count the number V_3 of all cubic vertices, V_4 the number of quartic vertices, and so on, we have that the number of internal lines is $I = \frac{1}{2}(\sum_{d=3} dV_d - E)$. This is because we have $\sum_{d=3} dV_d$ lines to start with, out of which E are chosen to be external. The remaining $(\sum_{d=3} dV_d - E)$ ones are contracted among themselves to form I internal lines. In our case we have $E = 4 + M$ where $M = |X|$ is the number of messenger particles. Using the argument from loop counting we have that the number of loops of our graph L is given by:

$$\begin{aligned} L = I - V + N &= \frac{1}{2}(\sum_{d=3} d \cdot V_d - 4 - M) - \sum_{d=3} V_d + 1 \\ &= \frac{1}{2}(\sum_{d=3}(d-2)V_d) - 1 - \frac{M}{2}, \end{aligned} \qquad (5.84)$$

where N is the number of connected components ($= 1$ in our case) . Thus we see that the amount of extracted $\hbar$s corresponds directly to the number of loops plus one[51]! We can thus write the amplitude $\mathcal{A}$ as a sum over reduced L-loop amplitudes $\bar{\mathcal{A}}^{(L)}$:

$$\mathcal{A}(p_1, p_2 \to r_1, r_2, X) = \sum_{L=0}^{\infty} \left(\frac{\kappa^2}{\hbar}\right)^{\left(L+1+\frac{|X|}{2}\right)} \bar{\mathcal{A}}^{(L)}(p_1, p_2 \to r_1, r_2, X). \qquad (5.85)$$

[50] as mentioned in the last section, this is true for gravity and SQED and we will extend this fact to schematically rescale the vertex coupling by $\hbar^{-\frac{d-2}{2}}$, for d the degree of the vertex in question.

[51] and the number of extracted couplings being twice that

Going back to the integrands we have:

$$\overline{\mathcal{F}_v'}(p_1{}^\mu) = \hbar^3 \mathring{i} \bar{q} \sum_{L=0}^{\infty} \left(\frac{\kappa^2}{\hbar}\right)^{(L+1)} \bar{\mathcal{A}}^{(L)}(p_1, p_2 \to p_1 + \hbar\bar{q}, p_2 - \hbar\bar{q})$$

$$= \mathring{i}\hbar\bar{q} \sum_{L=0}^{\infty} \kappa^{2(L+1)}\hbar^{(1-L)}\bar{\mathcal{A}}^{(L)}(p_1, p_2 \to p_1 + \hbar\bar{q}, p_2 - \hbar\bar{q}), \tag{5.86}$$

as well as the real kernel:[52]

[52] We changed the integration variable from r_i to $w_i = r_i - p_i$ thus the measure changes:

$$d\Phi_{2+|X|}(r_1, r_2, X) = d\Phi_{|X|}(r_X) \prod_{i=1,2} \tilde{d}^4 w_i \, \tilde{\delta}(2p_i \cdot w_i + w_i^2)\Theta(p_i^0 + w_i^0) \tag{5.87}$$

where we used the same reasoning as for the q_i variable change.

$$\overline{\mathcal{F}_r'}(p_1{}^\mu) = \hbar^2 \int d\Phi_{|X|}(r_X) \left[\prod_{i=1,2} \tilde{d}^4 w_i \, \tilde{\delta}(2p_i \cdot w_i + w_i^2)\Theta(p_i^0 + w_i^0)\right]$$

$$\times w_1^\mu \, \delta^{(4)}(w_1 + w_2 + r_X)$$

$$\times \mathcal{A}(p_1, p_2 \to p_1 + w_1, p_2 + w_2, r_X)\mathcal{A}^*(p_1 + \hbar\bar{q}, p_2 - \hbar\bar{q} \to p_1 + w_1, p_2 + w_2, r_X) \tag{5.88}$$

$$= \hbar^2 \int d\Phi_{|X|}(r_X)\left[\prod_{i=1,2} \hbar^3 \, \tilde{d}^4 \bar{w}_i \, \tilde{\delta}(2p_i \cdot \bar{w}_i + \hbar\bar{w}_i^2)\Theta(p_i^0 + \hbar\bar{w}_i^0)\right]$$

$$\times \hbar\bar{w}_1^\mu \, \hbar^{-4}\delta^{(4)}(\bar{w}_1 + \bar{w}_2 + \bar{r}_X)$$

$$\times \sum_{L=0}^{\infty}\left(\frac{\kappa^2}{\hbar}\right)^{(2L+2+|X|)}\bar{\mathcal{A}}^{(L)}(p_1, p_2 \to p_1 + \hbar\bar{w}_1, p_2 + \hbar\bar{w}_2, r_X)$$

$$\times \bar{\mathcal{A}}^{*(L)}(p_1 + \hbar\bar{q}, p_2 - \hbar\bar{q} \to p_1 + \hbar\bar{w}_1, p_2 + \hbar\bar{w}_2, r_X) \tag{5.89}$$

$$= \int d\Phi_{|X|}(r_X)\left[\prod_{i=1,2} \tilde{d}^4 \bar{w}_i \, \tilde{\delta}(2p_i \cdot \bar{w}_i + \hbar\bar{w}_i^2)\Theta(p_i^0 + \hbar\bar{w}_i^0)\right]$$

$$\times \hbar\bar{w}_1^\mu \, \delta^{(4)}(\bar{w}_1 + \bar{w}_2 + \bar{r}_X)$$

$$\times \sum_{L=0}^{\infty}\kappa^{2(2L+2+|X|)}\hbar^{2-2L-|X|}\bar{\mathcal{A}}^{(L)}(p_1, p_2 \to p_1 + \hbar\bar{w}_1, p_2 + \hbar\bar{w}_2, r_X)$$

$$\times \bar{\mathcal{A}}^{*(L)}(p_1 + \hbar\bar{q}, p_2 - \hbar\bar{q} \to p_1 + \hbar\bar{w}_1, p_2 + \hbar\bar{w}_2, r_X). \tag{5.90}$$

Schematically we have

$$\overline{\mathcal{F}_v'}(p_1{}^\mu) = \sum_{L=0}^{\infty} \mathcal{O}(\kappa^{2(L+1)}),$$

$$\overline{\mathcal{F}_r'}(p_1{}^\mu) = \sum_{L=0}^{\infty} \mathcal{O}(\kappa^{4(L+1)+2|X|}) \tag{5.91}$$

The contributions from the virtual kernel are lower order in the coupling κ for a given loop order. Both kernels contribute together provided that the following equation is verified:

$$L - 1 = 2L' + |X|. \tag{5.92}$$

Where L is the loop count for the virtual kernel and L', $|X|$ are the real kernel loop count and messenger particle count respectively. Note that for a tree level virtual kernel, the real-kernel match does not exist. The real kernel is only present for $L > 0$. When taking the classical limit we will only retain contributions from graphs that cancel the $\hbar$ divergences in each corresponding kernel. Thus at L loop level, the amplitude in the virtual kernel must cancel with:

$$\hbar^{1-L+O}, \tag{5.93}$$

where the O term is the order of $\hbar$ that is present as a result of the observable. In the case of particle 1's momentum, $O = 1$. Similarly, the amplitudes in the real kernel must cancel with:

$$\hbar^{2-2L'-|X|+O}. \tag{5.94}$$

Now we see that the LO contribution [53] to the impulse $\Delta p_1^{\mu,(0)}$ can only be from the virtual kernel at tree level. Thus we have the following equation,

$$\Delta p_1^{\mu,(0)} = \left\langle \int \mathrm{d}\overline{\Psi}(\bar{q}) \, \exp\left(-i\bar{q}^\mu b_\mu\right) \overline{\mathscr{J}_{\mathrm{v}}'}(p_1{}^\mu)^{(L=0)} \right\rangle. \tag{5.95}$$

And the integrand is given by the tree level 4 point amplitude.

$$\overline{\mathscr{J}_{\mathrm{v}}'}(p_1{}^\mu)^{L=0} = \mathring{i}\,\bar{q}^\mu \kappa^2 \hbar^2 \bar{\mathscr{A}}^{(0)}(p_1, p_2 \to p_1 + \hbar\bar{q}, p_2 - \hbar\bar{q}). \tag{5.96}$$

At Next-to-Leading Order (NLO), i.e. κ^4 order, both integrands contribute, as eq. 5.92 can be satisfied for $L = 1$, $L' = 0$ and $|X| = 2$. Thus we have the following equation:

$$\Delta p_1^{\mu,(1)} = \left\langle \int \mathrm{d}\overline{\Psi}(\bar{q}) \, \exp\left(-i\bar{q}^\mu b_\mu\right)\left(\overline{\mathscr{J}_{\mathrm{v}}'}(p_1{}^\mu)^{(L=1)} + \overline{\mathscr{J}_{\mathrm{r}}'}(p_1{}^\mu)^{(L'=0)}\right) \right\rangle. \tag{5.97}$$

The virtual integrand is now given by the 1-loop level amplitude, and the real integrand is given by the square of a the tree level amplitude. This process can go on indefinetely, and is general to the the type of observable and the theory. Here we considered the change of momentum a particle, which for a black hole very far away would be very difficult to measure. However, we can also consider an observable such as the four-momentum of the radiated particles, or more precisely its expection value. Of course the operator corresponding to this observable gives zero

[53] Here the expansion is in powers of the coupling constant, so even though we want $\hbar$s to cancel, the loop order will still affect the order of the contribution through the coupling constant κ and the LO corresponds to κ

when acting on the initial momentum states, and only gives a non-zero result when acting on the messenger states. Thus for this observable only the real integrand, starting with $|X| = 1$ will contribute, the LO contrybution being given by what is essentially the unitarity cut of a two loop amplitude. We see that regardless of observable, the objects that are needed are the amplitudes.

For each loop level, many diagrams can contribute, but the classical limit enforces that they must cancel the $\hbar$ orders given by eq. 5.94 and eq. 5.93. The cancellation order is dependent on the considered observable and filters the contributing diagrams. It can also be reformulated in the language of the method of regions.

To see the whole machinery in action, let us take SQED as an example theory, that shows the relevant subleties of the formalism.

5.5 SQED amplitudes

We want to couple a set of massive scalar fields to electromagnetism. We will use the minimal coupling prescirption to ensure that the resulting lagrangian exhibits the required gauge symmetry. The minimal coupling prescription works provided that our base mass lagrangian admits a conserved current. Our base mass lagrangian for two complex scalar fields is:

$$\mathscr{L}_m = \sum_{i=1}^{2} \partial_\mu \phi_i^\dagger \, \partial^\mu \phi_i - m_i^2 \phi_i^\dagger \phi_i. \tag{5.98}$$

Notice that under the following transformation:

$$\begin{aligned} \phi_i(x) &\to e^{-iQ_i\lambda}\phi_i(x), \\ \phi_i^\dagger(x) &\to e^{iQ_i\lambda}\phi_i^\dagger(x), \end{aligned} \tag{5.99}$$

or infinitesimally:

$$\begin{aligned} \delta\phi_i &= -\mathring{i}\phi_i Q_i \delta\lambda, \\ \delta\phi_i^\dagger &= \mathring{i}\phi_i^\dagger Q_i \delta\lambda, \end{aligned} \tag{5.100}$$

the above Lagrangian is unchanged. We will identitfy Q_i with the charge, in units of e, of each particle. Note the sign of the transformation is important. If we upgrade the parameter λ to a spacetime function $\lambda(x)$, the Lagrangian is not invariant anymore and invariance is restored if we replace all the derivatives ∂_μ with the gauge-covariant derivative D_μ, i.e. if along with the transformation above, we perform a gauge transformation of the photon field:

$$A_\mu \to A_\mu + \frac{1}{e}\partial_\mu\lambda \qquad (5.101)$$

or infinitesimally

$$\delta A_\mu = \frac{1}{e}\partial_\mu\delta\lambda, \qquad (5.102)$$

then the whole lagrangian:

$$\mathscr{L}_{ED} + \mathscr{L}_m(\phi_i, \partial_\mu\phi_i) \to \mathscr{L}_{ED} + \mathscr{L}_m(\phi_i, D_\mu\phi_i), \qquad (5.103)$$

is invariant under the above defined gauge transformation, with the gauge-covariant derivative defined as:

$$D_\mu = \partial_\mu + i\,e\,Q_i\,A_\mu. \qquad (5.104)$$

The final lagrangian is:

$$\mathscr{L} = -\frac{1}{4}F_{\mu\nu}F^{\mu\nu} + \sum_{i=1}^{2}\left[\left(D_\mu\phi_i\right)^\dagger\left(D^\mu\phi_i\right) - m_i^2\phi_i^\dagger\phi_i\right], \qquad (5.105)$$

with $F_{\mu\nu} \equiv \partial_\mu A_\nu - \partial_\nu A_\mu$. Expanding and then integrating by parts:

$$\mathscr{L} = -\frac{1}{4}\left(\partial_\mu A_\nu - \partial_\nu A_\mu\right)\left(\partial^\mu A^\nu - \partial^\nu A^\mu\right) + \sum_{i=1}^{2}\left[\left(\partial_\mu - i\,e\,Q_i\,A_\mu\right)\phi_i^\dagger\left(\partial_\mu + i\,e\,Q_i\,A_\mu\right)\phi_i - m_i^2\phi_i^\dagger\phi_i\right]$$

$$= \underbrace{\frac{1}{2}A_\mu\left[\eta^{\mu\nu}\partial^2 - \partial^\mu\partial^\nu\right]A_\nu + \sum_{i=1}^{2}-\phi_i^\dagger\left(\partial^2 + m_i^2\right)\phi_i}_{\mathscr{L}_0} + \underbrace{\sum_{i=1}^{2}q_i^2\,e^2\,A_\mu A^\mu\,\phi_i^\dagger\phi_i - i\,e\,Q_i\,A_\mu\left(\phi_i^\dagger\partial^\mu\phi_i - \left(\partial^\mu\phi_i^\dagger\right)\phi_i\right)}_{\mathscr{L}'}. $$
$$(5.106)$$

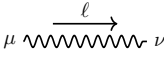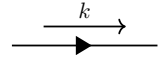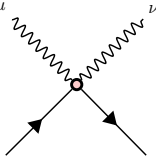Since we have a massless photon, and still have gauge freedom we have to implement gauge fixing in the usual way:
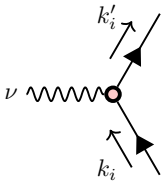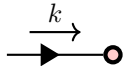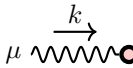
$$\mathscr{L}_{\text{eff}} = \mathscr{L} + \overbrace{\frac{-1}{2\xi}(\partial_\mu A^\mu)^2}^{\mathscr{L}_{\text{GF}}}$$

$$= \frac{1}{2}A_\mu\underbrace{\left[g^{\mu\nu}\partial^2 - \left(1 - \frac{1}{\xi}\right)\partial^\mu\partial^\nu\right]}_{\to \tilde{D}_\xi^{\mu\nu}(k) = \frac{-i}{k^2+i\varepsilon}\left[g_{\mu\nu}-(1-\xi)\frac{k_\mu k_\nu}{k^2}\right]}A_\nu + \sum_{i=1}^{2}-\phi_i^\dagger\underbrace{\left(\partial^2 + m_i^2\right)}_{\tilde{\Delta}_F(q^2)=\frac{i}{p^2-m^2+i\varepsilon}}\phi_i$$

$$+ \sum_{i=1}^{2}\underbrace{Q_i^2\,e^2\,\eta^{\mu\nu}}_{\times 2 i \to 4-\text{vertex}}A_\mu A_\nu\,\phi_i^\dagger\phi_i \underbrace{- i\,e\,Q_i\,A_\mu\left(\phi_i^\dagger\partial^\mu\phi_i - \left(\partial^\mu\phi_i^\dagger\right)\phi_i\right)}_{\times i \to 3-\text{vertex}}.$$
$$(5.107)$$

61

Where in the last lines we identify the terms contributing to the feyman rules. Our fields are given by the usual:

$$\phi(x) = \int \frac{d^3\mathbf{p}}{(2\pi)^{3/2}\sqrt{2\omega_\mathbf{p}}} \left[b_\mathbf{p} e^{-ip\cdot x} + c_\mathbf{p}^\dagger e^{ip\cdot x} \right]$$

$$\phi^*(x) = \int \frac{d^3\mathbf{p}}{(2\pi)^{3/2}\sqrt{2\omega_\mathbf{p}}} \left[b_\mathbf{p}^\dagger e^{ip\cdot x} + c_\mathbf{p} e^{-ip\cdot x} \right].$$

(5.108)

The Feynman rules are given in Table 5.2

Tbl 5.2: Feynman rules for SQED

For every		Write
	internal photon line	$\tilde{D}_\xi^{\mu\nu}(\ell) = \frac{-\mathring{i}}{\ell^2+i\varepsilon}\left[\eta_{\mu\nu} - (1-\xi)\frac{\ell_\mu\ell_\nu}{ell^2}\right]$
	internal scalar	$\tilde{\Delta}_F(k^2) = \frac{\mathring{i}}{k^2-m^2+i\varepsilon}$
	$\phi_i\phi_i^\dagger A_\mu A_\nu$ vertex	$2\mathring{i}Q_i^2 e^2 \eta^{\mu\nu}$
	$\phi_i(k_i)\phi_i^\dagger(k_i')A_\mu$ vertex	$\mathring{i}e Q_i (k_i^\mu - k_i'^\mu)$
	External scalar	$\times 1$
	$\left\{\begin{array}{c} \text{incoming} \\ \text{outgoing} \end{array}\right\}$ photon	$\times\left\{\begin{array}{c} \varepsilon_\mu \\ \varepsilon_\mu^{*\prime} \end{array}\right\}$, with $\varepsilon\cdot k = 0, \varepsilon'\cdot k' = 0$

where we consider only incoming momenta and the arrows denote incoming or outgoing particles.

For the photon, we will take the Feynamn gauge, setting $\xi = 1$ and thus $\tilde{D}_1^{\mu\nu}(\ell) = \tilde{D}^{\mu\nu}(\ell) = \frac{-\mathring{i}\eta^{\mu\nu}}{\ell^2+i\varepsilon}$. Notice that if we rescale all photon momenta

(taking them to be the loop momenta) by $\hbar$ or equivalently take them to be in the soft region: $|k| \sim |q| \ll |p|$, where p is the external momenta, then the photon propagator scales homgenously in $\hbar$, typically:

$$\frac{1}{(\ell - q)^2} = \frac{1}{\hbar^2} \frac{1}{(\bar{\ell} - \bar{q})^2}, \tag{5.109}$$

thus contributes $\mathcal{O}(\hbar^{-2})$ to the overall diagram. The matter propagator on the other hand, has inhomgenous $\hbar$ scaling, as we do not rescale the external momenta, (or equivalently the external momenta are not restricted by the regions). Note that we will not consider internal mass loops as the soft limit means that massive pair production is forbidden, thus massive propagators necessarily contain an external momentum. We can notheless expand a generic massive propagator in the soft limit:

$$\frac{1}{(\ell - p_i)^2 - m_i^2} = \frac{1}{\ell^2 - 2\ell \cdot p_i + \not{p_i^2} - \not{m_i^2}} = \frac{1}{\hbar^2 \bar{\ell}^2 - 2\hbar \bar{\ell} \cdot p_i}$$
$$= -\frac{1}{\hbar} \frac{1}{2\bar{\ell} \cdot p_i} \left(1 + \hbar \frac{\bar{\ell}^2}{2\bar{\ell} \cdot p_i} + \hbar^2 \frac{\bar{\ell}^4}{(2\bar{\ell} \cdot p_i)^2} + ...\right). \tag{5.110}$$

In other contexts one may say that the matter propagator has eikonalized (linearized). Before we compute the amplitudes let us set up some useful kinematic identities and variables. If we consider the two-to-two particle scattering, taking an all outgoing momentum convention we have the following masses:

$$m_1^2 = p_4^2 = p_1^2, \quad m_2^2 = p_2^2 = p_3^2, \tag{5.111}$$

and mandelstam variables:

$$s = (p_1 + p_2)^2, \quad t = q^2 = (p_1 + p_4)^2, \quad u = (p_1 + p_3)^2, \tag{5.112}$$

subject to the usual constraint:

$$s + t + u = 2(m_1^2 + m_2^2). \tag{5.113}$$

We can also change the external momentum variables to ones more amenable to the soft limit, namely:

$$p_1 = -\left(\tilde{p}_1 - \frac{q}{2}\right), p_2 = -\left(\tilde{p}_2 + \frac{q}{2}\right), p_3 = \left(\tilde{p}_2 - \frac{q}{2}\right), p_4 = \left(\tilde{p}_1 + \frac{q}{2}\right). \tag{5.114}$$

The new momentum variables $\tilde{p}_i$ are crucially orthogonal to momentum transfer q :[54]

[54] we use eq. 5.111

63

$$\tilde{p}_i \cdot q = 0, \tag{5.115}$$

and the physical scattering region, given by $s > (m_1 + m_2)^2$ and $q^2 < 0$ is the given by the same formulas:

$$s = \left(-\left(\tilde{p}_1 - \frac{q}{2} \right) - \left(\tilde{p}_2 + \frac{q}{2} \right) \right)^2 = (\tilde{p}_1 + \tilde{p}_2)^2 \tag{5.116}$$

and

$$t = \left(-\left(\tilde{p}_1 - \frac{q}{2} \right) + \tilde{p}_1 + \frac{q}{2} \right)^2 = q^2. \tag{5.117}$$

With all the ingredients in place, we can now go on to computing the amplitudes.

5.5.1 Tree level

We start with the tree level amplitude, the only LO contribution in for example eq. 5.95. The only possible diagram we can build with four external scalar legs, and vertices as defined in Table 5.2, is the following tree:

$$i\bar{\mathscr{A}}^{(0)}\left(\tilde{p}_1 - \frac{q}{2}, \tilde{p}_2 + \frac{q}{2} \to \tilde{p}_1 + \frac{q}{2}, \tilde{p}_2 - \frac{q}{2}\right) =$$

Tree

The amplitude is read off diagram and using Feynman rules for SQED we have:

$$\mathscr{A}^{(0)} = i\tilde{D}^{\mu\nu}(q) \cdot e^2 Q_1 Q_2 2\tilde{p}_1{}^{\mu} 2\tilde{p}_2{}^{\nu} = \frac{4e^2 Q_1 Q_2 \tilde{p}_1 \cdot \tilde{p}_2}{q^2}, \tag{5.118}$$

using the mandelstahm invariants described above we can infact write this as:

$$\bar{\mathscr{A}}^{(0)} = e^2 Q_1 Q_2 \frac{4m_1 m_2 \sigma}{\hbar^2 \bar{q}^2}, \tag{5.119}$$

where σ is the relativistic factor of particle 1 in the rest frame of particle 2:

$$\sigma = \frac{s - m_1^2 - m_2^2}{2m_1 m_2} = \frac{p_1 \cdot p_2}{m_1 m_2} = \frac{\tilde{p}_1 \cdot \tilde{p}_2}{m_1 m_2} + \mathcal{O}(\hbar). \qquad (5.120)$$

We now input the reduced version $\bar{\mathscr{A}}^{(0)} e^2 = \mathscr{A}^{(0)}$ of the amplitude, and take the $\hbar \to 0$ limit of eq. 5.95. We can safely take the $\hbar \to 0$ limit as the integrand contains no terms singular in $\hbar$ (the $\frac{1}{\hbar^2}$ is cancelled by the $\hbar^2$ pre-factor). Notice that the integration measure eq. 5.76 simplifies in the classical limit:[55]

$$\lim_{\hbar \to 0} \mathrm{d}\overline{\Psi}(\bar{q}) = \tilde{\mathrm{d}}^4 \bar{q}\, \tilde{\delta}(2\widetilde{\tilde{p}_1 \cdot \bar{q}}) \tilde{\delta}(2\widetilde{\tilde{p}_1 \cdot \bar{q}}). \qquad (5.122)$$

The integrand corresponding to the LO contribution to the impulse is then:

$$\Delta p_1^{\mu,(0)} = 4e^2 Q_1 Q_2 m_1 m_2 \sigma \int \tilde{\mathrm{d}}^4 \bar{q}\, e^{-i\bar{q}\cdot b}\, \bar{q}^\mu\, \frac{\cancel{\hbar^2}}{\cancel{\hbar^2} \bar{q}^2}. \qquad (5.123)$$

This can be analytically computed (see LO impulse SQED) to find a closed form for the LO impulse.

$$\Delta p_1^{\mu,(0)} = -\frac{e^2 Q_1 Q_2}{2\pi} \frac{\gamma}{\sqrt{\gamma^2 - 1}} \frac{b^\mu}{b^2} \qquad (5.124)$$

5.5.2 One loop

Already at one loop the number of possible diagrams one can for increases dramatically from 1 to 13. One can nonetheless relatively easily enumerate them. As we increase loop count, the number of diagrams increases exponentially. It is therefore very useful to have a systematic, programmatic way to handle these diagrams, and while we are at it, also to compute the amplitudes. Note that all the code needed to do these computations can be found on the repository for this book.

The first tool we will use is `QGRAF` [56], a fortran program that can generate Feynman diagrams for a given set of vertices and external legs. The first step to is to define the theory we are working in. This is essentially writing down the Feyman rules, without actually specifying what the graphical objects are. For SQED the model file is short:

SQEDmodel

```
* propagators
[Phi1,Phi1c,+]
```

[55] Compare to

$$\mathrm{d}\overline{\Psi}(\bar{q}) = \tilde{\mathrm{d}}^4 \bar{q}\, \tilde{\delta}(2p_1 \cdot \bar{q} + \hbar \bar{q}^2)\Theta(p_1{}^0 + q^0)$$
$$\tilde{\delta}(2p_1 \cdot \bar{q} + \hbar \bar{q}^2)\Theta(p_2{}^0 + q^0)$$
$$(5.121)$$

The theta functions cancel as $q^0 \to 0$ and p_i becomes classical. Changing to the special kinematic variables eq. 5.114 we can even eliminate the delta functions, since by constuction $\tilde{p}_1 \cdot \bar{q} = 0$.

```
[Phi2,Phi2c,+]
[Photon,Photon,+]

* vertices
[Phi1c,Photon,Phi1]
[Phi2c,Photon,Phi2]
[Phi1c,Photon,Photon,Phi1]
[Phi2c,Photon,Photon,Phi2]
```

This file also defines the names of the fields in question. We can then give QGRAF additional options, such as the number of external legs, and the number of loops, written in a qgraf.dat file that can look like this:

qgraf.dat

```
output= '{{output filename}}' ;
style= './styles/julia.sty' ;

model= './qgraf/SQEDmodel';

in= Phi1,  Phi2;
out= Phi1,Phi2;
loops= 1;
loop_momentum= k;

options=  notadpole,nosnail,onshell ;
```

where we specify what process we are interested in (two-to-two scattering). We also specify that we want to compute the one loop amplitude, and that we want to use the julia.sty style file. The julia.sty file is a style file that is used to generate the output in a format that can be read by a Julia [57] package built to process and visualise the outputted graphs. This package is called (maybe too broadly) QFT.jl is hosted on github . Let us see it in action. We can run QGRAF from the command line, and it will generate a file called {{output filename}} that contains the output of the program. We can then use this in a Julia file to visualise the diagrams.

```
using Images
using QFT
using QFT.Diagrams
using QFT.FieldGraphs
using QFT.Fields
import  Catlab.Graphics.Graphviz: pprint
include("SQED.jl")
diags=include("QGRAFout/julia/1lSQED.jl")
```

```
qDiags=[qDiagram(;diag...) for diag in diags]
grafs=(x → x.g).(qDiags)
println("::: {#fig-oneloopsqed  layout-ncol=3}")
for (i,graf) in enumerate(grafs)
println("```{dot}")
println("//| fig-width: 1.5")
    pprint(stdout,to_graphviz(graf,graph_attrs=Dict("layout"⇒"neato")))
    println("```")
end
println("all one loop graphs in (?:sqed)")
println(":::")
nothing
```

We can notice a few things about the diagrams above. Not all the diagrams contribute to the classical limit. Clearly the diagrams with internal matter loops cannot be allowed when the momenta incoming to the loop is soft [56]. In the classical limit this momenta will go to 0, and since the scalars are massive, they need momentum greater than their mass to be pair produced, thus these diagrams do not contribute. Another class of diagrams that does not contribute to the classical limit are the ones with photon loops that start and end on the same matter line. These do not contribute because they are scaleless. An integral is scaleless when its integrand $\mathcal{I}_{\text{scaleless}}(\{\ell_i\})$ scales homegenously under any rescaling of the loop momentum ℓ_i:

$$\mathcal{I}_{\text{scaleless}}(\{\ell_i\}) \xrightarrow{\ell_j \to \lambda \ell_j} \lambda^\eta \mathcal{I}_{\text{scaleless}}(\{\ell_i\}) \tag{5.125}$$

Thus any diagram that has a basis of loops that does not contain both scalar fields (i.e. does not cross over) cannot have its scale set by the momentum transfer, and is thus scaleless. Dimensionally regularised scaleless integrals vanish, thus we can also discard these diagrams. We can easily implement such a filter programatically, by checking that if cycles are present they touch either both types of scalars, or neither. To compute the cycle basis we use an algorithm derived from [58], implemented in the DirectedHalfEdgeGraphs.jl package.
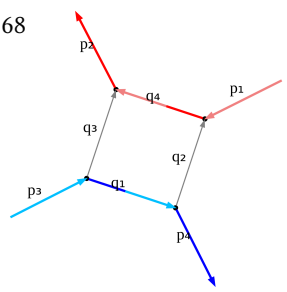
```
using Logging
Logging.disable_logging(Logging.Info)
function scaleless(g::AbstractFieldGraph)
  cycles =cycle_basis(g)
  isscaleless=false
  for c in cycles
    hs= collect(Iterators.flatten(half_edges.(Ref(g),c)))
    fields=unique!(typeof.(field.(Ref(g),hs)))
    if Bool(Phi1 in fields) ∨ Bool(Phi2 in fields)
      isscaleless=true
    end
```

67
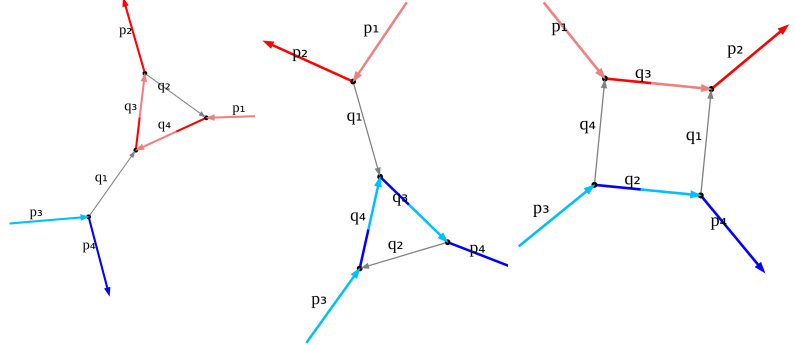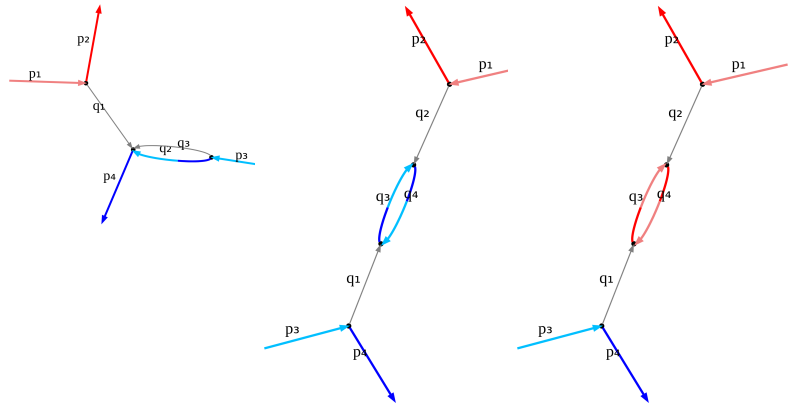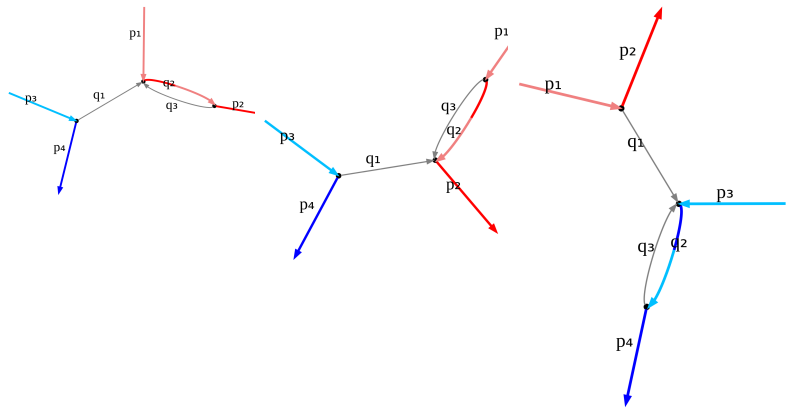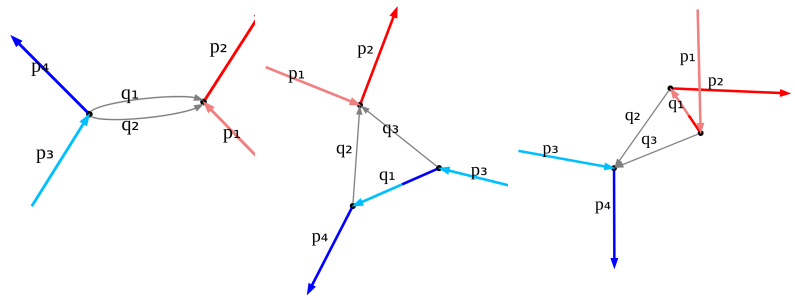
```
    end
    return isscaleless
end

noscalelessdiags=qDiags[.!scaleless.(grafs)]
classicaldiags=noscalelessdiags[2:end]
for (i,d) in enumerate(classicaldiags)
    d.ID=i
end

println(":: {#fig-onefilterloopsqed  layout-ncol=5 fig-cap-location=margin}")
for (i,graf) in enumerate(grafs[.!scaleless.(grafs)])
println("```{dot}")
println("//| fig-width: 1")
    pprint(stdout,to_graphviz(graf,graph_attrs=Dict("layout"⇒"neato")))
    println("```")
end
println("one loop graphs that contribute to the classical limit in (?:sqed)")
println(":::")
nothing
```
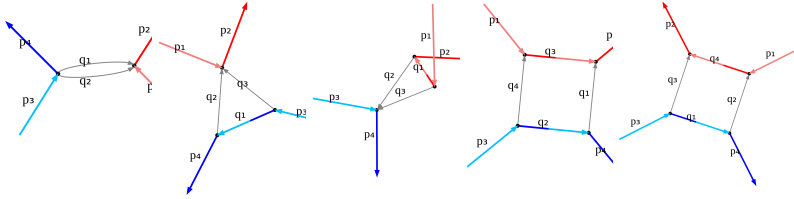

There is one final simplification we can do. The first diagram above
has two photon propagators, and two quartic vertices, which give it its
name: the double-seagull. The photon propagators have homogeonous
$\hbar^{-2}$ scaling (see eq. 5.109), the vertices only bring constants, and the
loop integration has $\hbar^4$ scaling. Together this means that the reduced
amplitude has $\hbar^0$ scaling. However in the virtual integrand the reduced
amplitude has to cancel with the transfer momentum's $\hbar$ scale (see
eq. 5.90). Thus the double seagull diagram dies in the classical limit.

We are left with only 4 diagrams, the two triangle diagrams, the box
and cross box, which we can now compute. At this point we can do
this manually, but again, putting in place a programattic framework
means that subsequent loops can be treated systematically[57]. We will
also extract one of these integrands by hand, for completeness and
comparison.

[57] at least at the unintegrated level

The first step is to define the Feynman rules in a computer readable
format. We will use Julia to apply these rules at every vertex and every
edge, but for the actual computation we will use FORM [59,60] which can
automatically contract indices and does expression manipulations in an

69
```

extremely fast way. The Feynman rules implementation in the package developped for this thesis make use of `Julias` defining paradigm of multiple dispatch. This allows us to define the rules for each vertex and each edge in a very compact way. We can define the rules for SQED as follows:

```julia
function feynmanRule(mime::MIME"text/FORM",p,f1::Photon,f2::Photo
  momen = repr(mime,p.symbol)
  indx1 = repr(mime,index(f1))
  indx2 = repr(mime,index(f2))
  "_i* prop(-1,0,$momen)*d_($indx1,$indx2)"
end

@symmetric function feynmanRule(mime::MIME"text/FORM",p,[f1::Phi1
  momen = repr(mime,p.symbol)
  "_i* prop(-1,1,$momen)"
end

@symmetric function feynmanRule(mime::MIME"text/FORM",p,[f1::Phi2
  momen = repr(mime,p.symbol)

  "_i* prop(-1,2,$momen)"
end

@symmetric function feynmanRule(mime::MIME"text/FORM",[(pᵩ₁,a)::T
              (pᵩ₂,b)::Tuple{Any,AdjointField{ScalarField{S}}},
              (pᵧ,γ)::Tuple{Any,Photon}]) where {S}
  p1 = repr(mime,pᵩ₁(index(γ)))
  p2 = repr(mime,pᵩ₂(index(γ)))
  q = repr(mime,charge(a))
  "_i*e*$q*($p2-$p1)"
end

@symmetric function feynmanRule(mime::MIME"text/FORM",[(pᵧ₁,γ₁)::
              (pᵧ₂,γ₂)::Tuple{Any,Photon},(pᵩ₂,b)::Tuple{Any,Adjoin
              (pᵩ₁,a)::Tuple{Any,ScalarField{S}}]) where {S}
  mu = repr(mime,index(γ₁))
  nu = repr(mime,index(γ₂))
  q = repr(mime,charge(a))
  "2*_i*$q^2*e^2*d_($mu,$nu)"
end
```

where we define `prop(n,i,p)` as representing a generic Feynman propagator, which we will denote:

$$D_-(n,i,p) = \mathrm{prop}(n,i,p) = (p^2 - m_i^2 + i\epsilon)^n \quad \text{thus} \quad \mathrm{prop}(-1,i,p) = \frac{1}{p^2 - m_i^2 + i\epsilon}.$$
$$(5.126)$$

We can now apply these feynamn rules to the graphs we have left, obtaining FORM readable integrands. For example the box diagram gives:

```julia
```{julia}
toform(stdout,classicaldiags[3])
```
```

```
*--#[d3l1:


L [d3l1|o.3.4|i.3.4|i|o|] = 1*i_* prop(-1,0,q1)*d_(nu1,nu2)*i_* prop(-
1,1,q2)*i_* prop(-1,2,q3)*i_* prop(-1,0,q4)*d_(nu7,nu8)*i_*e*qch1*(q2(nu1)-
p4(nu1))*i_*e*qch2*(q3(nu2)-p2(nu2))*i_*e*qch1*(p3(nu7)-
q2(nu7))*i_*e*qch2*(p1(nu8)-q3(nu8));
#procedure momentumRouting


Id q2 = p3 + -q4;
Id p1 = p2 + p4 + -p3;
Id q1 = p3 + -p4 + -q4;
Id q3 = p2 + p4 + q4 + -p3;

Id q4= l1;
#endprocedure
*--#]d3l1:
```

Notice that we also define the momentum routing by imposing the replacement rules, one per vertex. This can be done in many ways but to ensure proper scaling we set the loop momenta on the massless lines. This is done by the Julia program, using kruskal's algorithm [61] to find the maximal-mass spanning tree of the graph, and then setting the loop momenta to be those internal edges that are missing from the tree. Using FORM we can contract indices and apply the momentum conservation rules. Finallly we also apply the relableing rules described in eq. 5.114. The FORM version of the box integrand is then:

When applied to all 4 diagrams we obtain precisely the same integrands as those in [5]. Additionally we notice that the two triangles and the box diagram have overlapping propagators. In fact the denominators of the integrands for all three can be written as:

$$\Box_{i_1,i_2,i_3,i_4} = \frac{1}{\rho_1^{i_1}\rho_2^{i_2}\rho_3^{i_3}\rho_4^{i_4}}, \tag{5.127}$$

for powers $\{i\} \in \{0,1\}^4$, where the inverse propagators ρ_i are:

$$\rho_1 = \ell^2 + \mathring{\imath}\epsilon, \quad \rho_2 = (\ell-q)^2 + \mathring{\imath}\epsilon, \quad \rho_3 = (\frac{q}{2}-\ell+\tilde{p}_1)^2 - m_1^2 + \mathring{\imath}\epsilon, \quad \rho_4 = (-\frac{q}{2}+\ell+\tilde{p}_2)^2 - m_2^2 + \mathring{\imath}\epsilon \tag{5.128}$$

Listing 5.1 Box integrand in FORM

```
[d3l1|o.3.4|i.3.4|i|o|] =
      ( prop(-1,0,q - l1) )
    * ( prop(-1,0,l1) )
    * ( prop(-1,1,1/2*q - l1 + pb1) )
    * ( prop(-1,2, - 1/2*q + l1 + pb2) )
    * ( dot(q,q) - 2*dot(q,l1) - 2*dot(q,pb2) + 2*dot(q,pb1) +
        + 2*dot(l1,pb2) - 2*dot(l1,pb1) - 4*dot(pb2,pb1) )
    * ( dot(l1,l1) + 2*dot(l1,pb2) - 2*dot(l1,pb1) - 4*dot(pb2
    * ( qch2 ) * ( qch2 ) * ( qch1 ) * ( qch1 )
    * ( e ) * ( e ) * ( e ) * ( e );
```

Note that in the classical limit we can expand the massive propagators as shown in eq. 5.110 and obtain to first order in $\hbar$:

$$\rho_3 = 2\ell \cdot \tilde{p}_1 + \mathring{\imath}\epsilon, \quad \rho_4 = -2\ell \cdot \tilde{p}_2 + \mathring{\imath}\epsilon, \tag{5.129}$$

where we used eq. 5.115. The cross box can in fact extend this family, by adding just one more inverse propagator. We now have the complete description of the denominators of all 1-loop contributing diagrams. The numerators in fact do not complicate things much. They are all composed of scalar products of momenta. If these do not contain loop-momenta they are just constant factors in front of the integral. The scalar products that do contain loop momenta can be intelligently written as inverse powers of the propagators. This is the case for any feynman like integrand. Consider the following general integrand:

$$\mathcal{I} = \frac{\mathcal{N}}{\mathcal{D}} = \frac{\prod_{S'} N_{S'}}{\prod_{S} D_S} = \frac{\prod_{S'} \sum_{i \geq j} S'_{ij} p_i \cdot p_j}{\prod_{S} \sum_{i \geq j} S_{ij} p_i \cdot p_j}, \tag{5.130}$$

where S and S' are sets of coefficient matrices for all possible dot products. If we have a quadruplet $\{A, B, a, b\}$ such that $A_{a,b} \neq 0$ and $B_{a,b} neq 0$ and p_a or p_b is a loop momentum ℓ, say $p_a = \ell$ then it is useful to write this component of the integrand as:

$$\frac{N_B}{D_A} = \frac{\tilde{N}_B + B_{ab}\ell \cdot p_b}{A_{ab}\ell \cdot p_b + \sum_{\substack{i \geq j \\ i,j \neq a,b}} A_{ij} p_i \cdot p_j} = \frac{\tilde{N}_B}{D_A} + \frac{B_{ab}}{A_{ab}}\left(1 - \frac{\tilde{D}_A}{D_A}\right). \tag{5.131}$$

where the tilde means that we have remove the *ab* contribution. Thus we see that we obtain in the numerator, a sum of objects, none of which

contain the dot product: $\ell \cdot p_b$. We can do this for every quadruplet $\{A, B, a, b\}$, after every replacement and obtain an integrand containing only so called *irreducible* loop-momenta scalar products. In the cases we have here, they all dissapear, leaving us truely with a family of integrands like eq. 5.127. This can be readily fed into a IBP solver, such as `AIR` [62], `FIRE` [63] or `Kira` [64].

With such a solver we can obtain a complete family of integrals, that one can then look up. We are thus able to obtain the integrated integrands at NLO that are then used in eq. 5.90 and eq. 5.86. The algorithm described above was implemented in `FORM` and is able to rapidly process the 1-loop diagrams. The code is available at the repository for this document.

Importantly we still need to take the classical limit. At this point a problem shows up. The box and cross box integrals are divergent in the classical limit (some authors call this super classical). Let us see this for the box integral. We have from Listing 5.1 that the integral for the box diagram B is:

$$\mathring{i}B = e^4 Q_1 Q_2 \int \tilde{\mathrm{d}}^D \ell \, \Box_{1,1,1,1} (4\tilde{p}_1 \cdot \tilde{p}_2 + 2\ell \cdot (\tilde{p}_2 - \tilde{p}_1) - (q - \ell)^2)(4\tilde{p}_1 \cdot \tilde{p}_2 + 2\ell \cdot (\tilde{p}_2 - \tilde{p}_1) - (\ell)^2) \tag{5.132}$$

we can apply the procedure described above, turning messenger momenta into wavenumbers:

$$\mathring{i}B = e^4 Q_1 Q_2 \int \tilde{\mathrm{d}}^D \bar{\ell} \, \frac{\hbar^D}{\hbar^6} \Box_{\bar{1},\bar{1},\bar{1},\bar{1}} (4\tilde{p}_1 \cdot \tilde{p}_2 + \hbar 2\bar{\ell} \cdot (\tilde{p}_2 - \tilde{p}_1) - \hbar^2 (\bar{q} - \bar{\ell})^2)(4\tilde{p}_1 \cdot \tilde{p}_2 + \hbar 2\bar{\ell} \cdot (\tilde{p}_2 - \tilde{p}_1) - \hbar^2 (\bar{\ell})^2), \tag{5.133}$$

where $\Box_{\bar{i}_1, \bar{i}_2, \bar{i}_3, \bar{i}_4} = \frac{1}{\hbar^{2(i_1 + i_2) + i_3 + i_4}} \Box_{i_1, i_2, i_3, i_4}$ is the box family with wavenumber instead of messenger momenta, and $\hbar$s extracted. We notice that if we apply the scalar product reduction eq. 5.131, we will necessarily still have an integral of the form[58]:

$$e^4 Q_1 Q_2 16 (\tilde{p}_1 \cdot \tilde{p}_2)^2 \int \tilde{\mathrm{d}}^D \ell \, \Box_{1,1,1,1} = \mathcal{O}(\hbar^{D-6}) \tag{5.134}$$

whilst we need to cancel with the $\hbar$ in the classical limit (eq. 5.93), here we have one too many orders in the denominator (if D=4). Thus would get a divergent $(\frac{1}{\hbar})$ contribution when taking the classical $\hbar \to 0$ limit. If we consider now the cross box, which is the same family as above but with an extra minus sign:

$$\tilde{\rho}_4 = (\frac{q}{2} - \ell + \tilde{p}_2)^2 - m_2^2 + \mathring{i}\epsilon \simeq 2\ell \cdot \tilde{p}_2 + \mathring{i}\epsilon. \tag{5.135}$$

If we write that $\Box_{+i_1, +i_2, +i_3, +i_4} = \Box_{i_1, i_2, i_3, i_4}$ where the sign is the sign of the $\mathring{i}\epsilon$ prescription, then we can write the cross box integral as:

$$\int \tilde{\mathrm{d}}^D \ell \, - \Box_{1,1,1,-1} \tag{5.136}$$

[58] along with ones that are of the form $\Box_{1,1,1,0}$ and other permutations. These are not divergent in the classical limit, as they have one less propagator, thus one less $\hbar$, just enough to cancel what is left of the $\hbar$ in the numerator, and have an overall $\mathcal{O}(\hbar^0)$ scaling.

thus summing up the two divergent contributions from the box and cross box we have:

$$\Box_{1,1,1,1} - \Box_{1,1,1,-1} = \Box_{1,1,1,0}\left(\frac{1}{-2\ell \cdot \tilde{p}_2 + i\epsilon} - \frac{1}{2\ell \cdot \tilde{p}_2 + i\epsilon}\right) = -i\Box_{1,1,1,0}\tilde{\delta}(2\ell \cdot \tilde{p}_2),$$
(5.137)

where in the equation line we used *reverse unitarity* [65–67]. This idea was developed in the context of cross-section calculations in the for collider physics computations. It enables to set on equal footing real contributions [59] where we integrate over on shell momenta [60] and virtual integrals, where the integration is over all possible four-momentum [61]. The idea is to trade the on-shell delta functions and their n-th derivatives for differences of (powers of) propagators with alternating $i\epsilon$:

$$\frac{i}{(-1)^n n!}\frac{\mathrm{d}^n}{\mathrm{d}z^n}\tilde{\delta}(z) = \frac{1}{(z - i\epsilon)^{(n+1)}} - \frac{1}{(z + i\epsilon)^{(n+1)}}.$$
(5.138)

In our case eq. 5.138 implies the following identities:

$$\tilde{\delta}(-2\ell \cdot \tilde{p}_2) = i(\Box_{0,0,0,1} - \Box_{0,0,0,-1})$$
(5.139)

$$\tilde{\delta}(2\ell \cdot \tilde{p}_1) = i(\Box_{0,0,1,0} - \Box_{0,0,-1,0})$$
(5.140)

Since we where able to write this difference of propagators as a sort of cut, we could further compare the divergent part of the box and cross box with the corresponding real contribution, which is at tree level, with no cut messengers: $L' = 0$ and $|X| = 0$ such that eq. 5.92 is satisfied. We have:

$$\int \tilde{\mathrm{d}}^4\bar{w}\,\tilde{\delta}(2\tilde{p}_1 \cdot \bar{w} - \hbar\frac{\bar{q}}{2} \cdot \bar{w} + \hbar\bar{w}^2)\tilde{\delta}(-2\tilde{p}_2 \cdot \bar{w} + \hbar\frac{\bar{q}}{2} \cdot \bar{w} + \hbar\bar{w}^2)$$
$$\times \hbar\bar{w}^\mu$$
$$\times \kappa^4\hbar^2\mathscr{A}^{(0)}(\tilde{p}_1 - \hbar\frac{\bar{q}}{2}, \tilde{p}_2 + \hbar\frac{\bar{q}}{2} \to \tilde{p}_1 + \hbar\frac{\bar{q}}{2} + \hbar\bar{w}, \tilde{p}_2 - \hbar\frac{\bar{q}}{2} - \hbar\bar{w}_2)$$
$$\times \bar{\mathscr{A}}^{*(0)}(\tilde{p}_1 + \hbar\frac{\bar{q}}{2}, \tilde{p}_2 + \hbar\frac{\bar{q}}{2} - \hbar\bar{q} \to \tilde{p}_1 - \hbar\frac{\bar{q}}{2} + \hbar\bar{w}, \tilde{p}_2 + \hbar\frac{\bar{q}}{2} - \hbar\bar{w}_2).$$
(5.141)

where the $\bar{\mathscr{A}}^{(0)}$ we already computed in eq. 5.119, and we have eliminated the theta functions in prepartation of taking the classical limit. Thus it is essentially a cut of a one-loop box. Notice that in the classical limit we must cancel with $\hbar^3$ (eq. 5.94) which at leading order is again overdone. The $\tilde{p}_1 \cdot \tilde{p}_2$ contribution from each tree scales like $\frac{1}{\hbar^4}$, and is thus classically divergent as the box and cross box before it. We also notice it has the following form:

[59] such as ones in the real integrand eq. 5.51

[60] thus three dimensional momentum space

[61] as virtual particles can be off shell

$$e^4 Q_1 Q_2 16 (\tilde{p}_1 \cdot \tilde{p}_2)^2 \frac{1}{\hbar} \int \tilde{d}^4 \bar{\ell}\, \bar{\ell}^\mu \tilde{\delta}(2\tilde{p}_1 \cdot \bar{\ell}) \tilde{\delta}(-2\tilde{p}_2 \cdot \bar{\ell}) \Box_{\bar{1},\bar{1},\bar{0},\bar{0}}, \qquad (5.142)$$

where we've changed variables from $\bar{w}$ to $\bar{\ell}$ and removed the $\hbar(\frac{\bar{q}}{2} \cdot \bar{\ell} \pm \bar{\ell}^2)$ term in the delta functions, in prepation for the classical limit. We can now apply reverse unitarity (eq. 5.139, eq. 5.140) and focus on the integral without the prefactors:

$$\int \tilde{d}^4 \bar{\ell}\, \bar{\ell}^\mu \tilde{\delta}(2\tilde{p}_1 \cdot \bar{\ell}) \tilde{\delta}(-2\tilde{p}_2 \cdot \bar{\ell}) \Box_{\bar{1},\bar{1},\bar{0},\bar{0}} = \int \tilde{d}^4 \bar{\ell}\, \bar{\ell}^\mu \tilde{\delta}(2\tilde{p}_1 \cdot \bar{\ell}) i (\Box_{0,0,0,1} - \Box_{0,0,0,-1}) \Box_{\bar{1},\bar{1},\bar{0},\bar{0}}$$

$$= -\int \tilde{d}^4 \bar{\ell}\, \bar{\ell}^\mu (\Box_{0,0,1,0} - \Box_{0,0,-1,0})(\Box_{1,1,0,1} - \Box_{1,1,0,-1}),$$

$$= \int \tilde{d}^4 \bar{\ell}\, \bar{\ell}^\mu [(\Box_{1,1,1,-1} - \Box_{1,1,1,1}) + (\Box_{1,1,-1,1} - \Box_{1,1,-1,-1})].$$

$$(5.143)$$

We now notice something interesting, this cut integral has a sort of horizontal flip symmetry, i.e. if we average over the existing 'loop' momentum labelling and a new $\ell' = q - \ell$ we eliminate the ℓ^μ dependence in the numerator:

$$\frac{1}{2}[\ell^\mu + (q^\mu - \ell^\mu)] = q^\mu \qquad (5.144)$$

since the box families transform as:

$$\Box'_{i,j,m,n} = (-1)^m (-1)^n \Box_{j,i,-m,-n}. \qquad (5.145)$$

Thus we have that the cut integral with the $\bar{q}^\mu$ factored out:

$$\int \tilde{d}^4 \bar{\ell}\, \frac{1}{2}[(\Box_{1,1,1,-1} - \Box_{1,1,1,1}) + (\Box_{1,1,-1,1} - \Box_{1,1,-1,-1})]. \qquad (5.146)$$

We can apply the relabelling only this time only for the last two integrands, and the integral becomes, applying eq. 5.145:

$$\int \tilde{d}^4 \bar{\ell}\, \frac{1}{2}[(\Box_{1,1,1,-1} - \Box_{1,1,1,1}) + (\Box'_{1,1,-1,1} - \Box'_{1,1,-1,-1})] = \int \tilde{d}^4 \bar{\ell}\, (\Box_{1,1,1,-1} - \Box_{1,1,1,1}). \qquad (5.147)$$

If we now add the box and cross box contributions from eq. 5.137 we get:

$$\int \tilde{d}^4 \bar{\ell}\, (\cancel{\Box_{1,1,1,-1}} - \underline{\Box_{1,1,1,1}}) + \underline{\Box_{1,1,1,1}} - \cancel{\Box_{1,1,1,-1}} = 0. \qquad (5.148)$$

The classically divergent terms have cancelled leaving us with only the finite terms!

6 Conclusion

In this thesis we explored the landscape of theoretical research that surrounds gravitational waves. We showed the existence of gravitational waves theoretically. We motivated waveform generation techniques grounded in first principles' physics. It is only through such precise frameworks that we can hope to elucidate the nature of the objects that emit this gravitational radiation. We looked at NR and EOB two complementary approaches to waveform generation that enabled LIGO to make that field changing detection in 2016. Both approaches have their challenges, NR with stability and computational cost, and EOB with higher order perturbative calculations. Each increase in precision enables a more precise match of the signal, enabling a much richer analysis of the incoming wave. Purely analytical tools have recently come into the crosshairs of particle physicits aswell.

We then went on to understand these nascent formalisms built on techniques from particle physics. The EFT matching approach enables a simple map from EOB to amplitudes computed in the potential kinematic region. This, and EOB in general, struggle to use and implement dissipation however. The Hamiltonian framework has to be somehow augmented with the dissipative forces. This motivates frameworks that sidestep the EOB framework. We explored the most developed one currently: KMOC . We were able to express classical observables such as the impulse in terms of the classical limit amplitudes and their unitarity cuts. We then went on to implement a programmatic framework for expressing the necessary integrals that the amplitudes yield. We used custom code to apply Feynman rules, manipulate and filter the graphs. We matched the results from [5], and then implemented a scalar product reduction for preparing the input to IBP reduction programs.

The results and formalsims explored here show that amplitude techniques in gravitaional wave theory are a very promising and powerful tool. A lot of the recent high energy physics results can directly be put to use in this context, and can already outperfom traditional methods. The higher perturbative order frontier however is increasingly difficult. At some point in the near future, these computations will have exhausted the techniques currently in use for particle physics. The next step is to develop new techniques that can be applied to both fields. Important work needs to be done to have a fully amplitude based waveform generation framework. This might be the next revolution in gravitational wave theory.

References

[1] B. P. Abbott, R. Abbott, T. D. Abbott, et al., *Observation of Gravitational Waves from a Binary Black Hole Merger*, Physical Review Letters **116**, 061102 (2016).

[2] B. P. Abbott, R. Abbott, T. D. Abbott, et al., *GW170817: Observation of Gravitational Waves from a Binary Neutron Star Inspiral*, Physical Review Letters **119**, 161101 (2017).

[3] R. Abbott et al., *Observation of Gravitational Waves from Two Neutron Star–Black Hole Coalescences*, The Astrophysical Journal Letters **915**, L5 (2021).

[4] W. D. Goldberger and I. Z. Rothstein, *Effective Field Theory of Gravity for Extended Objects*, Physical Review D **73**, 104029 (2006).

[5] D. A. Kosower, B. Maybee, and D. O'Connell, *Amplitudes, Observables, and Classical Scattering*, Journal of High Energy Physics **02**, 137 (2019).

[6] R. A. Porto, *The Effective Field Theorist's Approach to Gravitational Dynamics*, Physics Reports **633**, 1 (2016).

[7] D. Neill and I. Z. Rothstein, *Classical Space–times from the S-matrix*, Nuclear Physics B **877**, 177 (2013).

[8] A. Shomer, *A Pedagogical Explanation for the Non-Renormalizability of Gravity*, (2007).

[9] E. Remiddi, *Differential Equations for Feynman Graph Amplitudes*, Il Nuovo Cimento A (1971-1996) **110**, 1435 (1997).

[10] Z. Bern, L. Dixon, and D. A. Kosower, *Dimensionally-Regulated Pentagon Integrals*, Nuclear Physics B **412**, 751 (1994).

[11] A. V. Kotikov, *Differential Equations Method. New Technique for Massive Feynman Diagram Calculation*, Physics Letters B **254**, 158 (1991).

[12] Z. Bern, L. Dixon, D. C. Dunbar, and D. A. Kosower, *Fusing Gauge Theory Tree Amplitudes Into Loop Amplitudes*, Nuclear Physics B **435**, 59 (1995).

[13] Z. Bern, V. Del Duca, L. J. Dixon, and D. A. Kosower, *All Non-Maximally-Helicity-Violating One-Loop Seven-Gluon Amplitudes in N=4 Super-Yang-Mills Theory*, Physical Review D **71**, 045006 (2005).

[14] E. I. Buchbinder and F. Cachazo, *Two-Loop Amplitudes of Gluons and Octa-Cuts in N=4 Super Yang-Mills*, Journal of High Energy Physics **11**, 036 (2005).

[15] C. Anastasiou, R. Britto, B. Feng, Z. Kunszt, and P. Mastrolia, *D-Dimensional Unitarity Cut Method*, Physics Letters B **645**, 213 (2007).

[16] S. Weinberg, *Gravitation and Cosmology: Principles and Applications of the General Theory of Relativity* (Wiley, New York, 1972).

[17] S. M. Carroll, *Spacetime and Geometry: An Introduction to General Relativity*, Higher Education from Cambridge University Press (2019).

[18] G. D. Birkhoff and R. E. Langer, *Relativity and Modern Physics* (Harvard University Press; [etc., etc.], Cambridge, 1923).

[19] S. Detweiler, *Pulsar Timing Measurements and the Search for Gravitational Waves*, The Astrophysical Journal **234**, 1100 (1979).

[20] M. Maiorano, F. De Paolis, and A. A. Nucita, *Principles of Gravitational-Wave Detection with Pulsar Timing Arrays*, Symmetry **13**, 2418 (2021).

[21] G. Hobbs et al., *The International Pulsar Timing Array Project: Using Pulsars as a Gravitational Wave Detector*, Classical and Quantum Gravity **27**, 084013 (2010).

[22] S. Mukherjee, S. Mitra, and S. Chatterjee, *Gravitational Wave Observatories May Be Able to Detect Hyperbolic Encounters of Black Holes*, Monthly Notices of the Royal Astronomical Society **508**, 5064 (2021).

[23] G. Kalin and R. A. Porto, *From Boundary Data to Bound States*, Journal of High Energy Physics **01**, 072 (2020).

[24] S. G. Hahn and R. W. Lindquist, *The Two-Body Problem in Geometrodynamics*, Annals of Physics **29**, 304 (1964).

[25] F. Pretorius, *Evolution of Binary Black-Hole Spacetimes*, Physical Review Letters **95**, 121101 (2005).

[26] M. Campanelli, C. O. Lousto, P. Marronetti, and Y. Zlochower, *Accurate Evolutions of Orbiting Black-Hole Binaries Without Excision*, Physical Review Letters **96**, 111101 (2006).

[27] A. Buonanno and T. Damour, *Transition from Inspiral to Plunge in Binary Black Hole Coalescences*, Physical Review D **62**, 064015 (2000).

[28] L. Blanchet, *Gravitational Radiation from Post-Newtonian Sources and Inspiralling Compact Binaries*, Living Reviews in Relativity **17**, 2 (2014).

[29] L. Blanchet, T. Damour, and B. R. Iyer, *Gravitational Waves from Inspiralling Compact Binaries: Energy Loss and Waveform to Second-Post-Newtonian Order*, Physical Review D **51**, 5360 (1995).

[30] R. Sturani, *Effective Field Theory Methods to Model Compact Binaries*, in *Handbook of Gravitational Wave Astronomy*, edited by C. Bambi, S. Katsanevas, and K. D. Kokkotas (Springer, Singapore, 2021), pp. 1–33.

[31] W. B. Bonnor and L. Rosenhead, *Spherical Gravitational Waves*, Philosophical Transactions of the Royal Society of London. Series A, Mathematical and Physical Sciences **251**, 233 (1959).

[32] K. S. Thorne, *Multipole Expansions of Gravitational Radiation*, Reviews of Modern Physics **52**, 299 (1980).

[33] L. Blanchet and T. Damour, *Radiative Gravitational Fields in General Relativity I. General Structure of the Field Outside the Source*, Philosophical Transactions of the Royal Society of London. Series A, Mathematical and Physical Sciences **320**, 379 (1986).

[34] A. Buonanno and T. Damour, *Effective One-Body Approach to General Relativistic Two-Body Dynamics*, Physical Review D **59**, 084006 (1999).

[35] T. Damour, *Gravitational Scattering, Post-Minkowskian Approximation and Effective One-Body Theory*, Physical Review D **94**, 104015 (2016).

[36] E. Brezin, C. Itzykson, and J. Zinn-Justin, *Relativistic Balmer Formula Including Recoil Effects*, Physical Review D **1**, 2349 (1970).

[37] H. Goldstein, C. P. Poole, and J. L. Safko, *Classical Mechanics* (Addison Wesley, 2002).

[38] K. Hiida and H. Okamura, *Gauge Transformation and Gravitational Potentials*, Progress of Theoretical Physics **47**, 1743 (1972).

[39] Y. Iwasaki, *Quantum Theory of Gravitation Vs. Classical Theory*): Fourth-Order Potential*, Progress of Theoretical Physics **46**, 1587 (1971).

[40] N. E. J. Bjerrum-Bohr, J. F. Donoghue, and P. Vanhove, *On-Shell Techniques and Universal Results in Quantum Gravity*, Journal of High Energy Physics **02**, 111 (2014).

[41] V. Vaidya, *Gravitational Spin Hamiltonians from the S Matrix*, Physical Review D **91**, 024017 (2015).

[42] F. Cachazo and A. Guevara, *Leading Singularities and Classical Gravitational Scattering*, **02**, 181 (2020).

[43] A. Guevara, *Holomorphic Classical Limit for Spin Effects in Gravitational and Electromagnetic Scattering*, Journal of High Energy Physics **04**, 033 (2019).

[44] C. Cheung, I. Z. Rothstein, and M. P. Solon, *From Scattering Amplitudes to Classical Potentials in the Post-Minkowskian Expansion*, Physical Review Letters **121**, 251101 (2018).

[45] G. Kälin, J. Neef, and R. A. Porto, *Radiation-Reaction in the Effective Field Theory Approach to Post-Minkowskian Dynamics*, (2022).

[46] G. Kalin and R. A. Porto, *From Boundary Data to Bound States. Part II. Scattering Angle to Dynamical Invariants (with Twist)*, Journal of High Energy Physics **02**, 120 (2020).

[47] G. Kälin and R. A. Porto, *Post-Minkowskian Effective Field Theory for Conservative Binary Dynamics*, Journal of High Energy Physics **11**, 106 (2020).

[48] A. Cristofoli, R. Gonzo, D. A. Kosower, and D. O'Connell, *Waveforms from Amplitudes*, Phys. Rev. D **106**, 056007 (2022).

[49] Z. Bern, J. P. Gatica, E. Herrmann, A. Luna, and M. Zeng, *Scalar QED as a Toy Model for Higher-Order Effects in Classical Gravitational Scattering*, arXiv:2112.12243 [Gr-Qc, Physics:hep-Th] **08**, 131 (2022).

[50] M. A. Srednicki, *Quantum Field Theory* (Cambridge University Press, Cambridge ; New York, 2007).

[51] S. Coleman, *Lectures of Sidney Coleman on Quantum Field Theory* (WSP, Hackensack, 2018).

[52] H. Lehmann, K. Symanzik, and W. Zimmermann, *Zur Formulierung quantisierter Feldtheorien*, Il Nuovo Cimento (1955-1965) **1**, 205 (1955).

[53] J. Collins, *A New Approach to the LSZ Reduction Formula*, (2019).

[54] G. 't Hooft and M. Veltman, *Regularization and Renormalization of Gauge Fields*, Nuclear Physics B **44**, 189 (1972).

[55] Z. Bern, C. Cheung, R. Roiban, C.-H. Shen, M. P. Solon, and M. Zeng, *Black Hole Binary Dynamics from the Double Copy and Effective Theory*, Journal of High Energy Physics **10**, 206 (2019).

[56] P. Nogueira, *Automatic Feynman Graph Generation*, Journal of Computational Physics **105**, 279 (1993).

[57] J. Bezanson, A. Edelman, S. Karpinski, and V. B. Shah, *Julia: A Fresh Approach to Numerical Computing*, arXiv:1411.1607 (2015).

[58] K. Paton, *An Algorithm for Finding a Fundamental Set of Cycles of a Graph*, Communications of the ACM **12**, 514 (1969).

[59] J. A. M. Vermaseren, *New Features of FORM*, (2000).

[60] J. Kuipers, T. Ueda, J. A. M. Vermaseren, and J. Vollinga, *FORM Version 4.0*, Comput. Phys. Commun. **184**, 1453 (2013).

[61] J. B. Kruskal, *On the Shortest Spanning Subtree of a Graph and the Traveling Salesman Problem*, Proceedings of the American Mathematical Society **7**, 48 (1956).

[62] C. Anastasiou and A. Lazopoulos, *Automatic Integral Reduction for Higher Order Perturbative Calculations*, Journal of High Energy Physics **2004**, 046 (2004).

[63] A. V. Smirnov and F. S. Chukharev, *FIRE6: Feynman Integral REduction with Modular Arithmetic*, Computer Physics Communications **247**, 106877 (2020).

[64] P. Maierhöfer and J. Usovitsch, *Kira 1.2 Release Notes*, arXiv:1812.01491 [Hep-Ph] (2018).

[65] C. Anastasiou and K. Melnikov, *Higgs Boson Production at Hadron Colliders in NNLO QCD*, Nuclear Physics B **646**, 220 (2002).

[66] C. Anastasiou, L. Dixon, and K. Melnikov, *NLO Higgs Boson Rapidity Distributions at Hadron Colliders*, Nuclear Physics B - Proceedings Supplements **116**, 193 (2003).

[67] C. Anastasiou, L. Dixon, K. Melnikov, and F. Petriello, *Dilepton Rapidity Distribution in the Drell-Yan Process at Next-to-Next-to-Leading Order in QCD*, Physical Review Letters **91**, 182002 (2003).